agriculture

MDPI

Review

Monitoring Agricultural Land Use Intensity with Remote Sensing and Traits

Angela Lausch [1,2,3,*], Jan Bumberger [4,5,6], András Jung [7], Marion Pause [3], Peter Selsam [4,5], Tao Zhou [2,8] and Felix Herzog [9]

1 Department of Computational Landscape Ecology, Helmholtz Centre for Environmental Research—UFZ, Permoserstr. 15, D-04318 Leipzig, Germany
2 Landscape Ecology Lab, Geography Department, Humboldt-Universität zu Berlin, Unter den Linden 6, D-10099 Berlin, Germany; xinyangzhoutao@163.com
3 Department of Architecture, Facility Management and Geoinformation, Institute for Geo-Information and Land Surveying, Anhalt University of Applied Sciences, Seminarplatz 2a, D-06846 Dessau, Germany; marion.pause@hs-anhalt.de
4 Department of Monitoring and Exploration Technologies, Helmholtz Centre for Environmental Research—UFZ, Permoserstr. 15, D-04318 Leipzig, Germany; jan.bumberger@ufz.de (J.B.); peter.selsam@ufz.de (P.S.)
5 Research Data Management—RDM, Helmholtz Centre for Environmental Research—UFZ, Permoserstraße 15, D-04318 Leipzig, Germany
6 German Centre for Integrative Biodiversity Research (iDiv) Halle-Jena-Leipzig, Puschstraße 4, D-04103 Leipzig, Germany
7 Faculty of Informatics, Institute of Cartography and Geoinformatics, Eötvös Loránd University, Pázmány Péter sétány 1/A, H-1117 Budapest, Hungary; jung@inf.elte.hu
8 School of Resources and Environmental Engineering, Ludong University, Middle Hongqi Road 186, Yantai 264025, China
9 Agroecology and Environment, Agroscope, 8046 Zürich, Switzerland; felix.herzog@agroscope.admin.ch
* Correspondence: angela.lausch@ufz.de; Tel.: +49-341-6025; Fax: +49-341-235-1939

Abstract

The intensification of agricultural land use (A-LUI) is a central driver of global environmental change, affecting soil health, water quality, biodiversity, and greenhouse gas balances. Monitoring A-LUI remains challenging because it is shaped by multiple management practices, ecological processes, and spatio-temporal dynamics. This review provides a comprehensive synthesis of existing definitions and standards of A-LUI at national and international levels (FAO, OECD, World Bank, EUROSTAT) and evaluates in situ methods alongside the rapidly expanding potential of remote sensing (RS). We introduce a novel RS-based taxonomy of A-LUI indicators, structured into five complementary categories: trait, genesis, structural, taxonomic, and functional indicators. Numerous examples illustrate how traits and management practices can be translated into RS proxies and linked to intensity signals, while highlighting key challenges such as sensor limitations, cultivar variability, and confounding environmental factors. We further propose an integrative framework that connects management practices, plant and soil traits, RS observables, validation needs, and policy relevance. Emerging technologies—such as hyperspectral imaging, solar-induced fluorescence, radar, artificial intelligence, and semantic data integration—are discussed as promising pathways to advance the monitoring of A-LUI across scales. By compiling and structuring RS-derived indicators, this review establishes a conceptual and methodological foundation for transparent, standardised, and globally comparable assessments of agricultural land use intensity, thereby supporting both scientific progress and evidence-based agricultural policy.

Academic Editors: Francesco Marinello and Tarendra Lakhankar

Received: 22 July 2025
Revised: 22 September 2025
Accepted: 20 October 2025
Published: 26 October 2025

Citation: Lausch, A.; Bumberger, J.; Jung, A.; Pause, M.; Selsam, P.; Zhou, T.; Herzog, F. Monitoring Agricultural Land Use Intensity with Remote Sensing and Traits. *Agriculture* **2025**, *15*, 2233. https://doi.org/10.3390/agriculture15212233

Keywords: land-use intensity; agricultural land-use intensity; agricultural intensification; remote sensing; earth observation; traits; in situ; monitoring; indicators; policy relevance

1. Introduction

Agricultural intensification represents a major economic development in recent decades on a global scale. However, this phenomenon is concomitant with significant environmental and economic changes, disruptions, and challenges. Agricultural intensification, otherwise termed land use intensity (A-LUI), is defined here as the augmentation in production output per unit of land through increased management intensity (utilisation of high yielding crops and livestock, inputs such as fertilisers, pesticides, drainage or irrigation, mechanisation) and/or the adaptation of landscape structure (increased field size through, e.g., land consolidation, removal of structural elements) [1]. While increasing A-LUI has facilitated the procurement of sustenance for an expanding global population, it goes along with substantial ecological concerns, including soil degradation, alterations in water quality and resources, biodiversity loss, and augmented greenhouse gas emissions, in addition to health hazards. For instance, the ongoing utilisation of synthetic fertilisers has resulted in soil acidification, thereby impacting the availability of nutrients to plants and the health of soil microbiota [2]. Furthermore, the excessive application of fertilisers can lead to significant nitrogen leaching and runoff of phosphorus, impacting water resources and soil fertility [3].

Use of heavy agricultural machinery leads to soil compaction, resulting in a reduction in both water and air permeability. This, in turn, has the potential to precipitate the occurrence of erosion and desertification over time [4]. The intensive use of water resources, which accounts for approximately 70% of total water consumption in agriculture worldwide [5], increases pressure on surface and groundwater, especially in regions where water is scarce. The quality of water is diminished by the mobilisation of salts due to low water tables and the introduction of fertilisers and pesticides into the underlying aquifers, which can threaten drinking water supplies [6,7]. Another pertinent issue is the escalating eutrophication of water bodies due to excessive nutrient inputs, which culminates in oxygen depletion and the demise of aquatic organisms [8]. Land use intensification exerts a profound influence on biodiversity [9–12]. The phenomenon of biodiversity loss [13] and the alteration in networks between biodiversity and ecosystem functions and services [14] are also impacted by land use intensification. The establishment of monocultures has resulted in the displacement of species-rich ecosystems, which in turn has been shown to lead to a decline in biodiversity, genetic impoverishment, and reduced resilience. Furthermore, the process of intensification has been shown to result in a multi-trophic homogenisation of grassland communities [15]. These developments have consequences for the resilience of ecosystems, resulting in the loss of essential ecosystem services such as pollination, pest control, and soil formation [16–18]. The expansion of agricultural land, frequently at the expense of forests, wetlands, and other semi-natural ecosystems, contributes to habitat fragmentation and destruction, biodiversity loss, and the release of greenhouse gases, which in turn further exacerbates climate change [13,19–22]. Consequently, the agricultural sector is a substantial contributor to global warming. In addition to the ecological consequences, the intensification of land use poses a significant health risk. The presence of persistent pollutants from herbicides in food can result in health complications, including cancer and neurological disorders [23]. The overuse of antibiotics in intensive livestock production has been demonstrated to promote the development of antibiotic resistance, which poses a significant threat to public health [24,25].

As scientific debate has long emphasised, accurate recording and quantification of A-LUI [26] is essential for the assessment of the impact of intensification on agroecological systems and for the development of sustainable management strategies. In situ measurements are of central importance, as they provide detailed information directly in the field (e.g., [27–29]). The merits of in situ measurements are twofold. Firstly, they enable direct observation of complex ecological and agronomic processes. Secondly, they facilitate the capture of locally specific variability that is often not considered in large-scale modelling. This is particularly true in heterogeneous landscapes, where minor variations in soil quality or microclimate or management practices can have substantial consequences for A-LUI. Consequently, such measurements are imperative. However, in situ measurements are often time-consuming, costly, and have limited spatial coverage, making their large-scale application and continuous monitoring difficult. Moreover, the comparability of results between different regions and studies is problematic due to a lack of standardisation.

RS has emerged as a key approach to quantify and assess A-LUI indicators on a large scale, in a timely and standardised manner, and over long periods of time [30,31]. As demonstrated in the works of [32–38], RS technologies facilitate spectral, spatial, and temporal analyses, providing detailed information on vegetation structure, soil condition, and other key land cover parameters. Furthermore, RS-based indicators of A-LUI, including yield estimates, vegetation indices (e.g., NDVI), and soil moisture parameters, which are crucial for the assessment of agroecological processes, have been derived for some time, including the advent of unmanned aerial vehicles (UAVs) and autonomous robotic platforms, in conjunction with the freely available space-based RS data (Landsat mission [39,40], the Copernicus mission Sentinel [41], and the hyperspectral mission (EnMAP) [42]). As demonstrated in the 2015 Copernicus Hyperspectral Imaging Mission (CHIME) [43], the LiDAR mission (GEDI) [44], and in the planned future missions such as the Hyperspectral Infrared Imager Mission (HyspIRI) [45] and the Fluorescence Explorer (FLEX) sensor [46], the derivation of standardised and improved A-LUI indicators will be significantly improved. The substantial body of literature on the derivation of A-LUI indicators using RS is indicative of this phenomenon [47–50]. As demonstrated in the works of Segarra et al. [51–56] and Hank et al. [38], the subject has been extensively researched.

A promising approach to capture and quantify A-LUI is to understand traits and trait variation in land cover, vegetation, and geodiversity [57]. Traits manifest at all spatial and temporal scales, making them ideal for standardised monitoring and the derivation of A-LUI indicators from local to global levels. All RS technologies record traits and trait variation in vegetation (example [58,59]), soil (example [60]), terrain and geomorphology (example [61,62]), and water (example [63]). RS allows the monitoring of traits and their status, related processes, disturbances or resource limitations in both terrestrial and aquatic ecosystems, and their interactions in a timely and standardised manner. Furthermore, RS data that capture traits have the capacity to establish a correlation between the sensitivity of the analysed environmental unit and various globally relevant pressures, including climate change and LUI with its socio-ecological consequences [64]. In addition, novel indicators for quantifying urban LUI have already been developed using RS and the trait approach [65,66]. Yet, to ensure the comparability of data and derived A-LUI indicators at both local and global scales, it is crucial to develop standardised methods for data collection and analysis. In recent years, there has been an increasing focus at the international level on the establishment of measurement standards. International organisations such as the Food and Agriculture Organisation of the United Nations (FAO) and the Intergovernmental Panel on Climate Change (IPCC) promote the establishment of international standards for the measurement and assessment of agricultural intensification across local and global scales. These organisations are increasingly recognising the value of RS and incorporating RS-based indicators into their standards and guidelines.

Nevertheless, the full potential of RS for the development of A-LUI indicators remains to be unlocked. In order to understand RS-based A-LUI indicators, derive new ones, and assess the suitability of different RS techniques for developing and categorising new indicators, we first need to define and structure these indicators and discuss them in context. We still lack a compendium offering a comprehensive overview of A-LUI indicators that can be derived using RS, so the objectives of this paper are as follows: (I) to define and compile standardised indicators for monitoring A-LUI at national, European, and global levels (FAO, OECD, World Bank, EUROSTAT); (II) to review and synthesise in situ methods for assessing A-LUI; (III) to introduce an RS-based definition of A-LUI by structuring them into five indicator categories: trait, genesis, structural, taxonomic, and functional A-LUI indicators; (IV) to illustrate the operationalisation of this taxonomy through numerous RS-based examples; (V) to link management practices, traits, and RS proxies to A-LUI indicators, validation strategies, and policy relevance; and (VI) finally to present innovative approaches for quantifying and evaluating A-LUI using RS.

2. Definition, Standards, and Programmes for Monitoring the A-LUI

2.1. Definition of A-LUI

Despite the significance of quantifying the A-LUI, the definition remains elusive, as the monitoring of anthropogenic changes and pressures/impacts on agricultural ecosystems/landscapes is a complex and multidimensional phenomenon [67] that is challenging to quantify [33,68]. As Diogo et al. [69] emphasise, the direction of change (positive or negative) of the A-LUI is also difficult to assess, as it depends on highly context- and scale-dependent processes that vary regionally, which have direct and indirect effects on the whole system and can mutually influence each other (increase or decrease). Conversely, the utilisation of inadequate (one-dimensional) indicators to quantify the A-LUI has been observed [70]. This is primarily due to the restricted availability of readily available local in situ data, such as pesticide, fertiliser, or machinery use, often due to data protection constraints and being frequently available only in aggregated form within reports. (1) The FAO reference does not define “intensity” (the term is not even used). It describes datasets but is not about their interpretation. (2) Limiting A-LUI to only the use of inputs is too narrow, particularly in the context of RS. Landscape simplification is another aspect of intensification, and it can actually be well captured by RS. Therefore, we refer to Diogo et al. [69] for an important indicator of A-LUI, which includes the main indicators of management intensity, landscape structure, and agricultural productivity.

2.2. Programmes for Monitoring A-LUI at National, European and Global Scale

One of the main challenges in monitoring A-LUI is the need to standardise measurement methods and indicators. In order to achieve national and international comparability in the monitoring of A-LUI, standardised programmes and indicators for the monitoring of A-LUI have been introduced at the national (Germany), European, and global level. The most important programmes and responsibilities for the monitoring of agricultural LCI for Germany, Europe, and the world are listed below.

National scale

Land Register: The land register records the types of land and their use in Germany. It is maintained by the state surveying and land registry offices. Most countries have detailed land register records of land type and ownership, maintained by the state surveying and land registry offices.

Agricultural Structure Survey: Regular surveys of agricultural land use, yields, livestock, etc., by National Statistical Offices.

IACS (Integrated Administration and Control System for Management Aid): In agriculture, the IACS system plays a central role in monitoring and managing data such as information on the use of plant protection products, fertiliser data, soil and water data, and yield and production data, as well as environmental and health data. The monitoring and control of IACS data in agriculture is carried out by different institutions and authorities, mainly at regional, national, and European level.

Europe

Corine: The European Environment Agency (EEA) coordinates various land use monitoring projects, including the production of Corine Land Cover maps.
LUCAS (Land Use/Cover Area Frame Survey): This is a regular statistical survey of land use and land cover in the EU.
Copernicus data: Copernicus is the European Earth Observation Programme (ESA) and provides extensive data on land use from satellite data (Sentinel-1-3).
Farm structure survey datasets (https://ec.europa.eu/eurostat/statistics-explained/index.php?title=Glossary:Farm_structure_survey_(FSS) accessed on 19 October 2025)
Agricultural census data (e.g., production, environmental indicators) at national levels and at sub-national levels (NUTS 1, NUTS 2, NUTS3). https://ec.europa.eu/eurostat/web/agriculture/information-data#Agricultural%20production accessed on 19 October 2025.

World

Global Land Cover (GLC): Several international initiatives produce global land cover maps, including projects supported by FAO and the United Nations Environment Programme (UNEP).
MODIS (Moderate Resolution Imaging Spectroradiometer): An instrument on NASA's Terra and Aqua satellites that provides global data on land cover and land use change.
Global Land Analysis and Discovery (GLAD): A University of Maryland project to monitor global land use using high-resolution satellite imagery.
FAO (Food and Agriculture Organisation of the United Nations), OECD (Organisation for Economic Co-operation and Development), and World Bank (World Bank) use indicators to monitor A-LUI worldwide.

Table A1 provides an overview of the main agricultural land use intensity (A-LUI) indicators reported by major international organisations (FAO, OECD, World Bank, EUROSTAT). The indicators span input dimensions (e.g., fertiliser and pesticide use), output dimensions (e.g., crop yields), and structural aspects (e.g., land use statistics).

3. Approaches to Monitoring A-LUI

The monitoring of indicators to measure and assess A-LUI relies on both methods: in situ approaches provide detailed local information, while RS approaches, as physically based systems, capture status and change over large areas, though the underlying causes of change may differ. Therefore, coupling both approaches is essential. Traits represent the crucial connecting element between in situ and RS methods, as they can be directly measured in the field or indirectly derived from RS data. However, RS systems capture only a subset of traits—those with spectrally observable properties—which are, therefore, referred to as "spectral traits." Figure 1 illustrates how the trait approach helps to bridge the two methodologies and underlines the complementary role of in situ and RS data for a comprehensive assessment of A-LUI.

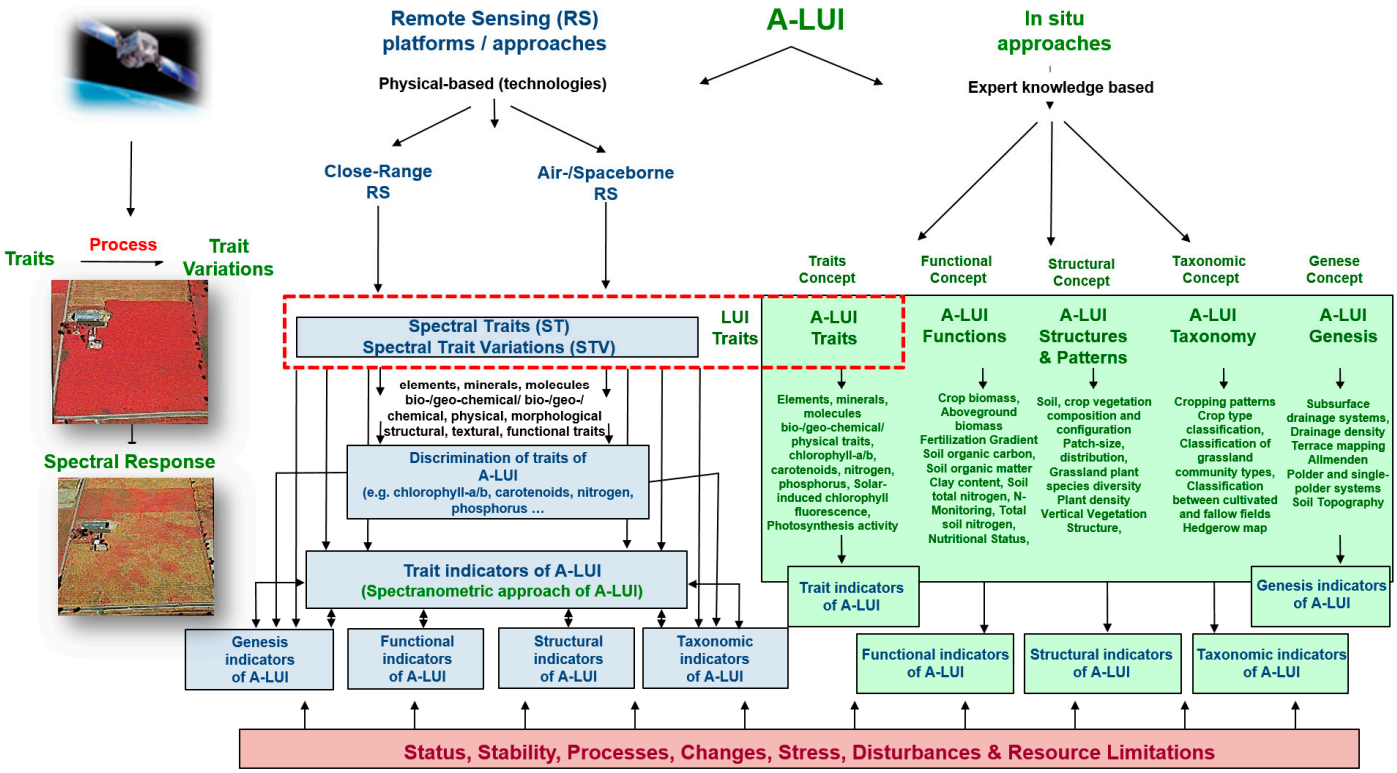

Figure 1. In situ and RS approaches and the five characteristics of A-LUI (trait indicators of A-LUI, genesis indicators of A-LUI, functional indicators of A-LUI, structural indicators of A-LUI, taxonomic indicators of A-LUI). Trait indicators of A-LUI are the most important link between in situ and RS monitoring approaches (modified after Lausch et al. [62]).

3.1. In Situ Approaches

The measurement and monitoring of land use intensity represent a pivotal facet of land use research, particularly in the context of sustainable resource utilisation and ecosystem conservation. In situ methods have been shown to be a valuable tool for the collection of detailed data and analysis of land use in different geographical and agricultural contexts.

The following observations were made during the course of field studies. One of the fundamental approaches to measuring land use intensity is through direct observation and measurement in situ. These methodological approaches provide direct insights into the environmental and agricultural conditions on the ground. (I) Direct field measurements entail detailed investigations at specific sites where scientists record land use patterns, plant species, soil conditions, and other relevant parameters. The methodology encompasses the measurement of plots, the collection of soil and plant samples, and the observation of agricultural practices. Direct measurements are imperative in order to generate accurate data on A-LUI and to understand the interactions between land use and environmental conditions. (II) Field mapping constitutes a complementary method in which researchers are tasked with the production of maps delineating land use types by traversing the study area on foot or by vehicle. The cartographic representations under consideration here were originally produced on paper or using early graphical systems. They provide a visual representation of the spatial distribution of land use. These data are of pivotal significance for subsequent analysis and interpretation of land use intensity.

Surveys and interviews: In addition to direct field measurements, surveys and interviews represent an integral component of the collection of land use intensity data, as they encompass the human and social aspects of land use. They also record information that

only the farmer will know, such as the type and quantity of pesticides and fertilisers used, etc. Structured interviews and surveys with landowners, farmers, and other land users can be used to collect information on land use practices, crop cycles, and irrigation methods. The collection of qualitative data facilitates the development of a more profound comprehension of the decision-making processes employed by land users, which are frequently influenced by economic, cultural, and political factors. Cultural and historical studies: The utilisation of cultural and historical studies is instrumental in facilitating a more profound comprehension of the historical evolution of land use patterns. The analysis of historical maps, archival records, and government reports provides valuable information on the long-term use and change in land areas and helps in understanding trends and shifts in land use.

The disciplines of analogue and digital cartography, as well as Geographic Information Systems (GIS), are discussed herein. The utilisation of mapping technologies and Geographic Information Systems (GIS) is of pivotal significance in the processes of recording and analysing land use intensity. These methodologies provide a comprehensive visual representation of the physical and agricultural traits of an area. Topographic maps: Topographic maps, produced by surveying, provide a basic representation of physical features such as contour lines, land cover, and infrastructure. These maps constitute a valuable source of data for the spatial analysis of land use. Aerial mapping: Prior to the advent of contemporary satellite technologies, aerial photographs were captured from aircraft and utilised to generate detailed cartographic representations. The interpretation of these images, frequently facilitated by the use of stereoscopes for three-dimensional viewing, enable a precise analysis of land use patterns and changes. The third point of the categorisation is Geographical Information Systems (GIS) and vector data. Geographic Information Systems (GIS) utilise vector data to display and analyse geo-referenced information on land use types and distributions. These systems facilitate sophisticated spatial analysis and monitoring of A-LUI indicators at local, national, and global levels.

The collection and analysis of agricultural yield data, as well as the maintenance of administrative records: The analysis of land use intensity is facilitated by quantitative and administrative information, which is provided by agricultural yield data and legal documents. Yield measurements: Yield data, frequently supplied by local or national agricultural authorities, offer insights into the productivity and utilisation of agricultural land. This information is indispensable for drawing conclusions on the intensity and efficiency of land use. Cadastral data: Cadastral data, encompassing land registry records and associated legal documentation, contains information pertaining to land ownership, delineated parcel boundaries and land use rights. These data are of crucial importance for the comprehension of formal land use patterns and their legal framework. IACS data: The IACS system occupies a pivotal position in the aggregation and administration of agricultural data within the European Union. The database under consideration encompasses a wide range of data, including, but not limited to, information pertaining to plant protection products; fertilisers; soil and water data; yield data; and production data. The systematised nature of these data facilitates the monitoring and evaluation of A-LUI.

Phenotyping laboratories: Contemporary phenotyping laboratories (e.g., Danforth Plant Science Centre, USA; IPK Gatersleben, Germany; JPPC, Germany; International Plant Phenotyping Network) utilise technologies such as automated imaging, sensors, drones, and robots to collect substantial data on plant growth, developmental disorders, soil, climate, and their interactions under laboratory conditions. This high-throughput phenotyping approach enables researchers to analyse numerous plants expeditiously and efficiently. Phenotyping laboratories are of significant importance in the context of A-LUI monitoring, as they facilitate the analysis and comprehension of the repercussions that intensive agricultural practices have on both plants and soils. This analysis encompasses

the assessment of the impact on plants, including the enhancement of yield and the cultivation of stress resistance, as well as the investigation of the sustainability of land use, encompassing issues such as soil degradation. The following aspects should be monitored: erosion and nutrient depletion; resource efficiency (reduced fertiliser use, water-saving irrigation techniques); biodiversity and ecosystem services (monitoring the genetic diversity of crops and analysing their interaction with the environment (changes in genotype, phenotype, epigenetics)). Phenotyping laboratories are particularly well-suited to the testing and development of new sensor systems in a range of realistic and controlled cultivation scenarios (e.g., the FLuorescence EXplorer (FLEX) [71]. The testing of sensor prototypes on different plant species under controlled conditions, such as varying light conditions, temperature, and humidity, is a further method of evaluation. For instance, the RS-based indicator of solar-induced chlorophyll fluorescence (SIF) has been the subject of study in phenotyping laboratories, with a focus on monitoring plant stress [72]. Moreover, these data are imperative for the validation of novel sensors and the assessment of their measurement accuracy and efficiency.

The implementation of in situ A-LUI monitoring techniques frequently necessitates a considerable investment of labour, often resulting in protracted monitoring processes. These methodologies are further constrained to specific geographical areas and temporal frames. Nevertheless, they furnish significant insights into land use and A-LUI, derived from highly accurate local information. These methodologies form the foundation for contemporary, technologically advanced RS technology and data analysis techniques. It is, therefore, evident that the combination of in situ and RS approaches is imperative for effective A-LUI monitoring.

3.2. RS Approach

3.2.1. Principles of Monitoring A-LUI Using RS

All RS technologies are non-contact and detect traits and trait variations in land cover from a few millimetres (close range) to thousands (air-spaceborne) of kilometres (see Figure 2) away. RS sensors are integrated on various RS platforms such as wireless sensor networks (WSN), laboratory and field platforms, lysimeters (soil), phenocameras, masts, drones, balloons, as well as air- and spaceborne platforms. Different RS technologies (RGB/photographic, multispectral, hyperspectral, TIR, laser, radio/RADAR, and LiDAR) are often used in combination on many platforms. As traits and trait variations exist locally and globally, RS allows objective and continuous monitoring and derivation of standardised A-LUI indicators from a local to global scale.

The collection of indicators that quantify A-LUI is a crucial RS application that began with the availability of spaceborne RS data in the 1970s [73]. The focus here was on land cover monitoring, LULC and crop classifications, land use change [73,74], and the determination of basic functional vegetation traits using indicators such as NDVI [75]. The free availability and opening up of RS missions (such as Landsat [76], the Copernicus missions [77], or the hyperspectral mission (EnMAP [42])) accelerated the use and development of further RS-based A-LUI indicators. RS approaches are certainly ideal for deriving A-LUI indicators, as RS is based on the following basic principle: RS captures traits and trait variations directly or indirectly in plants, vegetation diversity, geodiversity, geomorphology, terrain, and water diversity. The spectral reflectance and absorption of pixels are, thus, the result of interactions between light (the atmosphere), phylogenetic/genetic, biophysical, biochemical, physical, morphological, physiological, phenotypic, structural, taxonomic, and functional characteristics of the recorded traits of vegetation diversity, geodiversity [12,78], and anthropogenic changes and disturbances by A-LUI. RS-based monitoring can, thus, capture indicators of A-LUI, as A-LUI is subject to complex and multidi-

mensional influences, which are characterised by the interaction of abiotic–biotic compartments and anthropogenic factors (e.g., pesticide use, fertilisation, management) and their interactions.

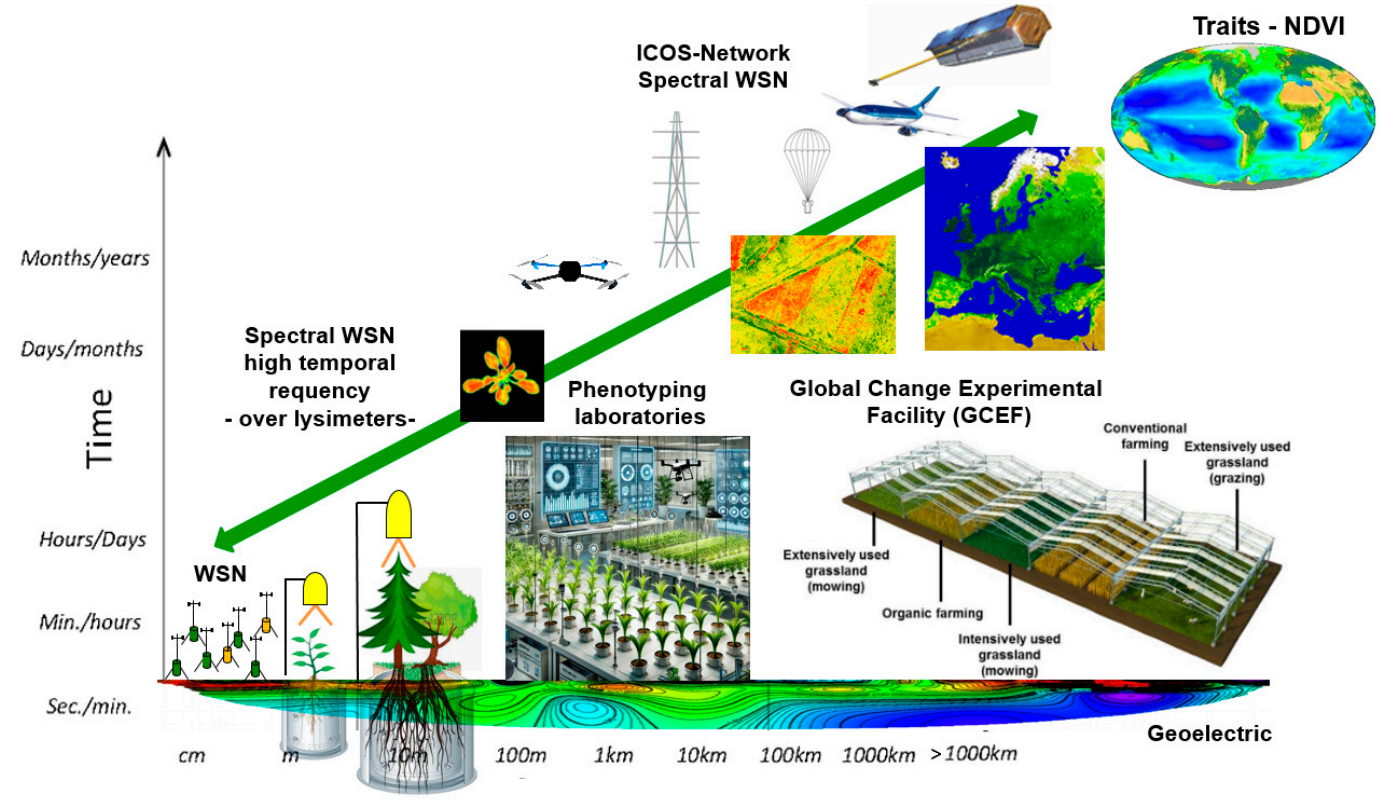

Figure 2. Different RS platforms; wireless sensor networks (WSN); WSN over lysimeters, phenotyping laboratories, global change experimental facility (GCEF), drones, towers, balloons, airborne- and spaceborne RS platforms with different RS technologies (RGB/photography, multispectral, hyperspectral, thermal, laser, RADAR, acoustic, and LiDAR) to monitor indicators of land use intensity on different spatial and temporal scales (modified from Lausch et al. [63]).

3.2.2. Challenges of Monitoring A-LUI Using RS

The recording of A-LUI through RS brings numerous advantages but also specific challenges associated with the particularities of agricultural practices and sensor characteristics (spectral, spatial, temporal). For example, Maudet et al. [79] clearly emphasised in a comparative study that there are significant differences between in situ indicators and land use data derived from RS. They demonstrated that land cover maps based on RS are not a reliable indicator of management intensity at the field level, as the classifications of these maps do not adequately capture the A-LUI caused by agricultural practices. In addition, the landscape structure described by the area diversity varies significantly depending on the classification systems used. These differences strongly depend on the number of intensity classes considered, which we analysed with regard to the sensitivity of a target variable [79]. The following challenges exist when deriving A-LUI from RS data:

(1) Limited coverage of agricultural practices

RS can identify different agricultural crops, but differentiating between intensive and extensive cultivation (e.g., conventional vs. organic farming, monocultures vs. crop rotation) is still a challenge. Spectral indices such as the NDVI only provide information on vegetation density and health but not direct information on the intensity of use, such as

the use of fertilisers, pesticides, or irrigation systems. In order to record the use of fertilisers, pesticides, or irrigation systems using RS, which is often performed using indirect indicators or a set of indicators

Recording management practices: The way agricultural land is managed, such as the frequency of ploughing, crop rotation, or the use of agrochemicals, is crucial for A-LUI. These management practices can only be derived from RS data with a high geometric resolution (<1 m).

(2) Seasonal dynamics

Agricultural areas go through different phases within a year (sowing, growth, harvest, fallow), which lead to significant changes in the vegetation. These seasonal variations can lead to misjudgements of the A-LUI if sufficient high-resolution, temporally dense data is not available. The challenge is to distinguish between natural seasonal variations and actual intensity changes. Multiple harvests: In regions with several harvests per year (e.g., in tropical areas), repeated RS images are required to correctly record the number and intensity of harvests. However, the temporal coverage of satellite images is often insufficient to fully document such multiple harvests. The use of RADAR data (Sentinel-1) in combination with optical RS data is expedient here, as they are recorded independently of cloud cover and at a high temporal density.

(3) Irrigation and water management

Irrigation is a central factor of A-LUI, but the detection of irrigation systems is only indirectly possible through RS, e.g., by quantifying soil moisture or vegetation health. Especially in regions with periodic rainfall, it is difficult to distinguish between naturally occurring moisture changes and human-induced irrigation. Recognising water stress: RS can indicate the condition of vegetation, but it is often difficult to distinguish between natural causes (e.g., drought, inadequate soil properties) and the effect of intensive irrigation practices or water stress.

(4) Fertiliser and pesticide use

The use of fertilisers and pesticides is a key factor in the intensity of agricultural production, but these inputs are virtually invisible to RS. While it is possible to infer the impact of these inputs on vegetation health (e.g., via spectral indices), there is no direct evidence of the amount or type of chemicals used.

Long-term soil degradation: Intensive use of fertilisers can have long-term effects on the soil, such as salinisation or nutrient depletion, but these are difficult to detect by RS. These effects are not directly reflected in the vegetation indices.

(5) Small-scale agricultural structures

In many parts of the world, particularly in developing countries, agriculture is small-scale and heterogeneous. Small farmers often cultivate very small plots of land with different utilisation intensities. As a result, there are numerous problems with the demarcation of field boundaries using RS. For example, different plant species or land use types can have similar spectral signatures, which makes differentiation difficult. Furthermore, natural field boundaries are often not sharp, e.g., due to transition zones or hedges, which makes precise demarcation difficult. The spatial resolution of many RS data is often not sufficient to reliably capture these small-scale differences. High-resolution RS data (<1 m) is required here, but this is often expensive or not regularly available. For example, Landsat or Sentinel-2 data cannot be used to determine roads, field paths, or small structures [80], which is crucial for deriving field structures. Furthermore, Figure 3 shows the problems of the spatial resolution of RS data in the detection of crop vegetation using the example of an oilseed rape plant, which was recorded at different flight altitudes (1–80 m). There are currently only a few RS-based sensors that are freely available and can quantify high-resolution landscape structures and patterns (e.g., detection of agricultural utilisation boundaries, small structures) with sufficient spatial accuracy (see Table A2). In order

to record the small-scale nature and utilisation structure, aerial image data (spatial resolution of 20 cm) is, therefore, repeatedly used, which is subsequently recorded vectorially and/or manually [81–84].

(6) Agroforestry and mixed cropping:

In agroforestry systems or mixed cropping, it is difficult to derive the intensity of agricultural use from RS, as the different plant species are intertwined and are often grown under trees. Tree canopies can obscure the underplanting, so that important information about the agricultural intensity is lost.

(7) Limited spectral information of RS data

While standard satellite sensors such as Landsat or Sentinel provide useful spectral information, these are often insufficient to capture subtle differences in the type and intensity of agricultural use. Hyperspectral RS sensors (e.g., EnMAP, DESIS) could provide more detailed information, but in many cases they are not widely available and their spatial resolution is limited to at least 30 × 30 m. Vegetation indices are often insufficient: spectral indices such as the NDVI can capture general biomass and vegetation health, but they do not provide detailed information on the intensity of agricultural activities (e.g., distinction between intensive and extensive cultivation).

(8) Climatic and topographical influences

Weather events such as drought or flooding influence vegetation development and can make it difficult to separate differences in A-LUI from natural or climate-related influences. Topography and land cover: In hilly or mountainous regions and in areas with widely varying land cover (e.g., grassland and arable land next to each other), RS data may have difficulty providing accurate A-LUI data, as topography or shading may affect the quality of the data.

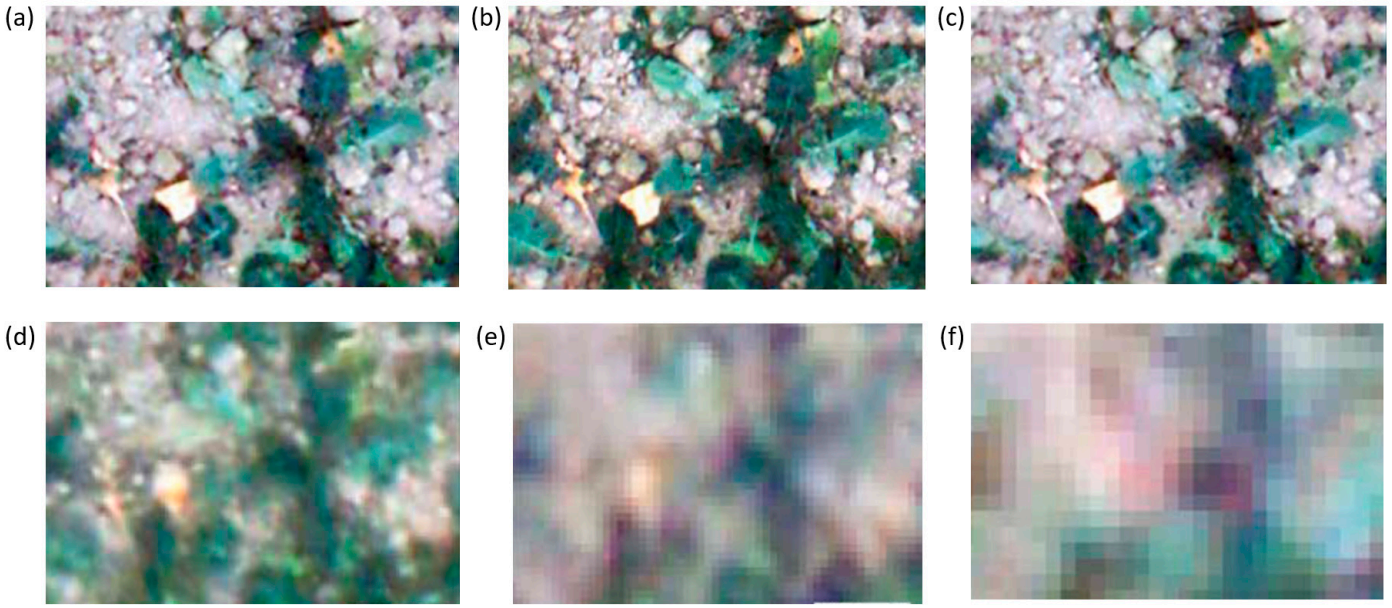

Figure 3. Problems of spatial resolution of RS data in the detection of crop vegetation. (**a**) Image of a rapeseed plant at a flight altitude of 1 m with a ground resolution of 0.6 mm per pixel. (**b**) Image of a rapeseed plant at a flight altitude of 5 m with a ground resolution of 1.5 mm per pixel. (**c**) Image of a rapeseed plant at a flight altitude of 10 m with a ground resolution of 2.5 mm per pixel. (**d**) Image of a rapeseed plant at a flight altitude of 20 m with a ground resolution of 5 mm per pixel. (**e**) Image of a rapeseed plant at a flight altitude of 40 m with a ground resolution of 10 mm per pixel. (**f**) Image of a rapeseed plant at a flight altitude of 80 m with a ground resolution of 20 mm per pixel (from Grenzdörffer [85]).

Table A3 provides a bridging overview that assigns each major challenge to one or more A-LUI definitions (trait, genesis, structural, taxonomic, functional) and lists potential RS- and AI-based solutions. This connection illustrates how the proposed framework can serve as a structured response to the practical difficulties of monitoring A-LUI with RS.

3.2.3. Separating A-LUI Indicators from Productivity and Spectral Signals

A key conceptual challenge in monitoring A-LUI with RS is the risk of conflating management intensity with signals of productivity potential or land cover change. High crop yields, for example, may result from intensive management (e.g., irrigation, fertilisation), but they may also reflect favourable soil and climate conditions. Similarly, RS-based indicators can inadvertently capture land cover conversion (e.g., expansion or abandonment) rather than intensity per se. To address this, we distinguish three components (Figure 4):

1. Management intensity signals—captured by traits and functional indicators (e.g., leaf nitrogen content, irrigation proxies, yield per unit input).
2. Biophysical potential signals—separated through normalisation with soil and climate data (e.g., adjusting NDVI or yield proxies for rainfall and soil fertility), or through modelling and domain adaptation approaches.
3. Land cover change dynamics—treated as a separate dimension under genesis indicators, where RS time series are used to track expansion, abandonment, or rotations.

Explicitly separating these dimensions can help avoid misinterpretations and ensure conceptual clarity and operational robustness.

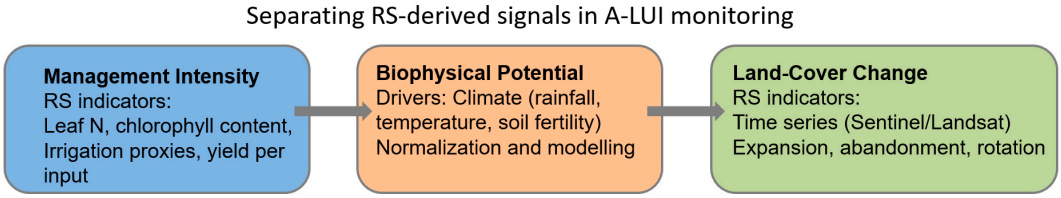

Figure 4. RS indicators capture management intensity (e.g., fertilisation, irrigation), while biophysical potential (climate, soil) is accounted for through normalisation and modelling. Land cover change dynamics are treated separately via RS time series to avoid conflating intensity with productivity or conversion signals.

4. Definition of A-LUI Using RS

In order to understand RS-based A-LUI indicators, to derive new ones and to understand the suitability of different RS technologies with regard to the development and categorisation of new indicators, a definition of A-LUI using RS data is required. A-LUI can be defined through RS as the combined expression of five complementary dimensions: trait, genesis, structural, taxonomic, and functional indicators (see Figures 5 and A1).

(I) *Trait Indicators of A-LUI:* "Trait indicators describe measurable biophysical and biochemical properties of plants, soils, or water that respond directly to management intensity". Examples using RS include leaf chlorophyll or nitrogen content derived from hyperspectral sensors (e.g., EnMAP, Sentinel-2 red-edge indices), leaf area index (LAI), or biomass estimated from multispectral vegetation indices such as NDVI or EVI, water stress, or photosynthetic activity monitored through solar-induced chlorophyll fluorescence (SIF) from the FLEX mission.

(II) *Genesis Indicators of A-LUI:* "Genesis indicators capture the temporal development and history of agricultural management practices, i.e., how intensity evolves over time".

Examples using RS include detect crop rotations, tillage events, or multiple harvests (Sentinel-1/2 time series); long-term Landsat archives documenting intensification trends such as the expansion of irrigated areas or the transition to monocultures.

(III) *Structural Indicators of A-LUI:* "Structural indicators describe the spatial configuration and arrangement of agricultural land, including field geometry and landscape elements". Examples using RS include field size and shape derived from high-resolution optical imagery (e.g., PlanetScope); hedgerows and boundary elements identified through LiDAR or UAV mapping; landscape diversity indices (e.g., number of crop types per hectare) based on classified RS data.

(IV) *Taxonomic Indicators of A-LUI:* "Taxonomic indicators refer to the diversity and composition of crop species or land use types within an agricultural landscape". Examples using RS include crop type classification using spectral signatures (e.g., distinguishing wheat vs. maize with Sentinel-2); detection of mixed cropping or agroforestry systems with hyperspectral UAV imagery; regional crop mapping from multi-temporal Sentinel-2 and Landsat data.

(V) *Functional Indicators of A-LUI:* "Functional indicators represent the ecological processes and services affected by agricultural intensity". Examples using RS include crop productivity (e.g., yield estimates per hectare) derived from vegetation indices and biomass models; soil moisture inferred from radar backscatter (Sentinel-1) as a proxy for irrigation intensity; carbon sequestration potential or emission estimates based on biomass and soil models combined with RS observations.

To provide a detailed understanding of these five key dimensions of A-LUI indicators, Sections 4.1–4.5 elaborate on each category individually, namely trait, genesis, structural, taxonomic, and functional indicators, illustrating their derivation and application using RS approaches.

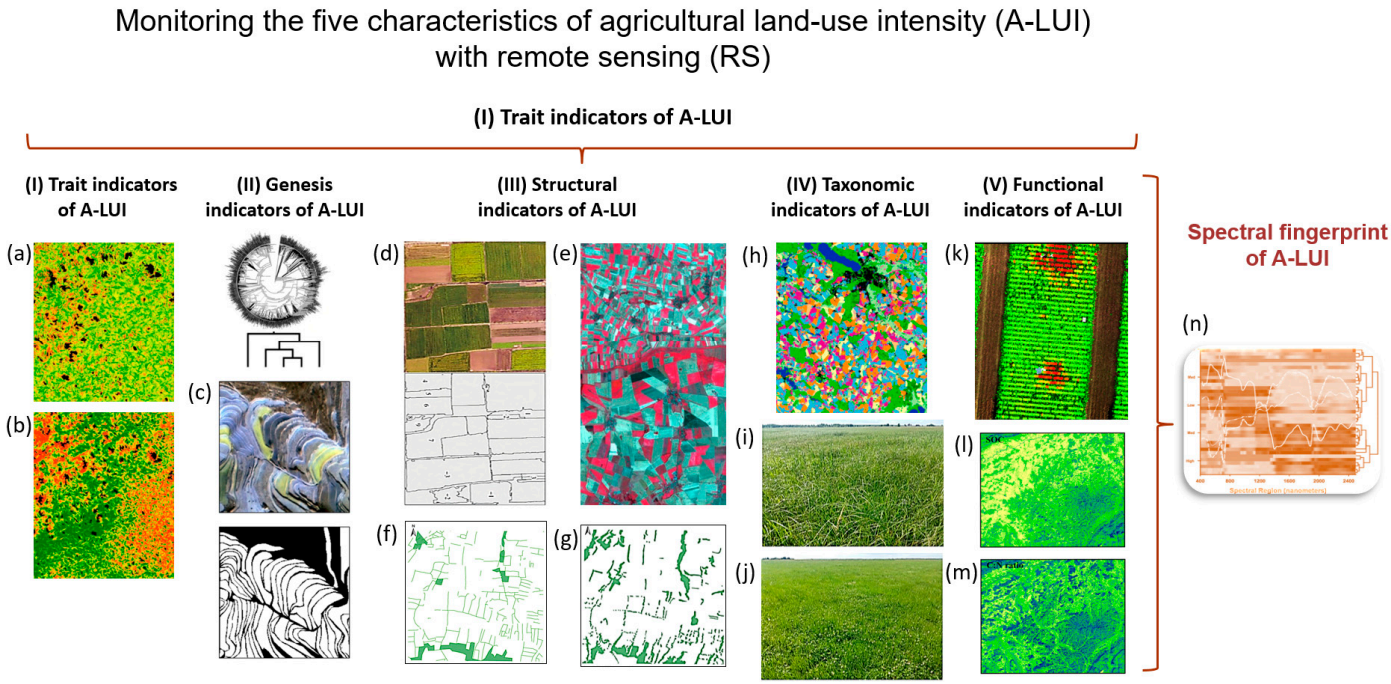

Figure 5. RS monitoring of the five characteristics of A-LUI: (I) the trait indicators of A-LUI, (II) the genesis indicators of A-LUI, (III) the structural indicators of A-LUI, (IV) the taxonomic indicators of A-LUI, and (V) the functional indicators of A-LUI. (**a**) Chlorophyll value; (**b**) phosphorus value (from Picado and Romero [86]); (**c**) terrace detection (from Yu et al. [87]); (**d**) perimeter boundaries of farmland blocks (from Wang et al. [88]); (**e**) shape, size, and small-scale nature of the border between Saxony-Anhalt and Lower Saxony; (**f**) hedgerow map classifications from an aerial

photography and (**g**) TerraSAR-X image (from Betbeder et al. [89]); (**h**) wall-to-wall crop type mapping using the benchmark 10-day interval composite of Landsat and Sentinel-2 time series (from Griffiths et al. [90]), types of grassland management intensity: (**i**) extensive, (**j**) intensive (from Bartold et al. [91]); (**k**) disease severity prediction in sugar beet using UAV multispectral data (from Günder et al. [92]); (**l**) mean SOC content and (**m**) C:N ratio maps predicted with Sentinel-1, Sentinel-2 and Landsat-8 data (from Zhou et al. [93]), (**n**) the spectral fingerprint of A-LUI can be determined using spectral RS data.

4.1. Monitoring the Trait Indicators of A-LUI Using RS

The recording and monitoring of traits form the basis for monitoring the genetic, taxonomic, structural, and functional A-LUI indicators using RS [94,95]. The monitoring of traits and trait variations (vegetation, soil, geomorphology, water) is, therefore, an essential basis for the assessment and management of A-LUI using RS. Traits are plant, soil, and hydrological properties that represent indicators of agricultural processes and their intensity. The targeted monitoring of such traits makes it possible to use resource inputs such as fertilisers, water, and pesticides more efficiently and, thus, make agricultural production more sustainable. The A-LUI traits refer directly to the extent of technological progress, the precision of the control of the resources used, and increases in efficiency in agriculture. The more precisely plant- and soil-related traits such as growth, yield, resistance to stress factors, or nutrient uptake can be monitored, the more effectively land use intensity can be controlled and optimised. Table A4 contains numerous examples, sensors, and references.

4.1.1. Trait Indicators of A-LUI—Spectranometric Approach

A particularly suitable approach for recording A-LUI is the spectranometric approach according to Greg Asner [95]. This method utilises, e.g., hyperspectral and multispectral RS data, which enables a detailed and direct recording of biochemical and structural characteristics of the vegetation (see Figure 6). The approach is characterised by several specific strengths: The method allows a detailed biochemical, structural, and functional characterisation of vegetation traits. Chemical characteristics such as nitrogen and chlorophyll content as well as concentrations of lignin, cellulose, and water content are precisely quantified using RS. As intensive agricultural use is typically associated with increased use of nitrogen fertilisers and pesticides, the resulting biochemical changes in the vegetation can be precisely recorded and spatially mapped. The hyperspectral approach allows precise quantification of plant structural characteristics such as leaf area index (LAI), leaf angle distribution, plant height, and biomass. These parameters are directly dependent on the type and intensity of cultivation, so that direct conclusions can be drawn about the intensity of land use. This method monitors the early detection of functional characteristics such as plant stress, for example, caused by water scarcity, over-fertilisation, or pest infestation. The detailed spectral signatures make stress symptoms visible at an early stage so that management decisions can be adapted and optimised in good time. By using hyperspectral RS technologies, which capture hundreds of narrow spectral bands, changes in plant physiology and soil can be measured and quantified in a differentiated manner. This allows a precise characterisation of the intensity of use at both field and landscape level. Finally, the spectranometric approach integrates hyperspectral data with ecological and agronomic models as well as satellite data from missions such as FLEX or Sentinel-3, enabling validated, precise, and in-depth statements about vegetation processes and the intensity of land use. The scientific significance of Greg Asner's approach lies particularly in making complex ecological relationships such as biodiversity, carbon storage, and the effects of human activities on ecosystems comprehensible in detail. In the

agricultural context, this enables a better understanding of sustainability and the ecological effects of different land use strategies. To summarise, the spectranometric approach offers a comprehensive, high-resolution, and differentiated method for the precise recording of A-LUI and, thus, represents an important basis for sustainable agricultural practices. Specific examples of monitoring the trait A-LUI indicators are as follows.

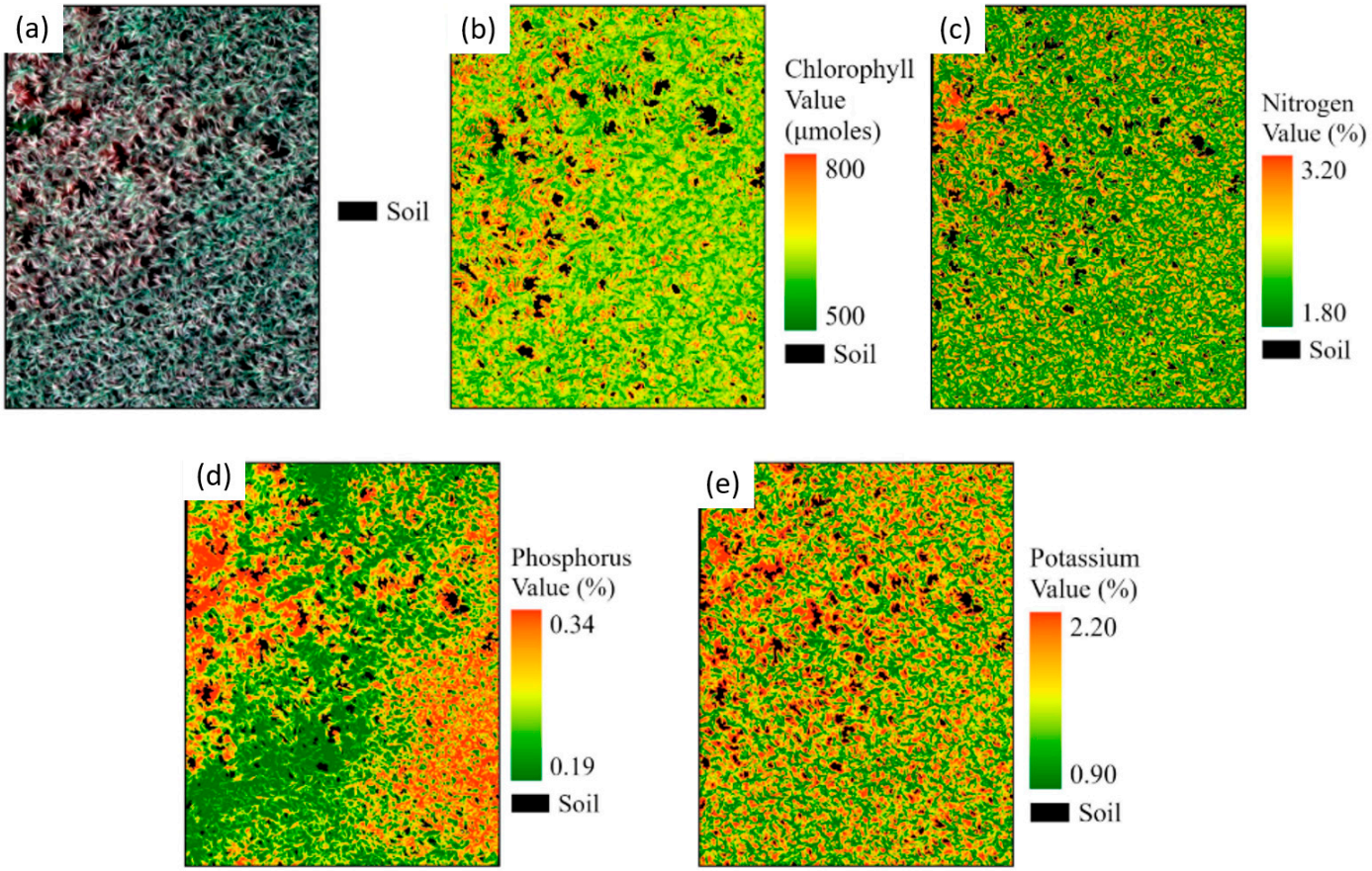

Figure 6. Mapping spatial nutritional variability of (**a**) sugarcane, (**b**) foliar chlorophyll, (**c**) foliar nitrogen, (**d**) phosphorus, (**e**) potassium concentrations using a MicaSense RedEdge-P camera attached to a drone and LiDAR data (from Picado and Romero [86]).

4.1.2. Trait Indicators of A-LUI—Chlorophyll Content

The measurement of chlorophyll content (Cab) using RS technology is of central importance, as this parameter is closely correlated with photosynthetic performance and, thus, plant vitality and productivity [96]. Chlorophyll serves as an effective indicator of A-LUI, as it reflects the influence of agricultural practices, fertiliser use, and plant health. Higher anthropogenic interventions, for example, through intensive fertilisation or the use of pesticides and precision agriculture, are directly reflected in changes in chlorophyll levels. An increased chlorophyll content often signals improved plant vitality, while stress factors such as drought, disease or nutrient deficiency can lead to a reduction in chlorophyll content. However, intensive management methods, including targeted plant protection measures, can partially compensate for such stress factors, which in turn results in more stable chlorophyll levels [96]. The importance of chlorophyll content arises from its role as an essential ecophysiological variable, which is closely linked to photosynthetic activity and, thus, to the vitality and productivity of plants [97]. In particular, the chlorophyll content provides information about nitrogen uptake and the general nutritional status of the vegetation. Plants in intensive farming show higher chlorophyll levels due to a

higher nitrogen supply, whereas extensive or less intensively farmed systems typically have lower chlorophyll concentrations [98].

Hyperspectral RS techniques, which are characterised by their high spectral resolution and sensitivity to biophysical parameters, are primarily used for RS of chlorophyll content [97] (see Figure 7). Current and future hyperspectral missions such as PRISMA [99], HISUI [100], SHALOM [101], CHIME [43], or EnMAP [42] and others enable the acquisition of detailed spectral signatures, which form the basis for a precise estimation of the chlorophyll content. The Copernicus Hyperspectral Imaging Mission (CHIME) of the European Space Agency (ESA) in particular, with a spatial resolution of 20 to 30 m and a temporal repetition cycle of around 10–12 days, opens up new perspectives for monitoring chlorophyll content in agricultural contexts [43,96]. There are two main traditional approaches to determine chlorophyll content by RS: empirical regression techniques and physically based modelling approaches. Empirical techniques usually use spectral indices calibrated to field measurements but often show site-specific and vegetation-dependent limited transferability [102]. Physically based models, on the other hand, which are based on radiative transfer models (RTMs), are more robust and transferable, but require complex calibration and are computationally intensive [98,103]. More recently, the hybrid approach has become established, which combines physical models with machine learning and, thus, unites the advantages of both methods: the robustness of physical models and the efficiency of machine learning methods. Especially in combination with active learning techniques, this approach shows promising results in chlorophyll estimation and other vegetation parameters [96,97]. Despite the progress, challenges remain, such as spectral saturation effects at high chlorophyll levels or interference from ground reflections in open vegetation stands. In addition, the relationship between chlorophyll and nitrogen content can vary from species to species, which makes it difficult to apply universal models [104]. Therefore, hybrid approaches combining physical and data-driven methods are currently the most promising way to improve chlorophyll estimation by RS and ensure more precise monitoring of plant condition and nitrogen uptake in agriculture.

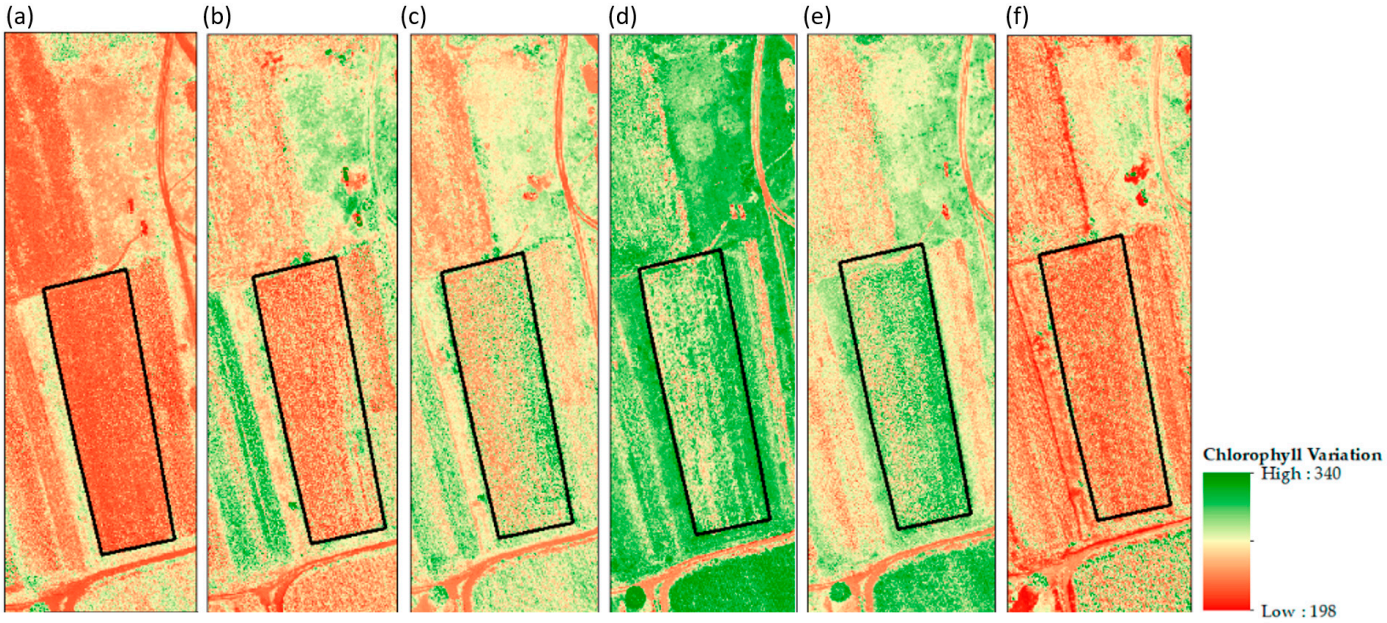

Figure 7. Spatial distribution of chlorophyll content over the maize field for vegetative stages based on UAV-MS data: (**a**) early vegetation, (**b**) mid vegetation, (**c**) late vegetation, (**d**) early reproductive, (**e**) mid reproductive, (**f**) late reproductive (from Brewer et al. [105]).

4.1.3. Trait Indicators of A-LUI—Chlorophyll Fluorescence

The Fluorescence Explorer (FLEX) sensor of the European Space Agency (ESA) [106] offers outstanding potential for the precise measurement of A-LUI (see Figure 8). By directly measuring solar-induced chlorophyll fluorescence (SIF), FLEX provides profound insights into the photosynthetic activity, vegetation health, and productivity of agricultural land [72,107]. The methodological suitability of FLEX for the assessment of A-LUI is based on several crucial factors: Firstly, FLEX directly measures photosynthetic activity, as SIF directly correlates with the photosynthetic rate of vegetation. Intensively used agricultural areas, characterised by increased use of fertilisers, irrigation, and pesticides, typically have higher fluorescence values, making FLEX a reliable tool for assessing A-LUI [72]. Secondly, the FLEX sensor allows early detection of plant stress, for example, caused by drought, nutrient deficiency, or over-fertilisation [108]. This early detection makes it possible to initiate targeted management measures before visible damage or significant yield losses occur [72]. Thirdly, with the FLORIS instrument (Fluorescence Imaging Spectrometer), FLEX has a high spectral and spatial resolution, which means that subtle differences in photosynthetic performance between intensively farmed areas can be precisely recorded. The spatial resolution of around 300 m allows detailed analyses and differentiated interpretations of land use intensity at a regional level [106]. Another methodological advantage is the integration of FLEX with Sentinel-3 satellite data. The synergetic use of optical and thermal sensors significantly improves the accuracy of deriving vegetation-relevant parameters such as leaf area index (LAI) and chlorophyll content. These parameters are essential for the comprehensive assessment of vegetation health and enable a differentiated assessment of agricultural utilisation intensity [107]. In addition, FLEX contributes significantly to the quantification of plant carbon sequestration, as SIF is closely linked to carbon uptake and, thus, to the global carbon cycle. This information is not only relevant for agricultural issues but also provides important insights for global climate modelling and sustainable development concepts [109].

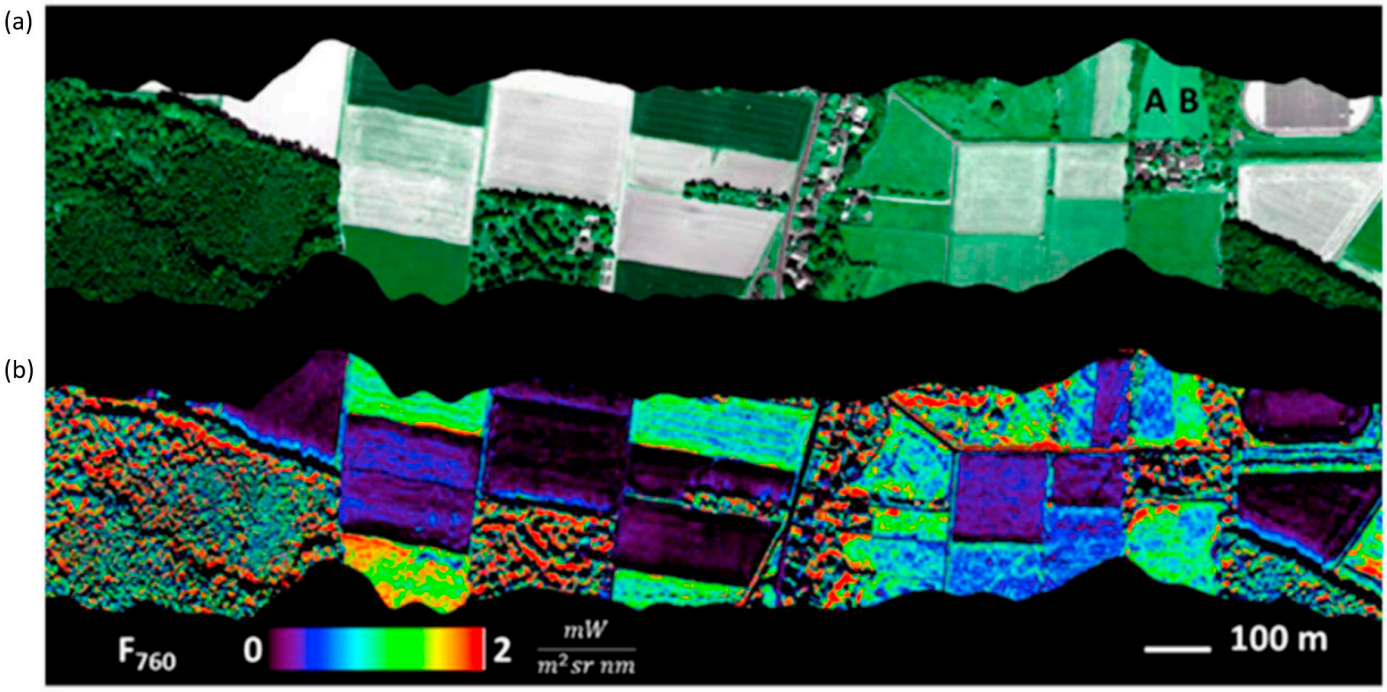

Figure 8. (**a**) Reflectance and (**b**) canopy SIF maps obtained with the HyPlant airborne sensor over an agricultural research site in Klein Altendorf, Germany. Lower SIF is evident in forests (left in

lower panel) and higher SIF in dense agricultural fields (middle and right in lower panel). Fluorescence emission reveals information on vegetation status which is not visible in the reflectance domain. For example, the two fields denoted as a and b display almost identical reflectance (**b**), whereas their fluorescence emission is very different (**a**,**b**) (from Mohammed et al. [72]).

4.1.4. Trait Indicators of A-LUI—Leaf Nitrogen Content

The monitoring of leaf nitrogen (leaf nitrogen, LN; leaf nitrogen content, LNC) as an indicator of A-LUI, provides important insights into the relationship between agricultural practices and plant physiology. Leaf nitrogen is an essential component of plant protein metabolism and plays a central role in photosynthesis. Intensively farmed agricultural areas, which are often characterised by increased use of fertilisers, generally have higher leaf nitrogen concentrations. This increased nitrogen availability promotes plant growth and increases productivity. A study by Dong et al. [110] emphasises that the allocation of nitrogen in leaf structures, especially in cell walls, increases with leaf mass per area (LMA), which indicates the importance of structural and metabolic components of leaf nitrogen. The intensity of land use influences not only the leaf nitrogen content but also the biodiversity of agroecosystems.

RS technologies have proven to be effective tools to measure LNC non-invasively and over large areas. There are a number of review studies on the detection of leaf nitrogen using RS technologies on different platforms [111–117]. Hyperspectral RS captures reflectance spectra of vegetation over a broad wavelength spectrum, which enables detailed analysis of leaf biochemistry. A study by Berger et al. [98] developed a hybrid method for estimating the aboveground nitrogen content of plants that combines physically based models with machine learning. This method identified specific wavelengths in the shortwave infrared (SWIR) range that are particularly relevant for nitrogen detection [98]. The use of hyperspectral RS technology opens up enormous potential for detecting the biochemical constitution of plant traits like the leaf nutrient content. For example, studies use hyperspectral technologies (such as EnMap [118] or Prisma [119]) to record the leaf nitrogen content. The use of UAVs RS technologies [120] in combination with advanced machine learning algorithms has increased the precision of LNC estimation. Zhang et al. [121] developed a self-supervised spectral–spatial transformer network using UAV imagery to accurately predict the nitrogen status of wheat fields. This model achieved high accuracy (0.96) and showed good generalisability for nitrogen status estimation [121]. Vegetation indices, such as the Normalised Difference Vegetation Index (NDVI), have traditionally been used to estimate LNC. However, more recent studies have developed more specific indices that are more sensitive to nitrogen variation. A study on estimating leaf nitrogen content in rice using vegetation indices emphasised the role of UAV-based RS in accurately determining nitrogen status at the field level [122]. The combination of different RS platforms, such as satellite imagery and UAVs, enables scalable and flexible monitoring of LNC. A comprehensive analysis of RS monitoring of nitrogen levels in rice and wheat crops over the last 20 years highlighted the importance of integrating different platforms to improve the accuracy and efficiency of nitrogen monitoring [111]. Traditional RS methods to determine leaf nitrogen (leaf N) content are usually based on indirect indicators, such as vegetation indices or chlorophyll-a+-b (Cab) content. However, these approaches reach their limits as the relationship between Cab and leaf N saturates at higher values and they are not very sensitive to early nutrient deficiency. A study by Y. Wang et al. [120] used Sentinel-2 satellite images to estimate various plant biochemical traits in large almond orchards in a two-year study. The traits, including leaf dry mass, leaf water content, and leaf Cab, were derived using a radiative transfer model and were used to explain the observed variability in leaf N. The resulting Sentinel-2 model for leaf N prediction showed high accuracy with an r^2 of 0.82 and an nRMSE of 13%. Both the model

performance and the contributing traits proved to be stable over the entire two-year period. The integration of these plant biochemical traits, thus, provides a more reliable and stable basis for leaf N prediction than conventional approaches, opening up promising prospects for application in precision agriculture (see Figure 9).

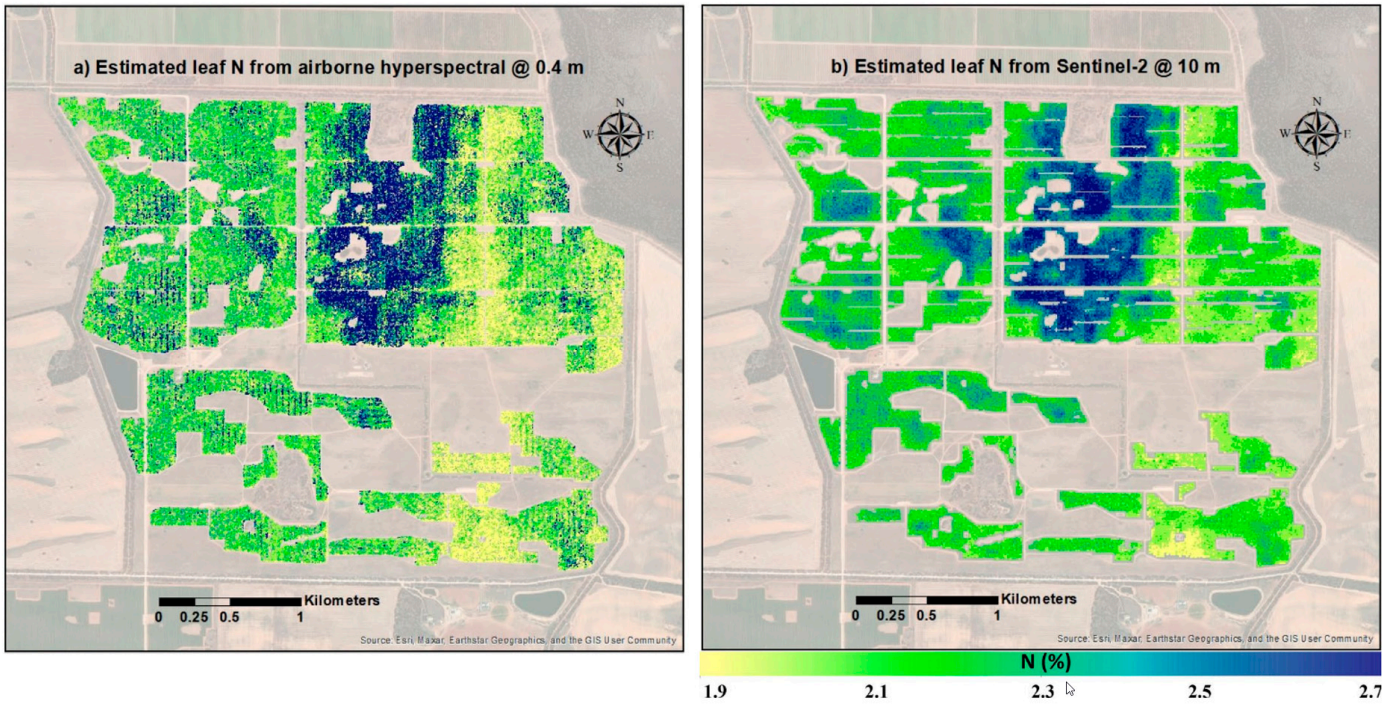

Figure 9. (a) Estimated leaf N maps from airborne hyperspectral data (0.4m spatial resolution) for the 2021, and (**b**) estimation leaf N from Sentinel-2 data (10m spatial resolution) (from Wang et al. [120]).

Table A4 presents a structured overview of trait-based A-LUI indicators, including concrete examples, the corresponding RS sensors, and the representative literature references.

4.2. Monitoring the Genesis Indicators of A-LUI with RS

Genesis indicators capture the temporal dynamics and historical development of A-LUI. They describe how management practices such as crop rotations, multiple harvests, tillage events, or land conversions evolve over time. RS is particularly suited to monitor these processes through dense time series, enabling the detection of management cycles and long-term trajectories of intensification.

4.2.1. Genesis Indicators of A-LUI—Subsurface Drainage

Subsurface drainage (DS) systems play an essential role in modern agriculture by efficiently draining excess water, thereby improving soil quality and agricultural productivity. Accurately locating and analysing these systems is crucial for sustainable land management, as unmapped drainage systems can lead to water quality degradation and increased nutrient inputs into water bodies [123]. Over the centuries, various civilisations such as the Egyptians, Chinese, and Indians developed their own drainage systems. In Europe, the drainage of agricultural land was established in the 17th century [124]. With the advent of motorised machinery in the 20th century, underground drainage systems spread rapidly, expanding agricultural land and making previously wet areas suitable for arable farming [125]. It is estimated that between 54% and 87% of the world's wetlands have been lost since 1700 AD [126]. In addition to their positive effects on agricultural

production, drainage systems also have undesirable side effects. They can accelerate the release of nutrients, especially nitrogen and phosphorus, into water bodies and, thus increase the risk of eutrophication [123]. In addition, draining carbon-rich wetlands can lead to increased CO_2 emissions [127].

RS offers an efficient alternative to time-consuming manual investigations using ground penetrating RADAR and electromagnetic induction and enable large-area detection of drainage systems [128,129] (see Figure 10). The first attempts to record underground drainage systems using airborne thermal infrared images were made as early as the 1970s [130]. Multispectral and hyperspectral imaging utilises near-infrared (NIR) and shortwave infrared radiation (SWIR) to detect soil moisture. Vegetation indices such as NDVI and NDWI help to identify wet areas where drainage systems may not be working effectively [131]. RADAR RS such as Sentinel-1 enable the detection of soil moisture differences and help to recognise drainage patterns, even under cloudy skies or at night [132]. High-resolution digital terrain models (DTM/DEM) based on LiDAR RS data help to analyse natural and artificial drainage paths. LIDAR can also detect microtopographies that indicate inadequate drainage [133]. Moist or water-saturated soils have different temperatures than dry soils. Thermal infrared images (TIR), for example from Landsat 8, can be used to recognise drainage, especially after precipitation or at night [134,135]. Studies have shown that the combination of optical and thermal images can significantly increase detection accuracy [136].

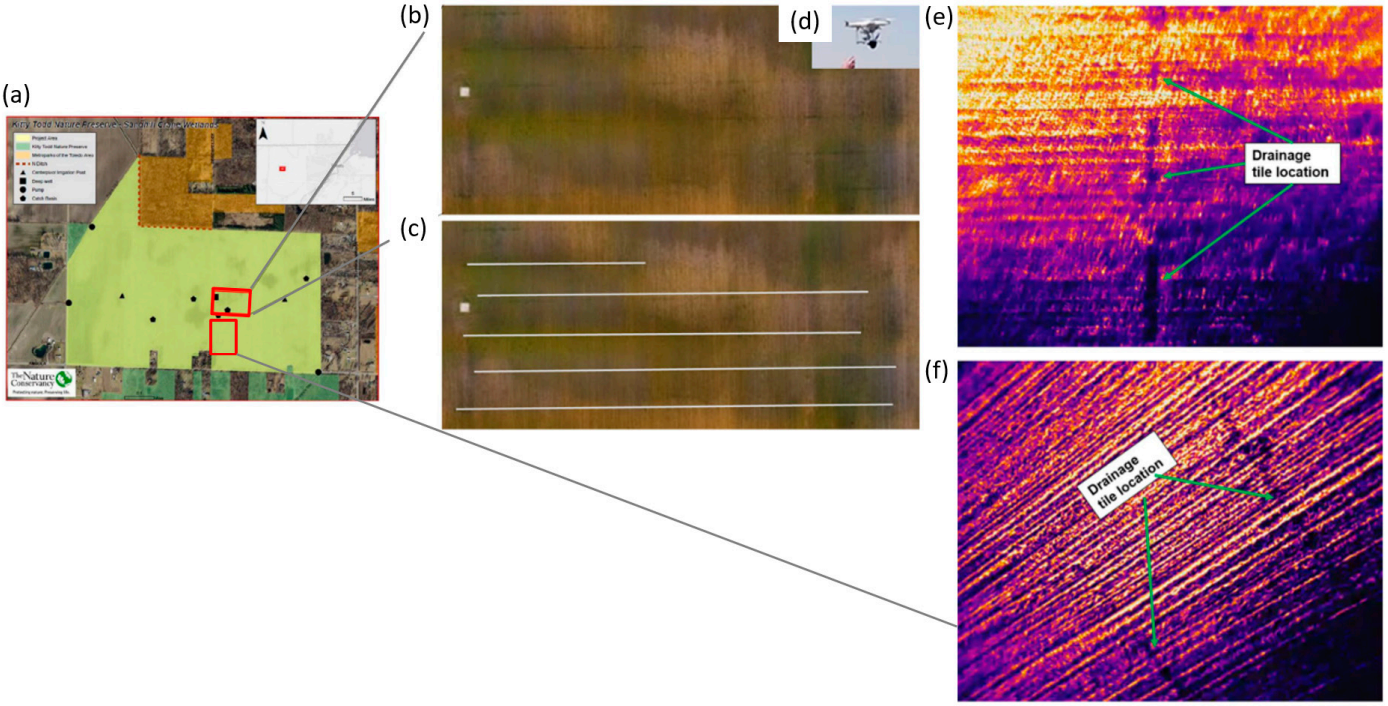

Figure 10. (**a**) Location of the study site within the Oak Openings regions in Ohio, USA. (**b**,**c**) section of visible image with dull colour linear feature interpreted as drainage tile with a parallel network, (**d**) the UAV used to acquire image, (**e**,**f**) a section of thermal infrared images of the study site with drainage tile (from Becker et al. [136]).

4.2.2. Genesis Indicators of A-LUI—Terrace Mapping

Terrace fields are an important indicator for the genesis of A-LUI because they reflect the long-term adaptation and transformation of the landscape by humans. Here are some key reasons. Terraces were built to intensify the cultivation of slopes and to minimise soil erosion. These cultivation terraces are often found in steep, mountainous regions.

In the study by Liu et al. [137], RS data (Sentinel-1/2) was used as an efficient alternative for recording terrace structures, as it enables large-scale monitoring. However, optical satellite images, especially in mountainous regions, are affected by high cloud cover and varying vegetation cover, which makes precise detection of terrace fields difficult. Previous studies on automated terrace mapping using high-resolution satellite imagery, such as the GF-2 satellite mission or WorldView-1/3, have focussed primarily on the Loess Plateau in China, a region with comparatively less topographical challenges [87,138,139] (see Figure 11). This work mainly utilised optical RS data and applied object-oriented or deep learning methods for classification [140]. The use of high-resolution satellite images and digital terrain models (DEM) with an accuracy of 1–2 m significantly improves the recognition accuracy of terrace structures. However, these methods are limited for large-scale analyses due to high costs and a considerable volume of data [137]. Especially in mountainous regions, such as the analysed landscape in Southwest China, there are still significant challenges in the RS of terraces. Complex planting patterns, including crop rotation and mixed cropping, make it difficult to clearly identify terraces due to spectral similarities between different land cover classes [141]. In addition, low- to medium-resolution satellite images have a limited ability to detect small-scale terrace structures, as these often only appear as mixed pixels in heterogeneous landscapes [142]. LiDAR (Light Detection and Ranging) and RADAR (Radio Detection and Ranging) are key RS technologies for the detailed detection of terrace structures. They provide precise topographical information that is essential for analysing and managing such landscapes. LiDAR, in particular, enables the creation of high-resolution, three-dimensional terrain models, which allow reliable mapping of terrace structures even in densely forested areas [143].

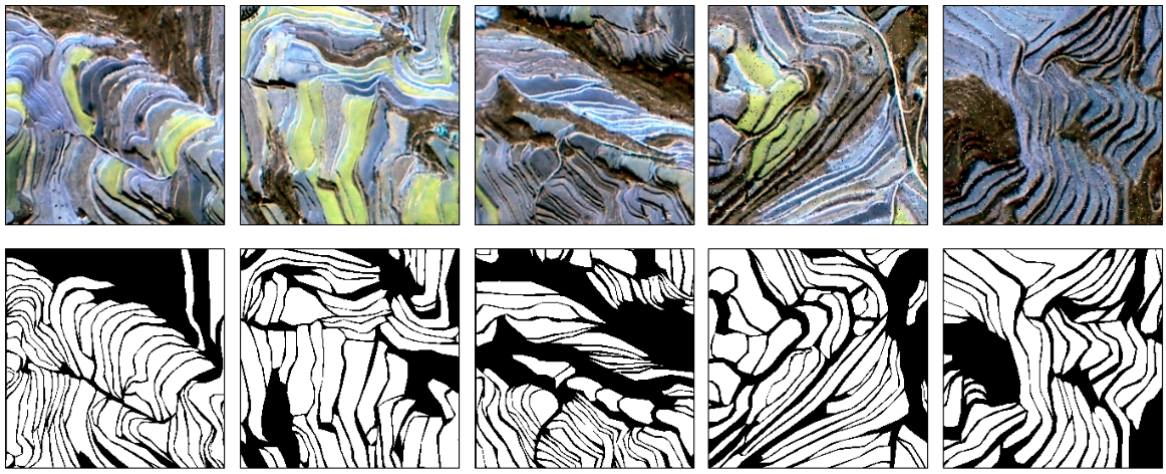

Figure 11. GF-2 RS data of fused images and their corresponding labels for detection of terrace. The top row shows the GF-2 RS dataset of fused images. The bottom row represents the true labels corresponding to the GF-2 sample set of fused images (from Yu et al. [87]).

An example of the application of this technology is provided by the study by Le Vot et al. [144], which aimed to reconstruct the historical development of land use on terraces. The aim of this study was to test the hypothesis of the resilience of these landscapes in the period from the 17th to the 21st century. For this purpose, current and archived geodata sets as well as LiDAR-based digital terrain models with a resolution of 1 m were used.

The analysis was carried out in an area that was recently affected by an extreme event and whose reconstruction was considered a challenge. The results showed that the optimal utilisation of the terraces corresponded to the demographic optimum in the mid-19th century. After the Second World War, there was a gradual abandonment of the terraces, with significant differences between mountain regions. Nevertheless, the terraces remained intact despite these developments and survived the extreme event under investigation. This confirms the hypothesis of resilience and provides important insights for future strategies to revitalise these landscapes in the context of climate change

In the study by Garzón-Oechsle et al. [145], a mobile LiDAR-based mapping system (MMS) without the use of UAVs was used to map the terrain around the documented stone architecture of the Manteños (ca. 650–1700 AD). The study area covered 1.2 km^2 in the cloud forests of Bola de Oro, Manabí, Ecuador. The resulting digital terrain models (DTMs), when combined with soil surveys and archaeological excavations, revealed a Manteño landscape that had been significantly altered by the construction of agricultural terraces, drainage channels, and water retention basins. These structures were designed to store and distribute water from seasonal rainfall and marine layers at higher altitudes. The extensive investment in this sophisticated landscape is likely due to the fact that the Chongón-Colonche Mountains were considered resilient areas to extreme climate changes associated with the El Niño–Southern Oscillation (ENSO) during the Medieval Climatic Anomaly (MCA, ca. 950–1250 AD) and the Little Ice Age (LIA, ca. 1400–1700 AD) [145].

4.2.3. Genesis Indicators of A-LUI—Allmenden

Allmenden refers to communally used areas that played a central role in pre-modern agricultural societies. The term originates from the medieval legal system and referred to areas that were not privately owned by individuals but were used jointly by several or all members of a village community. In Europe, commons were widespread and were an important addition to private farmland, particularly in the three-field economy. In England, Germany, and other parts of Europe, numerous commons were privatised in the 17th–19th centuries, which often caused social tensions. Remnants of historical commons have been preserved, for example, in alpine pastures, heathland, or traditional co-operative forests

Modern RS methods can be used to effectively record historical field systems and commons. The combination of different technologies, including LiDAR (Light Detection and Ranging) as well as multispectral and hyperspectral satellite images, is particularly powerful. LiDAR has the advantage of being able to penetrate vegetation and detect fine ground elevations and structures. This makes it possible to identify relics of earlier landforms, vaulted fields, hedge structures, and medieval paths. A practical application example is the discovery of former three-field farming areas and commons that are now covered by woodland or modern agriculture. Medieval plough tracks and plot structures, particularly in Great Britain, Germany, and France, can also be detected using this method. In addition, multispectral and hyperspectral satellite images make it possible to differentiate between different soil types and vegetation cover, allowing conclusions to be drawn about historical agricultural use. Deviating vegetation structures also help to identify historical field boundaries. Former agricultural areas often show characteristic vegetation patterns or soil features that can be visualised using these techniques. Hyperspectral analyses also offer the possibility of identifying differences in moisture content, soil chemistry, or erosion patterns, which provides additional insights into past land use practices.

Edisa Lozić [146] analysed the use of airborne LiDAR data to discover, document, and interpret agricultural land use systems in the early medieval microregion of Bled (Slo-

venia). By combining LiDAR data with archaeological, geological, and pedological analyses, significant environmental variations within a microregion were identified. These enabled a detailed reconstruction of early medieval settlements and their agricultural use. The study by Masini et al. [147] investigated the effectiveness of LiDAR data for reconstructing the urban form of a medieval village near Matera, southern Italy. The research shows how LiDAR data can be used to reconstruct the urban structure and architectural features of historical settlements, even in densely forested or difficult to access areas.

4.2.4. Genesis Indicators of A-LUI—Deforestation

The recording of deforestation to gain pasture or arable land is an essential indicator of A-LUI. It allows a detailed analysis of human interventions in the environment, especially with regard to changes in the carbon balance, biodiversity loss, resource utilisation, and soil changes. Modern RS technologies offer precise methods for measuring these environmental changes and assessing their ecological consequences over longer periods of time. Global deforestation shows significant losses of forest area in different regions of the world. The study "Forest Pulse: The Latest on the World's Forests" describes the latest trends in forest loss and deforestation and provides an up-to-date assessment of the global state of forests (https://gfr.wri.org/latest-analysis-deforestation-trends accessed on 19 October 2025). According to Smith et al. [148], the global forest cover was around 4.06 billion hectares, with approximately 420 million hectares lost between 1990 and 2020, mainly in tropical regions.

Slash-and-burn agriculture plays a significant role in the deforestation process and causes serious climate effects, including temperature increases, changes in precipitation patterns, and loss of biodiversity [149]. The use of unmanned aerial vehicles (UAVs) to analyse land cover during slash-and-burn has shown that multispectral imagery enables rapid and accurate assessment of land use change. In the future, this technology could serve as a standard method for recording slash-and-burn events [150]. The use of satellite imagery has proven to be one of the most efficient methods for the comprehensive and regular recording of deforestation. Optical satellites such as Landsat or MODIS provide high-resolution images that can be used to detect forest loss [151]. However, they are limited by weather conditions and cloud cover. RADAR systems such as Sentinel-1, on the other hand, work independently of light conditions and atmospheric influences, which makes them a reliable alternative for forest monitoring [152,153]. In addition, high-resolution satellite images make it possible to identify smaller deforested areas that are often overlooked in large-scale analyses [154]. The combination of different RS technologies can, thus, provide a comprehensive analysis of global deforestation and contribute to the development of effective conservation measures (see Figure 12).

Table A4 presents a structured overview of genesis indicators of A-LUI indicators, including concrete examples, the corresponding RS sensors, and the representative literature references.

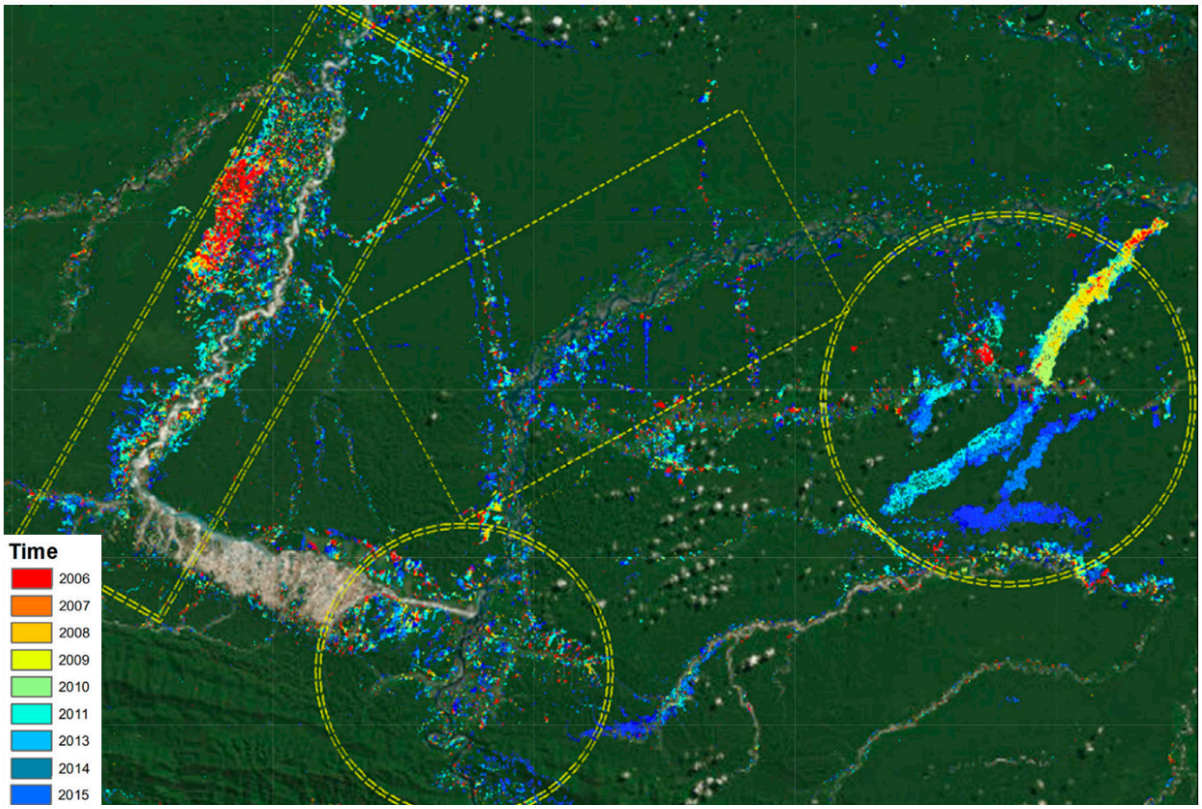

Figure 12. Deforestation events (2006–2016) were identified from Landsat time series (1990–2016) by analysing mean and standard deviation of photosynthetic vegetation indices. The example demonstrates how RS enables long-term monitoring of land cover change (from Tarazona et al. [154]).

4.3. Monitoring the Structural Indicators of A-LUI with RS

Structural indicators describe the spatial configuration and arrangement of agricultural land, including field size, shape, boundaries, and the presence or loss of semi-natural elements such as hedgerows, buffer strips, or terraces. These structural properties are closely linked to management intensity, as land consolidation, removal of landscape elements, and increasing field sizes typically indicate intensification. RS offers powerful tools to capture such patterns, ranging from high-resolution optical imagery and LiDAR data to radar-based mapping of field boundaries and landscape complexity. By quantifying structural diversity and fragmentation, RS enables a systematic assessment of how land use intensity reshapes the agricultural landscape.

4.3.1. Structural A-LUI Indicators—Crop Composition and Configuration

The quantification of landscape structure and the derivation of structural indicators play a decisive role in the monitoring of A-LUI. For example, the extraction of farmland boundaries from RS data is a key A-LUI indicator and supports agricultural planning, resource conservation, and sustainable development. Field boundaries are defined by changes in the type of crops planted, which are visible in RS data as discontinuities in grey value, colour, or texture. Wang et al. [88] provide a comprehensive overview of Farmland Boundary Extraction using RS data. Spatially high-resolution satellite images (≤1 m) such as WorldView-2/-3 (0.3–0.5 m), QuickBird (0.61 m), Pleiades (0.5 m), or GeoEye-1 (0.41 m) are particularly suitable for capturing field boundaries, as they allow fine structures such as narrow field paths and small plots to be captured. Medium-resolution satellite data (1–5 m) such as Sentinel-2 (10 m, with super-resolution at 5 m), Landsat 8 and 9 (30 m, for

large-scale land use analyses), GF-2 (1 m, Chinese satellite), or RapidEye (5 m, multispectral available) are also suitable for large-scale analyses [88] (see Figure 13).

RS data enable the quantification of field sizes and their spatial distributions, which allow conclusions to be drawn about the degree of A-LUI and its management practices. Large, contiguous areas on which a single plant species is cultivated are indicative of industrial agricultural practices [155]. The arrangement of such monocultures can be easily recognised by RS and is a structural characteristic of intensive use. High-resolution satellites (Sentinel-2, WorldView, RapidEye) show that these agricultural areas appear as numerous small, geometric fields that are often separated by paths or hedges. Here, the degree of A-LUI is shown by small, highly parcelled fields, which gives an indication of the maximum utilisation of the available land [67]. Kümmerle et al. [31] use the image texture of Landsat data to derive the patch size, whereby the texture explained up to 93% of the variability of the field sizes in the study area in the border region between Poland, Slovakia, and Ukraine. The patch size (field size) indicator also offers a unique opportunity of investigating changes in land use that have occurred due to post-socialist land reform strategies, as many large agricultural areas have been parcelled out through privatisation. For example, Figure 14 shows a Landsat RS dataset in the 1990s, which clearly shows the state border between Saxony-Anhalt and Lower Saxony north of the Harz Mountains due to the change in patch size and small-scale parcelling.

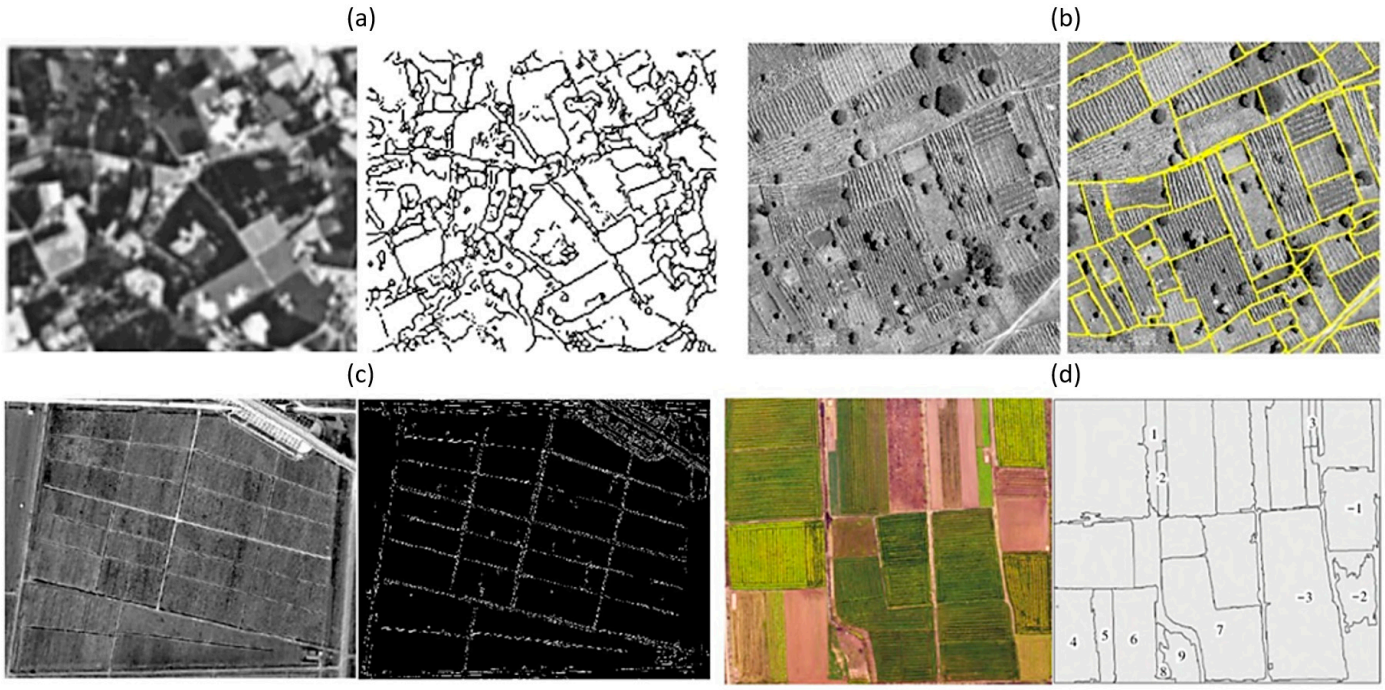

Figure 13. (**a**) Linear threads in farmland, (**b**) demarcation lines, (**c**) boundary objects, (**d**) perimeter boundaries of farmland blocks. Such boundary features allow quantification of field size and shape, which are indicators of A-LUI (from Wang et al. [88]).

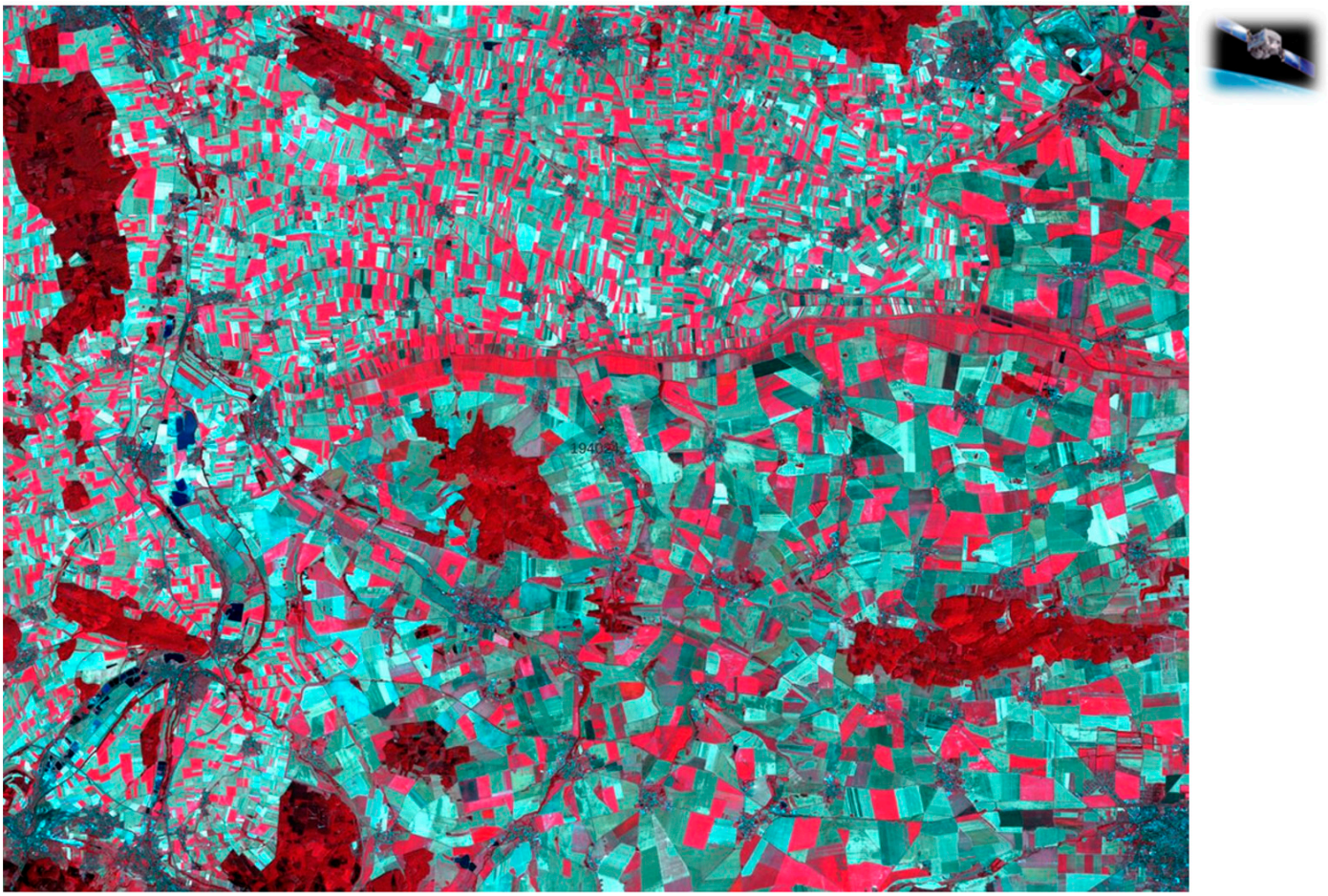

Figure 14. State border between the former FRG and GDR (different farming practices) after the fall of the Wall is clearly visible due to the shape, size, and small-scale nature of the border between Saxony-Anhalt and Lower Saxony north of the Harz Mountains in the 1990s, Germany.

In the study by Roilo et al. [67], various A-LUI indicators (e.g., field size, LULC_homogeneity) are used to analyse their effects on biodiversity. To calculate the field size, they used the LULC classification (2020, at 20 × 20 m resolution) [156], which was subsequently converted into polygons. The problem here is that not all crops could be properly classified using Sentinel-2 RS data. Furthermore, no roads and field paths could be included in the classification, which meant that the actual field size and the agricultural pattern could only be insufficiently quantified. In the study by Martin et al. [84], which deals with the effects of farmland heterogeneity on biodiversity, field size is emphasised as an important indicator. In order to improve the accuracy of the derivation of field size, it is often derived vectorially from aerial image data [82]. In this study, Mohr et al. [83] used aerial image data in combination with in situ data and interviews to answer the following question: Why has farming in Europe changed since the 1960s? In the study by Baessler and Klotz [157], historical and temporal time series of aerial image data were used to analyse changes in agricultural land use on landscape structure and arable weed vegetation over the last 50 years. The Interspersion and Juxtaposition Index (IJI) quantifies the mixing of different land use types and reflects the heterogeneity of the landscape. Higher IJI values indicate a more complex, diversified landscape, which has potentially positive effects on biodiversity [158].

The Shape Index is also used to analyse differences in land use patterns and management practices between different regions, such as East and West Germany. Such analyses can provide information on the impact of different management practices on landscape

structure and function [159]. Furthermore, shape indicators can be used, for example, to estimate operational efficiency, to justify the merging of two field plots or to facilitate land consolidation projects [160]. In his study, Oksanen [160] uses various shape indicators such as convexity, compactness, triangularity, rectangularity, ellipticity, the ratio of principal moments, the radius of the inscribed circle, and the kerb index to classify the real field plots in order to quantify the operational efficiency (time and distance of the necessary travelling distance). Griffel et al. [161] examine the relationship between field shape and size and empirically derived crop efficiency to support assumptions related to the prediction of crop costs, greenhouse gas emissions, labour requirements, and other factors that affect the willingness to grow energy crops. Salas and Subburayalu [162] used Airborne Hyperspectral AVIRIS and HYDICE datasets to assess the potential of an optimised shape index to discriminate between tillage types (maize-min and maize-notill) and between grass/pasture and grass/trees, tree, and grass.

The indicator homogeneity of agricultural areas is a very good indicator for quantifying the A-LUI. Areas with high A-LUI are characterised by high homogeneity in species distribution and homogeneous spectral characteristics in contrast to organically cultivated areas with increased diversity of species (no use of pesticides) [163]. Blüthgen et al. [163] were able to prove through in situ measurements at 150 grassland sites in the Biodiversity Exploratories in three regions in Germany (Alb, Hainich, Schorfheide) that the vascular plant diversity in grassland sites in two regions (Alb and Hainich) decreased significantly with the A-LUI. Important work on the assessment of homogeneity from RS data of landscapes can be found in Rocchini et al. [164], which provides an overview of the current state of RS-based techniques for deriving spectral heterogeneity as a proxy of species diversity. Based on these approaches, Rocchini et al. [165] developed the Rao's Q diversity index, which is considered a remotely sensed spatial heterogeneity indicator for taxonomic and functional plant species diversity [166].

4.3.2. Structural A-LUI Indicators—Surface Roughness of the Vegetation

Closely related to homogeneity is the surface roughness of the vegetation, which describes the structural variability of the vegetation surface and provides valuable information on plant architecture, stand density, species distribution, cultivation methods, and thus, A-LUI. Intensively managed fields with monocultural cultivation generally have low roughness (homogeneous stands), while more extensive, more diverse forms of cultivation or agroforestry systems have higher roughness. Steele-Dunne et al. [167] provide an overview of RADAR RS of agricultural canopies (see Figure 15). RADAR RS technologies can be used for a variety of applications resulting from the detection of the surface roughness of vegetation in agricultural areas. These range from crop classification, vegetation dynamics, vegetation phenology, water stress, and soil moisture derivation. Much of our understanding of vegetation backscatter from agricultural vegetation plots comes from SAR field-scale classification and monitoring studies [167]. Howison et al. [168] used Sentinel-1 RADAR data to quantify the spatial dynamics of surface roughness of vegetation in agricultural landscapes. Herrero-Huerta et al. [169] used the roughness of plant features (soya beans) using UAV aerial image data to estimate biomass in agricultural systems. Alfieri et al. [170] used the roughness, canopy structure, and configuration of vineyards to estimate the evapotranspiration loss required for irrigation and effective utilisation of limited water resources.

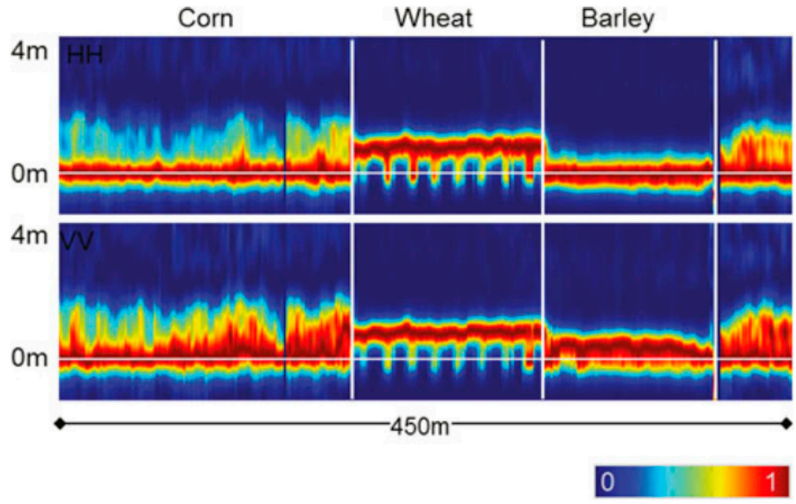

Figure 15. Normalised thermographic reflectivity profile across three fields (corn, wheat, and barley) based on RADAR RS data (from Steele-Dunne et al. [167]).

4.3.3. Structural A-LUI Indicators—Soil Roughness

Soil roughness is a crucial indicator for A-LUI as it allows direct conclusions on tillage practices, water balance, erosion processes, and vegetation development. Soil roughness is an inhomogeneous medium consisting of different types of soil textures, different shapes and sizes of stones, clods, SM gradients, organic matter, etc. The microwave signal incident on this layer is modified, scattered, and attenuated due to the physical and structural properties of this medium [171]. Soil roughness, thus, reflects various physical and agronomic processes. For example, the intensity of soil cultivation (e.g., ploughing, harrowing) changes the soil roughness considerably. High roughness often indicates intensive mechanical interventions, while low roughness indicates minimal soil turnover or conservation agriculture (see Figures 16 and 17). Different crops and management practices produce specific roughness patterns. During a vegetation cycle, a gradual smoothing of the soil can be observed due to natural processes (rain, wind, biological activity) or renewed roughness formation due to agricultural interventions. Furthermore, high soil roughness favours water infiltration, as depressions can store water. Too little roughness, on the other hand, favours surface runoff and increases the risk of erosion. Heavily tilled and, therefore, less rough soils are more susceptible to erosion, especially in dry areas. Roughness can, therefore, be used as an indicator for the risk of erosion and the sustainability of cultivation. Soil roughness influences the temperature and moisture distribution on the surface. High roughness can reduce soil warming and influence evaporation rates. By monitoring roughness, conclusions can be drawn about plant growth. Heavily cultivated soils with low roughness could, for example, indicate a high use of fertilisers and irrigation. It can be analysed very well using RS methods such as RADAR and LiDAR technologies as well as optical sensors [172].

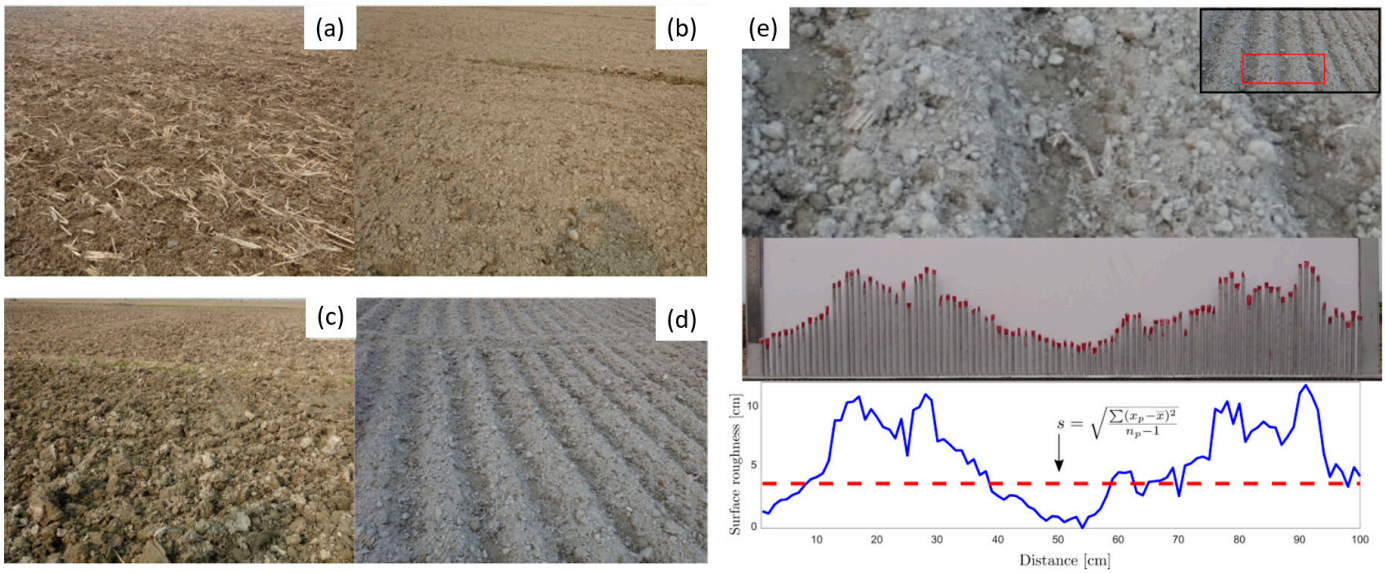

Figure 16. Field photographs to illustrate the surface roughness conditions in different agricultural plots on the Kosi Fan. (**a**) shows the photograph of a stubble field, (**b**) harrow field, (**c**) ploughed field, (**d**) furrow field, (**e**) surface undulation profile extracted by processing the photographs captured for the pin-profile using a digital camera in the field (from Singh et al. [171]).

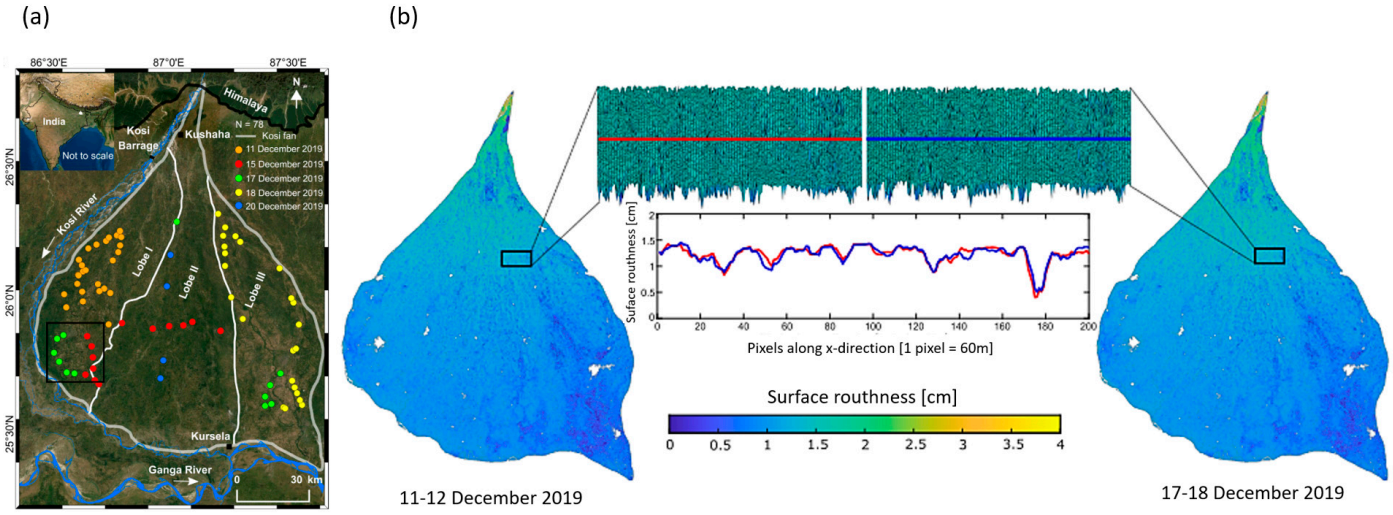

Figure 17. (**a**) Image in the top left shows the location of the Kosi megafan in the Himalayan Foreland, (**b**) spatial distribution of surface roughness prediction from Sentinel-1, Sentinel-2, and Shuttle RADAR Topographic Mission (SRTM) data. (from Singh et al. [171]).

Table A4 presents a structured overview of structural indicators of A-LUI indicators, including concrete examples, the corresponding RS sensors, and the representative literature references.

4.4. Monitoring the Taxonomic A-LUI Indicators with RS

Taxonomic indicators capture the land use types within agricultural landscapes. They reflect whether farming systems are dominated by monocultures or characterised by mixed cropping, rotations, or agroforestry practices. Such diversity strongly influences ecological resilience and is a central dimension of land use intensity. RS enables taxonomic differentiation by exploiting spectral signatures, multi-temporal observations, and

classification algorithms to distinguish crop types, detect rotations, or identify mixed stands.

4.4.1. Taxonomic A-LUI Indicators—Cropping Patterns

The monitoring of cropping patterns using RS is a key indicator of A-LUI. They enable precise characterisation of cropping intensity, harvest frequency, diversity, and management strategies. With the help of RS such as multispectral, hyperspectral, and RADAR data, changes can be analysed on a large scale, and long-term trends in agriculture can be identified [155,173,174].

Extensive agriculture shows more variable patterns with longer fallow periods, especially in semi-arid or mountainous regions, and relies on crop rotation, mixed cropping, or agroforestry. Single cropping indicates low intensity, while double/multi-cropping indicates high A-LUI, often under irrigated conditions in tropical and subtropical areas. Intercropping increases vegetation variability and is often used in sustainable agricultural systems. High A-LUI is associated with short or no fallow periods, while low A-LUI has longer fallow periods for soil regeneration. Long-term changes in cropping patterns can be indicators of soil degradation, water scarcity, or climate change, which is why the adoption of diversification strategies such as agroforestry and mixed cropping as sustainable measures against overexploitation is essential. Mahlayeye et al. [173] give a very good overview of the detection of cropping patterns using RS. Optical sensors are most commonly used for mapping single cropping, especially those with high spatial resolution, such as UAVs. These sensors enable the precise identification of single crop fields but are often only suitable for smaller areas. For large-scale (regional/global) analyses, on the other hand, medium to coarse resolutions are usually used, such as Spot, Landsat 8, MODIS, or Sentinel-2 [175,176]. In addition to optical sensors, microwave sensors with high temporal resolution, such as RADARSAT-2 or Sentinel-1 [177], are also used, particularly for rice cultivation in Asia or maize in Africa. Some studies have combined microwave and optical sensors for more precise crop mapping [178]. In addition, hyperspectral or LIDAR sensors are increasingly being used [179–181]. Studies on the mapping of individual crops are based on phenology and the spatial distribution of crops. Mapping individual crops using single images may be insufficient, as plants change during the growing season. Continuous monitoring of plant development is, therefore, necessary. Overall, the analysis shows that single crop cultivation can be successfully mapped at both local and regional levels with high spatial and temporal resolution [173]. The mapping of multiple cropping and sequential cropping systems is carried out at different levels using optical sensors with high temporal resolution [173]. MODIS satellite data are frequently used [182,183], while Indian RS (IRS) satellites and the Wide Field Sensor (WiFS) [184] and Sentinel-2 [174] are also used in some studies. The detection of triple cropping patterns was also carried out [182]. Microwaves (Sentinel-1 C-band time series data) and optical sensors enable the creation of detailed temporal profiles of sequential crops [185,186]. Commonly mapped crops are maize, rice, wheat, and soybeans, with studies on sequential cropping patterns increasingly being conducted in tropical regions characterised by long rainy seasons

Mapping sequential cropping patterns is more complex than single cropping, as different crops are planted in the same growing season, requiring a longer growing season and more continuous ground cover [173]. In particular, high-resolution multispectral and hyperspectral imaging provide valuable insights into the structure and dynamics of mixed crops. Vegetation indices such as the NDVI (Normalised Difference Vegetation Index) or the EVI (Enhanced Vegetation Index) help to differentiate between different plant species based on their spectral reflectance properties, while hyperspectral sensors enable even more precise differentiation by analysing specific wavelength ranges.

4.4.2. Taxonomic A-LUI Indicators—Crop Classifications

A study on high-resolution mapping of the German agricultural landscape using RS provides detailed insights into parcelling and field structures through crop classification. RS-based classifications of agricultural land use for the years 2017–2020 for the German agricultural landscape (grid of 10 m × 10 m) provide detailed insights into area size, distribution, and crop types cultivated (https://ows.geo.hu-berlin.de/webviewer/landwirtschaft/index.html accessed on 19 October 2025 [90], see Figure 18. Crop types such as rapeseed or sugar beet can be differentiated very well. However, species that are spectrally very similar in the course of the growth phases or in their appearance (e.g., winter wheat and triticale) or that differ solely in terms of their type of utilisation (e.g., silage maize and grain maize) cannot yet be recorded with sufficient accuracy using RS. Patterns of land use intensity, such as crop rotation or fallow periods, can be effectively captured by time-series RS data, providing insights into the sustainability of agricultural practices. Preidl et al. [156] used Sentinel-2A imagery data for crop classification on the national scale (Germany).

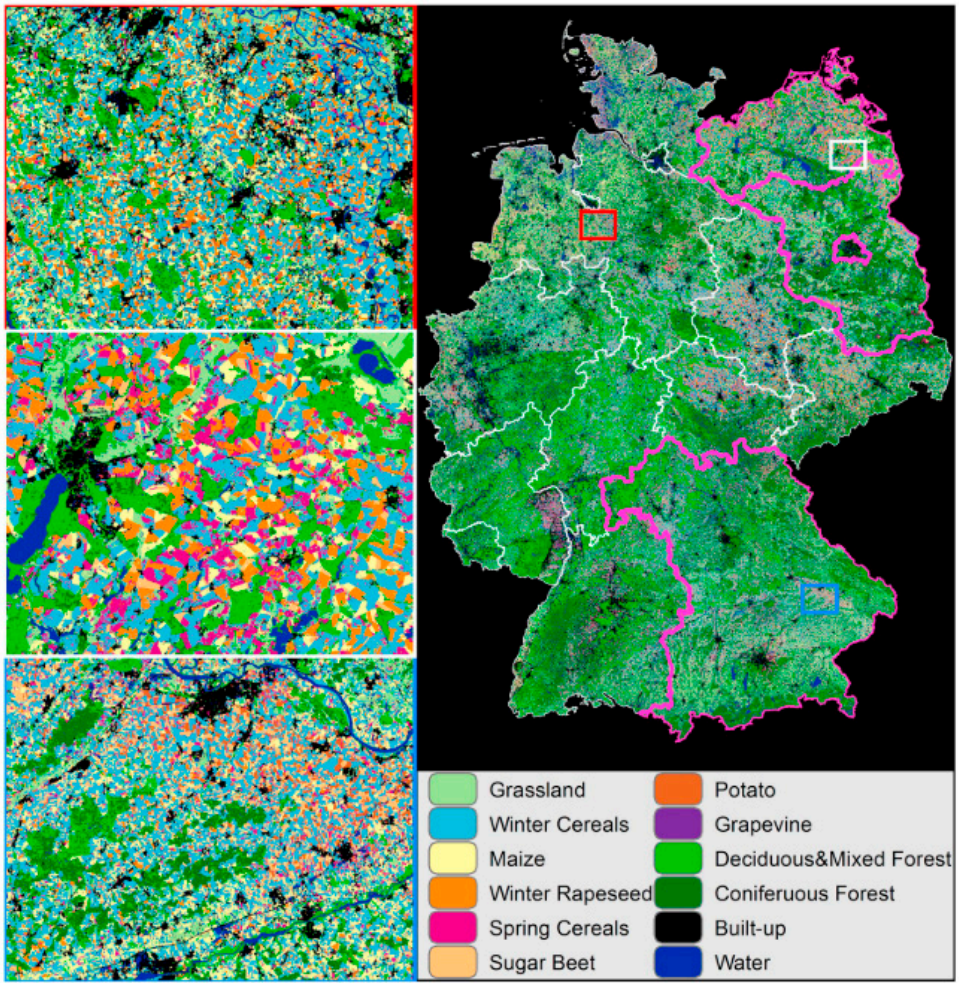

Figure 18. Results of the wall-to-wall crop type mapping using the benchmark 10-day interval composite of Landsat and Sentinel-2 time series for Germany (from Griffiths et al. [90]).

The global distribution of A-LUI is crucial for understanding agricultural land use. Previous studies used coarse-resolution data, which are unsuitable for heterogeneous landscapes. To fill this gap, Zhang et al. [187] developed the global, spatially continuous CI dataset GCI30 with 30 m resolution using Landsat 7 ETM+, Landsat 8 OLI, and Sentinel-2 MSI time series during 2016–2018. GCI30 captures global patterns and spatial details,

with monocultures dominating 81.57% of cropland. Regional differences reflect natural and anthropogenic influences [187]. Howison et al. [168] developed a new RADAR-based RS technique for large-scale quantification of A-LUI. The method utilises the temporal stability of RADAR signals to capture differences in land use and provides more precise tracking of A-LUI at the landscape scale.

4.4.3. Taxonomic A-LUI Indicators—Intensification of Grassland

The intensification of grassland utilisation (e.g., more frequent mowing, increased grazing) significantly impairs biodiversity and ecosystem services. However, detailed information on utilisation intensity is usually locally limited. Numerous studies show [35,188] that mowing events can be mapped over large areas using satellite image time series. Time-series phenology can overcome limitations of classification-based mapping approaches, especially when characterising grassland use intensity, using the frequency and timing of mowing events as important indicators [189]. Lange et al. [188] developed a method for the RS-based derivation of grassland intensity for Germany (www.ufz.de/land-use-intensity accessed on 19 October 2025). Based on Sentinel-2 time series (spatial resolution of 20m) from 2017 to 2018, the NDVI time series data and available in situ indicators (grazing intensity, mowing frequency, and fertiliser use) of the Biodiversity Exploratories for Germany [190] were used to train and derive a continuous A-LUI index for grassland for Germany using Convolutional Neural Networks (CNN). An overall classification accuracy of up to 66% for grazing intensity, 68% for mowing, and 85% for fertilisation was achieved. Weber et al. [35] developed a rule-based algorithm for mapping mowing and grazing events in Switzerland (2018–2021) based on Sentinel-2 and Landsat-8 data. The validation was carried out with time-series data from public webcams. The review (2020–2021) showed that ≥78% of the recorded events reflect actual management, but up to 57%—especially grazing events at higher altitudes—were not recognised. Bartold et al. [91] present a comprehensive study on the classification of management intensity of grasslands in two different regions of Poland (see Figure 19). By using Sentinel-1 and Sentinel-2 data synergistically, different intensity types could be identified, allowing conclusions to be drawn about herbicide use.

Table A4 presents a structured overview of taxonomic indicators of A-LUI indicators, including concrete examples, the corresponding RS sensors, and the representative literature references.

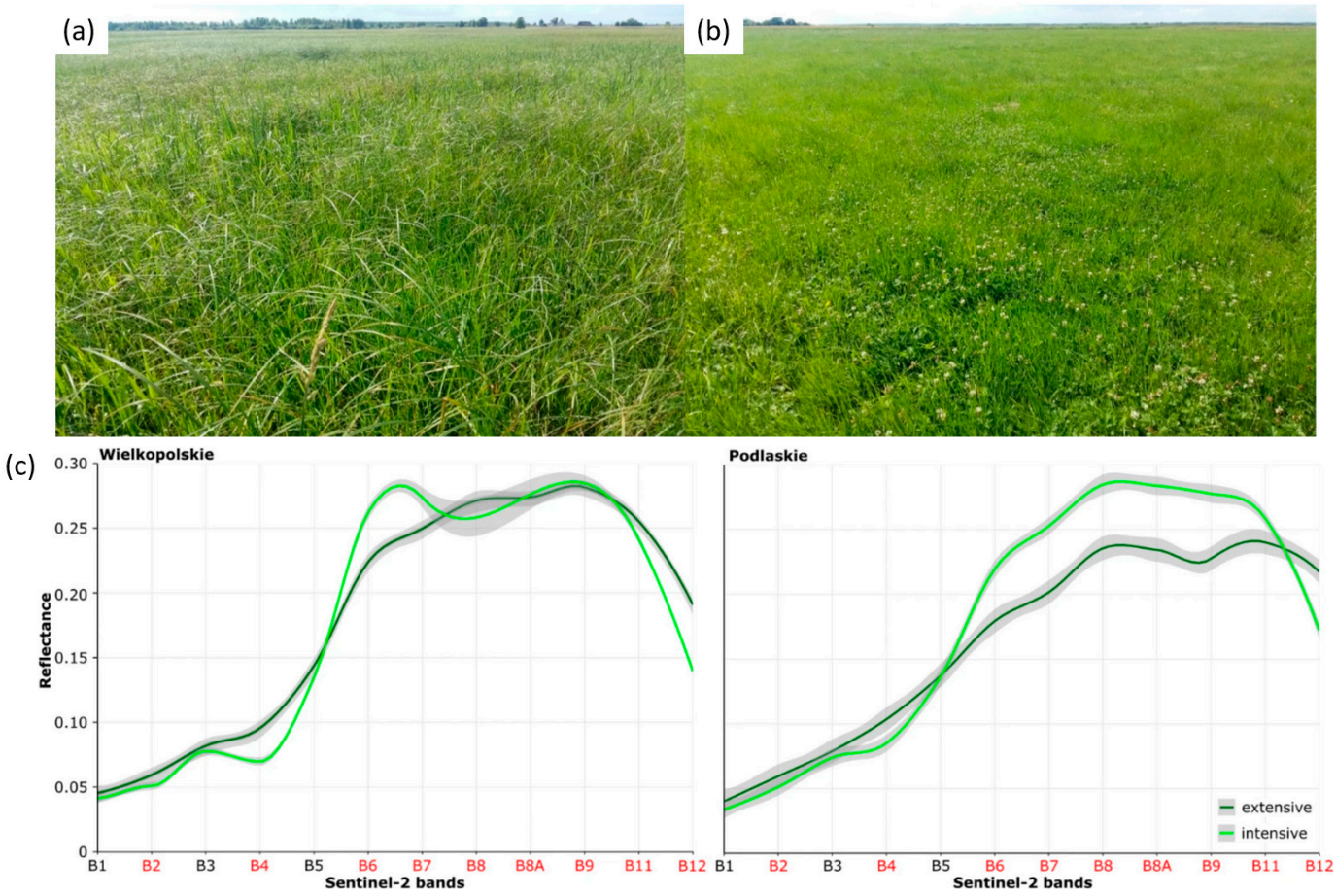

Figure 19. Types of grassland management intensity at the Podlaskie study sites: (**a**) extensive, (**b**) intensive; (**c**) comparison of spectral curves for intensive and extensive grasslands averaged with the loess algorithm (span = 0.35, confidence interval = 0.95) based on Sentinel-2, (from Bartold et al. [91]).

4.5. Monitoring the Functional A-LUI Indicators with RS

Functional indicators describe the ecological processes and ecosystem services that are directly affected by A-LUI. They include aspects such as crop productivity, soil fertility, carbon and nutrient cycling, irrigation demand, and greenhouse gas emissions. These functions are critical for assessing sustainability, as they link agricultural practices to environmental impacts and resource efficiency. RS contributes to functional monitoring by providing proxies for biomass production, evapotranspiration, soil moisture, and photosynthetic activity. Combined with modelling approaches, RS-derived functional indicators allow for large-scale assessments of agricultural performance, efficiency, and environmental trade-offs.

4.5.1. Functional A-LUI Indicators—Plant Density and Biomass Production

RS for recording plant density and biomass production is essential for analysing vegetation structures and assessing the A-LUI, as it reflects the direct effects of management practices on vegetation. RS technologies enable the area-wide analysis of vegetation parameters using the Normalised Difference Vegetation Index (NDVI), the Soil-Adjusted Vegetation Index (SAVI) and the Enhanced Vegetation Index (EVI) to minimise soil and atmospheric influences in order to determine plant density and biomass production. Recent studies, for example, by Sousa Júnior et al. [191], demonstrate the successful use of Landsat 8 to estimate aboveground biomass in agricultural mosaics. The combination of different sensor systems, especially optical- and RADAR-based RS technologies, improves

the accuracy of biomass estimates [192]. The use of unmanned aerial vehicles (UAVs) offers an efficient alternative due to high spatial resolution and flexibility [193,194]. Da et al. [194] combined UAV-derived spectral, textural, and structural features for biomass monitoring of soybean and achieved a model accuracy of R^2 = 0.85. Spaceborne RS data are also used to assess plant biomass. Breunig et al. [195] used PlanetScope and Sentinel-1 SAR data to monitor intercrop biomass in Southern Brazil. Hagn et al. [196] analysed Sentinel-2 data to model crop-specific biomass yield potential in precision farming. Their results showed a strong correlation between relative biomass potential (r = 0.62–0.73) and soil properties such as soil organic carbon (SOC) and total nitrogen (TN). However, optical satellite systems such as Landsat and Sentinel-2 are weather-dependent and do not collect data under cloudy conditions. To overcome this limitation, Planet developed the Biomass Proxy product [197], which provides a daily, ready-to-analyse biomass estimate with 10 m spatial resolution. The Biomass Proxy algorithm fuses Sentinel-1 and Sentinel-2 data and enables continuous monitoring of vegetation. This facilitates the early detection of growth anomalies, the assessment of crop yields, and the identification of potential environmental hazards and supports informed agronomic decision-making. The difference map of Aboveground Biomass (AGB) estimates of 18 August 2017 and 26 August 2017 derived from PlanetScope (PS) optical, Sentinel-1 SAR, and hybrid (optical plus SAR) datasets is shown in Figure 20.

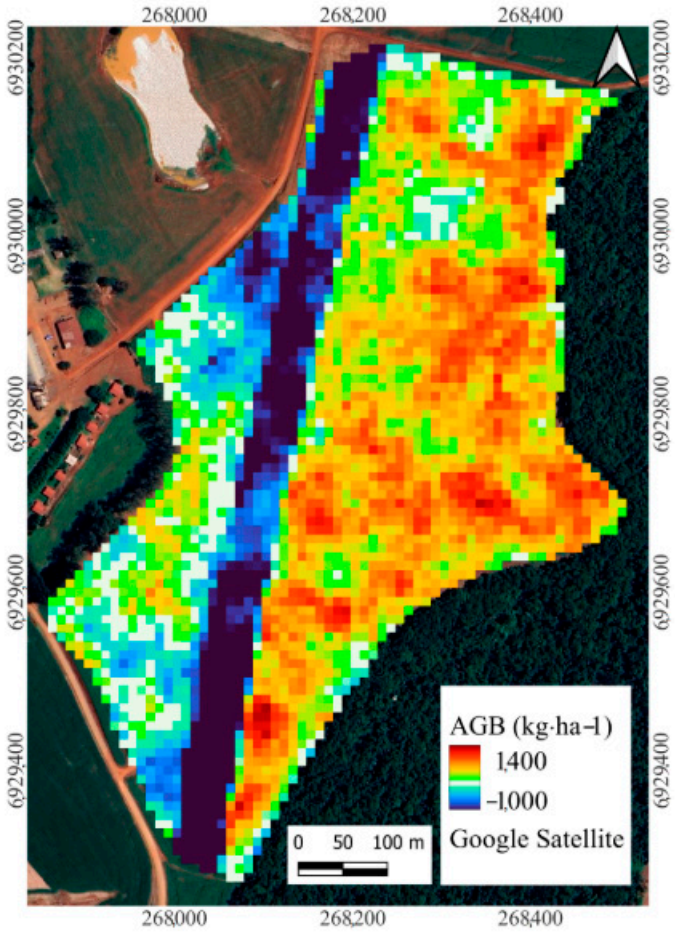

Figure 20. Difference map of Aboveground Biomass (AGB) estimates of 18 August 2017 and 26 August 2017 derived from PlanetScope (PS) optical, Sentinel-1 SAR, and hybrid (optical plus SAR) datasets. Reddish tones indicate AG increase and blue tones indicate AGB decrease. White areas indicate low AGB variation (from Breunig et al. [195]).

4.5.2. Functional A-LUI Indicators—Pesticide, Herbicide, and Fungicide

The use of pesticides and herbicides is an important indicator for assessing the A-LUI. The use of pesticides and herbicides causes vegetation-related changes and stress reactions in plant populations, which can be recorded using RS via vegetation anomalies. Herbicides specifically influence metabolic processes by disrupting biochemical reactions, e.g., triazines (atrazine) lead to the inhibition of photosynthesis, glyphosate to the blocking of amino acid synthesis, or auxin analogues (2,4-D) to the impairment of cell growth. These effects can be detected in the short term by spectral analyses of RS data

The RS-based recording of pesticide intensity is a growing field of research with the aim of making crop protection more efficient and environmentally friendly, as well as being able to detect the use of pesticides and herbicides. The use of satellite images, drones, and hyperspectral sensors allows conclusions to be drawn about the use and distribution of pesticides. While current applications are primarily focussed on laboratory analyses with hyperspectral sensors (e.g., ASD, MSV-500) [198–202], space-based RS data such as Sentinel-2 are also being used [203]. Spectral reflectance data, particularly in the red and near-infrared range, enable the calculation of vegetation indices such as NDVI, whose changes indicate herbicide applications and associated stress reactions [203]. Hyperspectral RS captures detailed spectral signatures that can identify specific pesticide applications and their effects [199]. For example, hyperspectral imaging combined with machine learning has been used to detect herbicide stress early and identify new sites of action. Zhang et al. [200] extracted the Physiological Reflectance Index (PRI) and NDVI from hyperspectral images and classified glyphosate-induced plant damage using Support Vector Machine (SVM). Chu et al. [201] used neural networks to identify different herbicide damage to wheat, finding significant spectral differences in the wavelength ranges 518–531 nm, 637–675 nm, and at the red edge. Pon Arasan et al. [204] analysed UAV-based mapping methods to optimise herbicide use. Bartold et al.[91] combined Sentinel-1 and Sentinel-2 data to classify management intensities in Polish grasslands and identified herbicide applications. Bautista et al. [91] investigated the efficiency of drone applications with cyhalofop-butyl in Spanish rice fields using NDVI analyses with Sentinel-2. Sentinel-2 and Landsat-8/9 are suitable for general monitoring, while PRISMA and EnMAP enable more precise spectral analyses. WorldView-3 offers high spatial resolution for detailed field studies. The combination of these satellites allows the monitoring of pesticide and herbicide use. Exemplary application of SugarViT (Vision Transformer based model for disease severity) for disease severity prediction in sugar beet using UAV multispectral data is shown in Figure 21; each prediction is completely independent of its surrounding predictions [92].

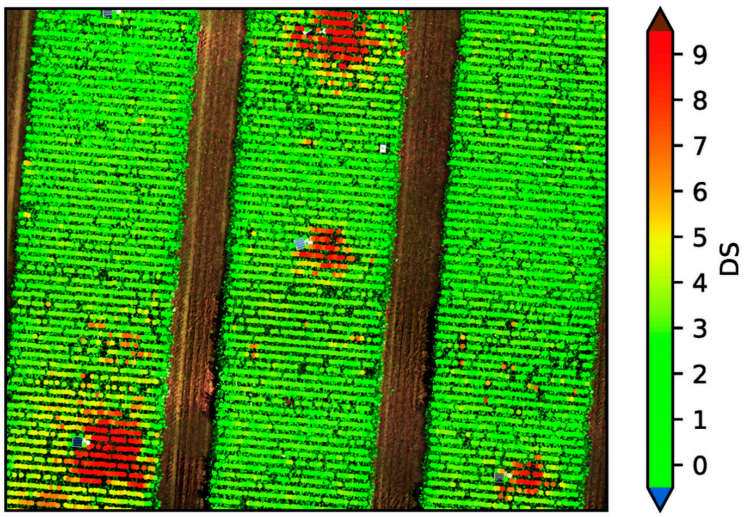

Figure 21. Exemplary application of SugarViT (Vision Transformer based model for disease severity) for disease severity prediction in sugar beet using UAV multispectral data. Each prediction is completely independent of its surrounding predictions. The model shows a highly consistent prediction behaviour (from Günder et al. [92]).

4.5.3. Functional A-LUI Indicators—Fertilisation Intensity

Recording fertilisation intensity using RS is central to precision farming and allows conclusions to be drawn about A-LUI. For example, the intensive use of fertilisers and pesticides promotes a homogeneous and vital vegetation pattern by increasing plant growth and yield quality. Precise nutrient monitoring includes plant traits and nutrient information, with imaging spectroscopy as a key method to determine the nutrient status of crops and soil availability quickly and non-destructively. However, there are challenges as macro- and micronutrients, stress factors, and phenological development stages have similar spectral signatures, which favours confusion at different scales.

Vegetation indices such as the Normalised Difference Vegetation Index (NDVI) quantify plant health and density and provide information on fertilisation and management practices. NDVI is often used to measure plant vigour and derive fertiliser recommendations. Li et al. [205] demonstrated UAV-based hyperspectral imaging to optimise nitrogen stress indices in maize. The Normalised Difference Red Edge Index (NDRE) more precisely determines the chlorophyll and nitrogen content of plants, which Li et al. [205] confirmed for maize. The chlorophyll index also serves as an indicator for nutrient status, whereby hyperspectral data enable an exact determination of the chlorophyll content [205]. Yin et al. [206] used ensemble learning models and Sentinel-2 data to quantify the nitrogen concentration and aboveground biomass of potato plants with a coefficient of determination $R^2 = 0.74$. Almawazreh et al. [207] used UAV to investigate the effects of nitrogen fertilisation on the canopy temperature of agricultural crops in Southern India. Increased nitrogen applications reduced the leaf temperature of maize by 2.1 °C and finger millet by 1.3 °C under sunny conditions. Hossen et al. [208] developed an AI-based, near real-time multispectral sensor solution for drones to accurately estimate the nitrogen content in the soil.

4.5.4. Functional A-LUI Indicators—Soil Organic Carbon (SOC)

Soil organic carbon (SOC) is a key component of soil quality and plays a crucial role in the global carbon cycle [209]. Higher A-LUI (e.g., heavy fertilisation, frequent tillage) generally leads to a decrease in soil organic carbon, as ploughing, erosion, and humus decomposition mineralise carbon more quickly and release it as CO_2. Furthermore, A-LUI influences plant cover and biomass production, which in turn has an impact on carbon storage in the soil. Precise mapping and monitoring of SOC is necessary to develop sustainable agricultural practices and optimise carbon storage in soils.

RS enables efficient and cost-effective monitoring of large areas, provides data from regions that are difficult to access, and allows the continuous recording of SOC dynamics with high temporal resolution [210]. Research on satellite-based SOC mapping started in the 1990s with Landsat TM data, where first correlations between spectral signatures and SOC concentrations were found [211]. These early studies showed promising results, but the spatial resolution was limited to 30 m and correlations often only reached R^2 values of around 0.5, indicating high uncertainties [212]. In the 2000s, high-resolution RS data was combined with ground-based measurements to better map the spatial variability of SOC. Initial attempts to couple soil chemical properties with the Normalised Difference Vegetation Index (NDVI) method from Landsat data demonstrated the importance of vegetation cover for SOC modelling [213]. Studies show that multispectral, hyperspectral, and RADAR sensors on satellite platforms can provide crucial data for SOC mapping [214].

However, optical RS is subject to certain limitations, particularly due to cloud cover. One possible solution is to combine optical- and RADAR-based data [215]. With the introduction of the Sentinel-1 and Sentinel-2 satellites in the 2010s, SOC mapping improved significantly. Sentinel-2 provides multispectral images with a resolution of up to 10 m, while Sentinel-1 provides RADAR images that can be used regardless of weather conditions [215,216]. RADAR data, in particular SAR, has potential for SOC mapping [214,217,218], but parameters such as polarisation, band frequency, orbit, and time window significantly influence the accuracy of the models [219,220]. For example, SAR signals interact differently with vegetation layers depending on wavelength, which means that C-band and L-band systems differ in their applicability. Nevertheless, comprehensive analyses comparing different optical- and RADAR-based sentinel satellites (Sentinel-1/2/3) for SOC mapping are still rare. In recent years, deep learning algorithms and hybrid models have proven to be particularly promising. Recent studies combine optical (Sentinel-2) and RADAR-based (Sentinel-1) RS data to further improve accuracy [221]. In addition, AI-based methods such as Random Forest, Light Gradient Boosting Machine (LGBM), and neural networks have been successfully used for SOC mapping [222,223]. Mean SOC content and C:N ratio maps predicted by 100 runs of BRT in Model V at a resolution of 100 m and their corresponding standard deviation maps (Model V: all available predictors, Sentinel-1-predictors, Sentinel-2 predictors, Landsat-8 predictors, climate predictors, topography predictors) [93] (see Figure 22).

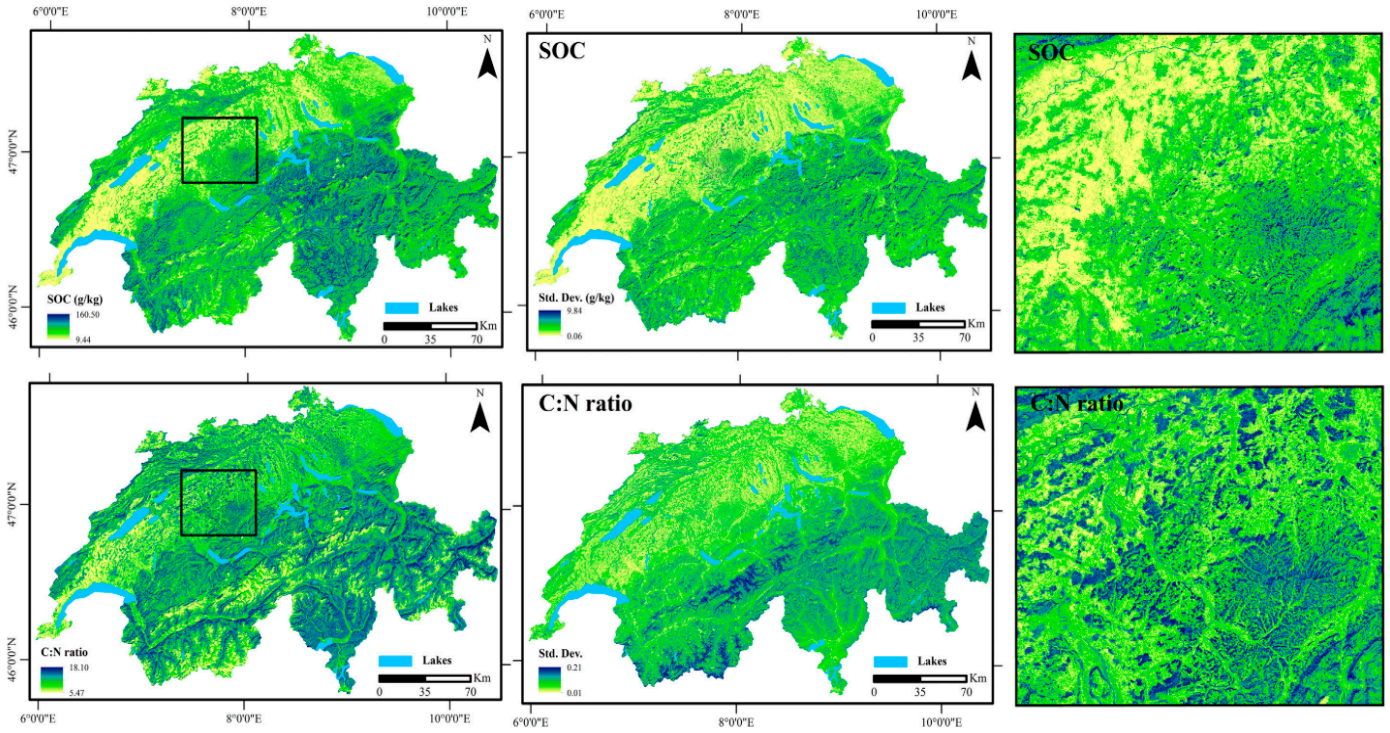

Figure 22. Mean SOC content and C:N ratio maps (100 m resolution) predicted by 100 runs of boosted regression trees (BRT) using multiple predictors (Sentinel-1, Sentinel-2, Landsat-8, climate, and topography). Standard deviation maps indicate model uncertainty (from Zhou et al. [93]).

Table A4 presents a structured overview of functional indicators of A-LUI indicators, including concrete examples, the corresponding RS sensors, and the representative literature references.

5. Examples of Trait–Sensor Linkages

RS offers the ability to monitor A-LUI through proxies that reflect underlying plant and soil traits. While our framework is primarily conceptual, Table A5 provides an illustrative subset of trait–sensor linkages to demonstrate how the taxonomy can be operationalised. The examples cover biochemical, structural, phenological, and genesis traits that respond sensitively to management intensity, and they highlight three key aspects: (1) Sensor characteristics. Different traits are best captured by specific RS technologies. For example, leaf nitrogen and chlorophyll are well resolved with red-edge indices or hyperspectral sensors, while canopy structure is better observed through LiDAR metrics or SAR backscatter. Thermal sensors and radar are essential for detecting water status and irrigation practices, whereas taxonomic composition and diversity require multi-temporal optical classification. (2) Expected directionality with intensity. Intensive management practices such as fertilisation, irrigation, or high sowing density are typically associated with increased canopy greenness, higher LAI and biomass, and more frequent disturbance signals from tillage or harvesting. Conversely, long-term intensive use often leads to declining soil organic matter or reduced crop diversity. These relationships provide measurable signatures of intensity, but their interpretation must be contextualised. (3) Confounding factors. Trait–intensity relationships are not deterministic. Cultivar differences, soil fertility gradients, and climatic variability can mimic or mask management effects. For example, high chlorophyll content may reflect either fertiliser application or inherently fertile soils; frequent harvest signals may stem from double-cropping systems or from regionally specific phenologies. A key research challenge is, therefore, to separate management-driven intensity signals from background biophysical potential and land cover dynamics. This Table A5 is not intended as a complete mapping, but as a demonstration of how conceptual trait categories can be translated into implementable RS indicators. Developing a systematic and validated trait–sensor–management matrix across crop types, agroecological zones, and sensor platforms represents a crucial agenda for subsequent research. Such work will require integration with farm records, independent proxy datasets, and uncertainty quantification to ensure policy-relevant and globally comparable intensity assessments.

While Table A5 focuses on traits and their observable RS proxies, a further step is needed to explicitly link these to management practices and their broader policy relevance. Table A6 extends the trait-based perspective by integrating concrete management actions (e.g., fertiliser application, irrigation, tillage, crop rotation, field consolidation, or hedgerow management) with the traits and processes they influence, the corresponding RS observables, and the resulting A-LUI indicator categories. In addition, the Table specifies validation needs—such as ground sampling, farm records, flux tower data, or biodiversity field surveys—and highlights the potential for direct policy applications, ranging from nutrient efficiency reporting to monitoring compliance with agri-environmental schemes or biodiversity conservation targets.

Together, Tables A5 and A6 illustrate the pathway from plant and soil traits to RS observables, and from there to validated A-LUI indicators that are directly relevant for management and policy. This integrative perspective underscores the importance of trait-based frameworks not only for scientific monitoring but also for supporting evidence-based governance of agricultural intensification.

6. Linking Management, Traits, and RS to A-LUI Indicators, Validation, and Policy

The monitoring of A-LUI requires an integrative perspective that connects management practices with biophysical responses and policy-relevant indicators. Figure 23 provides such a schematic overview, linking management inputs (e.g., fertiliser, irrigation, crop protection, tillage, crop rotations) to plant and soil traits, which serve as the central mediators between human interventions and the biophysical signals recorded by RS. These traits—biophysical, biochemical, and structural properties—can either be measured in situ or derived indirectly from RS data. RS observables and indices such as vegetation indices (NDVI, EVI), solar-induced chlorophyll fluorescence (SIF), soil moisture, or canopy structural metrics derived from LiDAR represent the quantifiable expressions of these traits.

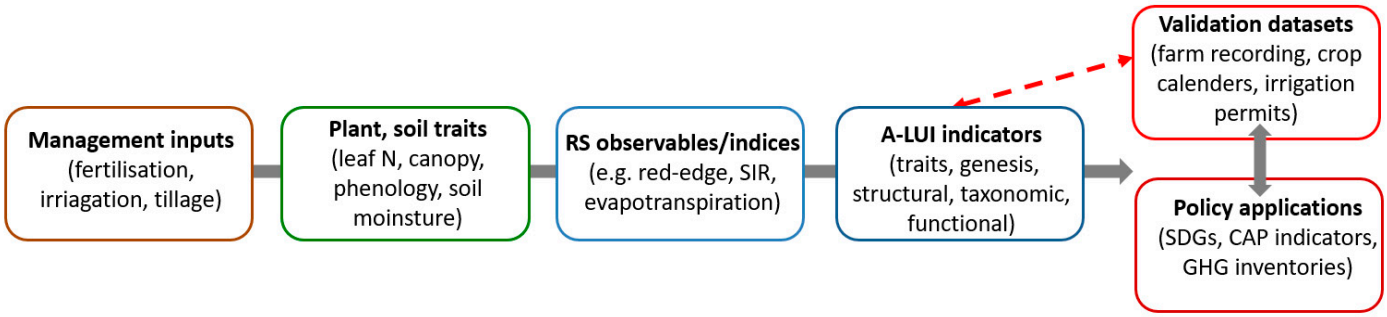

Figure 23. The diagram illustrates the conceptual flow: from management practices (e.g., fertilisation, irrigation, tillage) through trait responses (leaf nitrogen, canopy structure, phenology, root traits, soil organic matter) to RS observables (spectral indices, SIF, SAR, thermal, LiDAR). These feed into the five proposed A-LUI indicator categories (trait, genesis, structural, taxonomic, functional), which can be validated against in situ and administrative data and aligned with policy frameworks (e.g., SDGs, CAP indicators, IPCC inventories).

The framework illustrates how RS-derived observables feed into the five categories of A-LUI indicators: trait, genesis, structural, taxonomic, and functional indicators. Each category addresses a distinct dimension of A-LUI, ranging from biochemical leaf properties (trait indicators) to temporal dynamics (genesis indicators), landscape configuration (structural indicators), crop and species composition (taxonomic indicators), and ecosystem processes (functional indicators). However, RS alone cannot fully capture the underlying causes of change. Hence, the integration of validation datasets—such as ground-based measurements, experimental phenotyping, and farmer-reported management data—is essential to calibrate and verify RS products.

7. From Inputs–Outputs–Impacts to A-LUI Indicators: Advancing the Framework

To better position our proposed A-LUI taxonomy against prior syntheses, we provide a cross-walk between established frameworks of LUI and our five indicator categories. Earlier frameworks have typically emphasised the three-pillar structure of inputs, outputs, and system-level impacts, with some extensions towards land use change intensity, efficiency measures, and socioeconomic drivers. While these approaches provide a solid foundation, they often remain generic and do not explicitly capture the specific opportunities and challenges of RS-based monitoring.

Our new definition (trait, genesis, structure, taxonomic, function) builds on these established dimensions but introduces several novel contributions. In particular, the structural and taxonomic categories add an explicit consideration of field geometry and crop diversity, dimensions often overlooked in previous frameworks. The genesis category uniquely accounts for temporal trajectories of land use intensity, such as crop rotations,

multiple harvests, or abandonment, which are central for RS time-series analysis. Moreover, the taxonomy operationalises agricultural management metrics (e.g., irrigation, fertilisation) through RS proxies, thereby making input intensity directly observable. Finally, by providing a structured indicator appendix and a bridging analysis between challenges, framework categories, and RS/AI solutions, the taxonomy explicitly addresses operational and policy readiness. Table 1 highlights both the conceptual overlaps and the distinct advances of our framework, clarifying how the proposed taxonomy extends beyond previous reviews and offers a more operational and policy-relevant structure for monitoring agricultural land use intensity

Table 1. Cross-walk between established A-LUI frameworks and the proposed A-LUI indicator taxonomy, highlighting overlaps and novel contributions.

Established LUI Framework	Typical Dimensions/Indicators	Corresponding A-LUI Indicator Categories	Conceptual Overlap	Novel Contributions in This Study
Inputs (fertiliser, irrigation, energy, labour, pesticides)	Input intensity, chemical/energy flows	Trait; Functional	Inputs affect plant/soil traits measurable by RS (leaf N, chlorophyll, soil moisture)	Operationalisation of inputs through RS proxies (e.g., irrigation from Sentinel-1, N status from hyperspectral)
Outputs (yield, production, harvested biomass)	Productivity, output per hectare	Functional	Yield proxies and biomass reflect outputs	Explicit RS yield models, link to SDG indicators, inclusion of uncertainty quantification
System-level impacts (biodiversity, soil quality, GHG emissions)	Ecosystem services, species diversity, carbon balance	Structural; Taxonomic; Functional	Impacts partly addressed via land cover, diversity, ecological functions	New explicit categories: Structural (field geometry, fragmentation) and Taxonomic (crop diversity mapping via RS)
Land use/cover change intensity	Expansion, abandonment, conversion rates	Genesis	Sometimes treated as part of 'impacts'	New focus on temporal dynamics and trajectories (e.g., crop rotations, double cropping, abandonment)
Efficiency measures	Output per input (yield per fertiliser, water use efficiency)	Trait; Functional	Implied in productivity frameworks	Potential to derive efficiency metrics from RS (e.g., biomass per water unit via evapotranspiration modelling)
Socioeconomic drivers (markets, subsidies, governance)	Institutional and policy-related intensity factors	Not directly covered	Socioeconomic context linked indirectly	RS–policy linkages highlighted; positioned as future integration pathway
Cross-scale integration (local–regional–global)	Aggregated indicators for monitoring	All categories + indicator appendix	Often missing in prior reviews	Indicator appendix as reference tool; bridging table (challenges → solutions) for operational uptake

8. New Approaches for the Quantification and Evaluation of A-LUI Using RS

8.1. RS and AI for Recording A-LUI

The precise recording of A-LUI is central to quantifying the impact of agricultural management on ecosystems and developing sustainable strategies. Recently, RS and artificial intelligence (AI) have established themselves as key technologies for recording agricultural utilisation intensities on a large scale, promptly and objectively [224]. RS data and its time series such as Sentinel-2, Landsat-8, MODIS, or WorldView-3 provide high-resolution information on vegetation, soil surface, and hydrology, allowing numerous indicators to be derived (see Table A7), which are closely related to agronomic interventions

such as fertilisation, tillage, detection of crop rotations, harvest cycles, and tillage patterns or multiple harvests per year as characteristics of A-LUI [225,226].

A critical step in interpreting these data are the integration of AI methods, in particular machine learning and deep learning, which can recognise complex, non-linear patterns in large, heterogeneous datasets. AI models such as Convolutional Neural Networks (CNNs), Support Vector Machines (SVMs), or Random Forests (RF) have been successfully used many times in the literature to quantify characteristics such as nutrient availability, plant health, or management practices [226–228]. For example, Castaldi et al. [229] used Sentinel-2 data to derive soil organic carbon, indicating many years of intensive use. Shi et al. [230] combined RGB images with Backpropagation Neural Networks (BPNN) to estimate nitrogen accumulation and biomass in rice fields. This allows conclusions to be drawn about fertiliser intensity and growth potential. Sahabiev et al. [231] extended these approaches by incorporating soil characteristics (e.g., organic carbon, soil texture) into ML models for the spatial prediction of nutrient distributions. A particularly relevant example in the context of utilisation intensity is the use of CNNs to detect crop cycles, which is made possible by the time series of satellite images (e.g., Sentinel-2 or MODIS). The detection of multiple harvests or intensive crop rotations is possible by analysing NDVI time histories [232,233]. In this context, Wang et al. [226] demonstrated that a combined LSTM-CNN model, trained with weather and soil data, was able to provide very precise predictions of the winter wheat harvest in China—a direct measure of output intensity. Various methods have also been established for nutrient intensity. Jaihuni et al. [234] used deep learning to estimate the spatio-temporal distribution of nitrogen, potassium, and phosphorus.

Despite these successes, challenges remain: The technical complexity of RS data processing requires specialised expertise and high-performance infrastructures [224]. High-resolution data material, such as UAV-based hyperspectral images, is often only available locally. There is a lack of standardised definitions and indicators for deriving A-LUI, which makes comparability between regions difficult [235]. In addition, many deep learning models are difficult to interpret—a problem that recent work on Explainable AI (XAI) aims to counteract.

Nevertheless, future prospects are extremely promising. New architectures such as edge cloud computing or the edge cloud continuum make it possible to process large amounts of data in a decentralised manner on sensors and drones [224]. At the same time, methods such as transfer learning or few-shot learning allow models to be adapted for new regions with little training data [226,236]. This could make globally standardised, AI-supported maps of land use intensity a reality—a valuable tool for agricultural policy, climate protection, and sustainable land use worldwide [224].

8.2. Semantic Web and Linked Open Data for the Monitoring of A-LUI

Semantic web integration (SWI) and linked open data (LOD) approaches are designed to make heterogeneous datasets interoperable, machine-readable, and reusable across institutions and platforms. For A-LUI monitoring, this is highly relevant because RS-derived indicators, in situ measurements, farm management records, and policy data often exist in separate silos and use inconsistent terminologies. Semantic technologies provide a way to bridge these gaps by assigning shared vocabularies and ontologies to different data sources [237,238]. At their core, semantic technologies such as RDF (Resource Description Framework), OWL (Web Ontology Language), and SPARQL (a query language) create a common structure that allows datasets to be linked through concepts rather than file formats. For example, different databases may store information on "crop type," "fertilisation," or "irrigation." Through a shared ontology, these concepts can be

harmonised, enabling automated queries and reasoning across datasets. For A-LUI monitoring, the main advantage is the ability to connect three layers of information: (1) RS indicators (e.g., crop type maps, soil moisture, vegetation indices, yield proxies). (2) Farm and management data (e.g., fertiliser application, irrigation logs, crop rotations). (3) Policy and sustainability frameworks (e.g., SDG 2.4.1 on sustainable agriculture, FAO agri-environmental indicators). This integration allows complex questions to be addressed consistently, such as "Which wheat fields in Region X received irrigation in 2023 and show high biomass in Sentinel-2 indices?" or "How do RS-derived nitrogen proxies correspond to reported fertilisation levels in regional statistics?" A practical example illustrates this potential. RS-derived crop classification maps (e.g., from Sentinel-2) can be linked to farm irrigation and fertilisation records. Using an ontology that defines shared concepts like "crop type" and "management practice", a query could identify all irrigated maize fields with high NDVI values in a given season. The semantic web layer then produces a harmonised map or table that combines RS and farm data into a single, policy-relevant product. For practitioners, this means that information which today is scattered across agencies (satellite data at space agencies, farm logs at agricultural offices, policy indicators at statistical bureaus) could be accessed in one place, with automated links ensuring consistency. For researchers, this enhances reproducibility and data transparency, as datasets can be cited and queried through open standards. At present, such applications remain in pilot and prototyping stages, with operational deployment still limited. Therefore, we present semantic web and linked open data approaches as a future prospect for A-LUI monitoring. Their adoption could greatly enhance the integration of RS and management data, improve cross-scale comparability, and facilitate alignment with international monitoring frameworks (Figure 24).

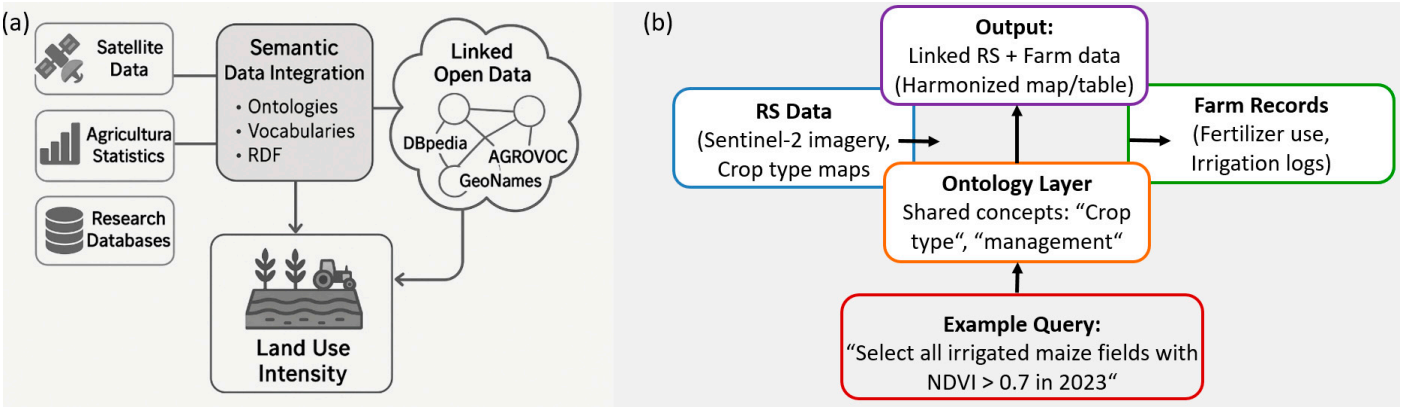

Figure 24. (**a**) Semantic data integration for assessing A-LUI. Integration of diverse data sources (satellite data, soil data, agricultural statistics, research databases, socioeconomic information, model data) linked open data (LOD), AGROVOC (AGRO = Agriculture, VOC = Vocabulary of the FAO). (**b**) A schematic figure visualise this concept for practitioners: RS data (satellite imagery → crop type map), Farm records (fertiliser log, irrigation schedule), Ontology layer: Shared concepts like "crop type," "management practice," "season" represented as semantic links, SPARQL query box: Example query: "Select all irrigated maize fields with NDVI > 0.7 in 2023.", Output: harmonised map or table showing linked information.

9. Conclusions and Further Research

This review synthesised current concepts, definitions, and methodological approaches for monitoring A-LUI with a particular focus on RS- and trait-based indicators. By proposing a structured taxonomy that distinguishes trait, genesis, structural, taxonomic, and functional indicators, we aimed to bring conceptual clarity and to align RS-

derived measures more explicitly with established A-LUI dimensions. The review highlights how traits can serve as a common denominator between in situ measurements and RS proxies, and how linking traits to measurable observables helps to bridge methodological and disciplinary gaps.

At the same time, our synthesis demonstrates the limitations and uncertainties inherent in RS-based monitoring of A-LUI. Cultivar-specific differences, mixed pixels, sensor saturation, and phenological variation can bias indicator derivation and interpretation. While we have outlined representative examples and conceptual solutions, systematic validation strategies remain a major research need. Future work should, therefore, prioritise long-term, multi-scale validation efforts that combine ground measurements, phenotyping infrastructures, and RS observations.

Another frontier is the development of operational frameworks that can integrate existing datasets (e.g., FAO, OECD, Eurostat) with Earth Observation-derived indicators in a transparent and standardised manner. Progress in open-source data infrastructures and community repositories provides promising entry points, but dedicated projects are needed to ensure consistency, accessibility, and long-term comparability.

Looking ahead, further research should address the following:

The design of multi-scale validation protocols to quantify uncertainty and improve indicator robustness.
The integration of hyperspectral, thermal, and radar missions with AI-based approaches for trait retrieval and intensity mapping.
The differentiation of management intensity signals from biophysical potential and land cover dynamics through coupled RS–model frameworks.
The systematic assessment of smallholder and heterogeneous landscapes, where high-resolution data and advanced image analysis are crucial.
The establishment of specialised studies focusing on cultivar-specific effects, phenological corrections, and management practices that cannot yet be robustly inferred from RS alone.

In conclusion, while significant progress has been made in conceptualising and operationalising RS-based A-LUI monitoring, a globally consistent and validated framework is still in development. By clarifying definitions, structuring indicator categories, and highlighting limitations, this review provides a foundation for subsequent studies to address these open challenges and to move towards an integrated, transparent, and scalable monitoring of agricultural land use intensity.

Author Contributions: A.L., F.H.: conceptualisation, methodology, writing—original draft preparation, writing—review and editing, visualisation, J.B.: supervision; P.S., J.B., M.P., T.Z., A.J.: investigation, resources, visualisation, writing—review and editing. All authors have read and agreed to the published version of the manuscript.

Funding: This research received no external funding.

Data Availability Statement: No data were integrated in this paper.

Acknowledgments: Our special thanks go to the Helmholtz Centre for Environmental Research—UFZ and the TERENO project, funded by the Helmholtz Association and the Federal Ministry of Education and Research, for providing the remote sensing research. The authors gratefully acknowledge the German Helmholtz Association for supporting the activities of research data science approaches and advanced data technologies. András Jung was supported by project No. TKP2021-NVA-29, which was implemented with the support of the Hungarian Ministry of Culture and Innovation from the National Fund for Research, Development, and Innovation under the TKP2021-NVA funding programme.

Conflicts of Interest: The authors declare no conflicts of interest.

Abbreviations

A-LUI	Agricultural Land-Use Intensity
AGROVOC	Agricultural Vocabulary (FAO controlled vocabulary)
AI	Artificial Intelligence
CHIME	Copernicus Hyperspectral Imaging Mission for the Environment
EnMAP	Environmental Mapping and Analysis Programme
ET	Evapotranspiration
EUROSTAT	Statistical Office of the European Union
EVI	Enhanced Vegetation Index
FAO	Food and Agriculture Organisation of the United Nations
FLEX	Fluorescence Explorer
GEDI	Global Ecosystem Dynamics Investigation
GHG	Greenhouse Gas
GIS	Geographic Information System
GLAD	Global Land Analysis and Discovery
GLC	Global Land Cover
GPP	Gross Primary Productivity
HISUI	Hyperspectral Imager Suite
HyspIRI	Hyperspectral Infrared Imager
IACS	Integrated Administration and Control System
IPCC	Intergovernmental Panel on Climate Change
LAI	Leaf Area Index
Landsat	Land Satellite (USGS/NASA Earth observation programme)
LiDAR	Light Detection and Ranging
LUCAS	Land Use/Cover Area Frame Survey
ML	Machine Learning
MODIS	Moderate Resolution Imaging Spectroradiometer
NDVI	Normalised Difference Vegetation Index
OECD	Organisation for Economic Co-operation and Development
PlanetScope	High-resolution satellite constellation operated by Planet Labs
PRISMA	PRecursore IperSpettrale della Missione Applicativa
RS	Remote Sensing
SAR	Synthetic Aperture Radar
SDG	Sustainable Development Goal
Sentinel-1	C-band Synthetic Aperture Radar mission (Copernicus)
Sentinel-2	Multispectral optical imaging mission (Copernicus)
Sentinel-3	Ocean and land monitoring mission (Copernicus)
Sentinel-5P	Tropospheric monitoring mission (Copernicus)
SHALOM	Spaceborne Hyperspectral Applicative Land and Ocean Mission
SIF	Solar-Induced Fluorescence
SOC	Soil Organic Carbon
UAV	Unmanned Aerial Vehicle
World Bank	World Bank (International Financial Institution)

Appendix A

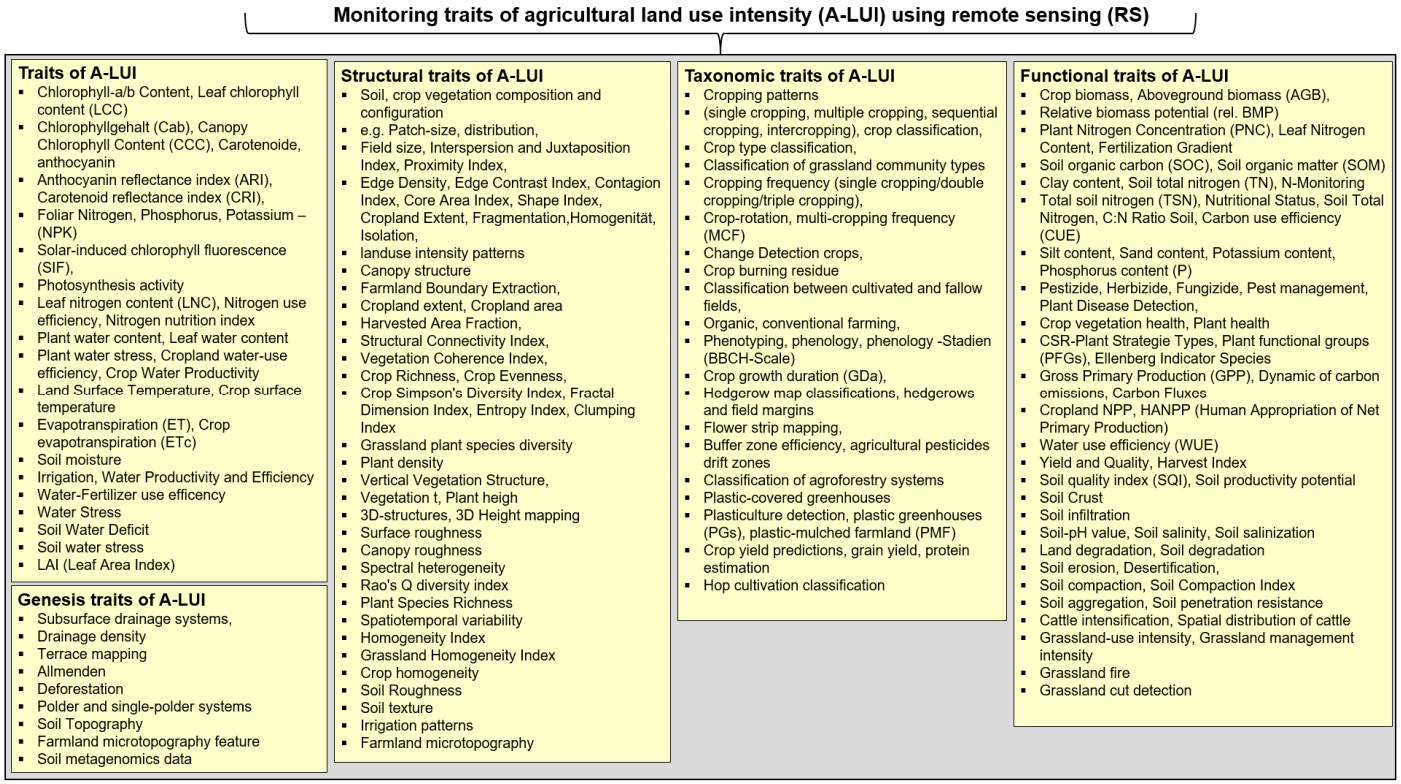

Figure A1. Monitoring the five characteristics of A-LUI using RS. These are traits of A-LUI, genesis traits of A-LUI, structural traits of A-LUI, taxonomic traits of A-LUI, functional traits of A-LUI with examples.

Table A1. Geographical area of monitoring, temporal availability of indicators, link, and selected examples of indicators for measuring and monitoring A-LUI; carried out by the FAO, OECD, World Bank and EUROSTAT.

	FAO	OECD	World Bank	EUROSTAT
Geographical area of monitoring	• Worldwide coverage, with a special focus on developing countries	• Primarily OECD member countries, focus on highly developed industrialised nations	• Developing countries and emerging markets	• European Union (EU) and some enlargement countries
Time availability of the indicators	• Indicators of land use intensity have been available since the 1960s, • Increased surveillance since the 1990s	• Data and analyses on land use intensity since the 1980s, • Regular reports since the early 2000s.	• Data on land use intensity since the 1990s, • Comprehensive database (WDI) since the 2000s.	• Harmonised data on agriculture and land use since the 1990s, • Regular (every three to five years) surveys since the 1990s
Link	• FAO database FAOSTAT • https://www.fao.org/statistics/data-dissemination/agrifood-	• OECD • https://www.oecd.org/, (data access: 11 July 2024)	• World Development Indicators (WDI) • https://databank.worldbank.org/source/world	• Farm Structure Surveys (FSS) • https://ec.europa.eu/eurostat/web/micro-

	systems/en, (data access: 11 July 2024)		-development-, (data access: 11 July 2024)	data/farm-statistics?utm_source=chatgpt.com (data access: 22 October 2025)
Indicators (selective examples)				
Indicator	**FAO**	**OECD**	**World Bank**	**Eurostat**
Agricultural area	Total area for agriculture (arable land, permanent grassland, permanent crops)	Agricultural land, including arable land, permanent crops, and pastures	Agricultural land (sq. km)	Utilised agricultural area (UAA)
Arable land	Land for crops, including repeatedly cultivated soils and fallow land	Arable land, including temporary crops and fallow land	Arable land (hectares)	Arable land
Permanent grassland	Land for perennial grasses and forage plants	Permanent pastures and meadows	Permanent meadows and pastures (hectares)	Permanent grassland
Permanent crops	Land for perennial crops such as fruit trees and vineyards	Permanent crops, such as orchards and vineyards	Permanent crops (hectares)	Permanent crops
Harvest yields	Amount of crop per unit area	Crop yields, measured by specific crop outputs per hectare	Cereal yield (kg per hectare)	Crop production per unit area
Use of fertilisers	Amount of fertiliser per hectare	Fertiliser consumption (kg per hectare of arable land)	Fertiliser consumption (kg per hectare of arable land)	Consumption of fertilisers per unit area of agricultural land
Pesticide use	Amount of pesticides per hectare	Pesticide sales and usage	Pesticide consumption (kg per hectare of arable land)	Pesticide sales and consumption
Irrigated area	Proportion of artificially irrigated agricultural land	Area equipped for irrigation (hectares)	Irrigated land (% of total agricultural land)	Irrigated area
Machine inventory	Number and type of machines per unit area	Agricultural machinery, such as tractors per hectare	Agricultural machinery (tractors per 100 sq. km of arable land)	Number of tractors and other agricultural machinery per unit area of agricultural land
Labour input	Labour hours per unit area	Labour input in agriculture, measured by hours worked per hectare	Employment in agriculture (% of total employment)	Labour force in agriculture
Livestock density	Number of animals per unit area of pastureland	Livestock density, measured as livestock units per hectare of pasture land	Livestock production index	Livestock density per unit area of pasture land
Carbon sequestration in the soil	Amount of carbon sequestered in the soil	Soil organic carbon content	Soil organic carbon content	Soil organic carbon content
Ground cover	Type and extent of ground cover	Land cover types and changes	Land cover (% of land area)	Land cover and land use
Erosion risk	Risk of soil erosion due to water or wind	Soil erosion rates	Soil erosion rates	Soil erosion and degradation risk
Biodiversity	Diversity of plant and animal species on farmland land (e.g.,	Farmland biodiversity indices (e.g., Farmland	Agricultural biodiversity indices (e.g.,	Biodiversity indicators in agricultural landscapes

	Farmland birds, pollinators, butterflies)	birds, pollinators, butterflies)	Farmland birds, pollinators, butterflies)	(e.g., Farmland birds, pollinators, butterflies)
Water consumption in agriculture	Amount of water used for irrigation	Agricultural water withdrawal	Agricultural water withdrawal (% of total water withdrawal)	Water use in agriculture
Agricultural production per unit of input	Efficiency of the means of production in agriculture	Total factor productivity in agriculture	Agricultural value added per worker	Output per hectare of agricultural land
Energy consumption in agriculture	Energy consumption in agriculture	Energy use in agriculture	Energy use in agriculture	Energy consumption in agriculture
Sustainability indicators	Sustainability of agricultural practices	Sustainable agriculture practices indicators	Sustainable land management indicators	Sustainable farming practices
Climate impact of agriculture	Greenhouse gas emissions from agriculture	Greenhouse gas emissions from agriculture	Agricultural methane emissions (kt of CO2 equivalent)	Greenhouse gas emissions from agriculture
Nutrient balance in the soil	Balance of nitrogen and phosphorus in the soil	Nitrogen and phosphorus balance	Soil nutrient balance	Nutrient balance in agricultural soils
Bioproductivity	Productivity of biological systems on agricultural land	Biological productivity of agricultural systems	Agricultural productivity indexes	Biological productivity of agricultural lands
Plant protection measures	Measures to combat pests and diseases	Pest and disease control practices	Pest and disease control indicators	Plant protection measures and their impact
Energy efficiency in agriculture	Efficiency of energy consumption in agriculture	Energy efficiency in agricultural practices	Energy productivity in agriculture	Energy efficiency indicators in farming
Utilisation of genetic resources	Utilisation and conservation of genetic resources in agriculture	Use and conservation of genetic resources	Genetic resource management indicators	Conservation and use of agricultural genetic resources
Landscape diversity	Diversity of landscapes and agroecosystems	Landscape diversity and heterogeneity	Landscape diversity indicators	Landscape heterogeneity and diversity in agricultural areas
Soil compaction	Degree of soil compaction caused by agricultural machinery	Soil compaction indicators	Soil compaction risk	Soil compaction due to agricultural practices
Waste management in agriculture	Handling agricultural waste	Agricultural waste management practices	Waste management in agriculture	Management and recycling of agricultural waste
Soil moisture	Moisture content of the soil	Soil moisture levels	Soil moisture content indicators	Soil moisture monitoring in agricultural lands
Landscape fragmentation	Fragmentation of natural and agricultural landscapes	Landscape fragmentation and its impact on agriculture	Landscape fragmentation indexes	Impact of landscape fragmentation on agriculture
Sustainable land use practices	Spreading sustainable agricultural practices	Adoption of sustainable agricultural practices	Sustainable land management practices	Implementation of sustainable farming practices
Water utilisation efficiency	Efficiency of water utilisation in agriculture	Water use efficiency in agricultural practices	Agricultural water productivity	Water use efficiency in irrigated agriculture
Agroecological indicators	Indicators for the assessment of agroecological systems	Agroecological assessment indicators	Agroecological practices	Assessment of agroecological systems

Erosion due to wind	Loss of topsoil due to wind erosion	Wind erosion rates	Wind erosion indicators	Impact of wind erosion on agricultural land
Soil fertility	Level of soil fertility and its changes	Soil fertility levels	Soil fertility indicators	Changes in soil fertility
Land use changes	Changes in the utilisation of agricultural land	Changes in agricultural land use	Land use change indicators	Agricultural land use changes
Irrigation efficiency	Efficiency of irrigation methods	Irrigation efficiency	Efficiency of irrigation systems	Efficiency of water use in irrigation systems
Climate adaptation measures	Measures to adapt to climate change	Climate adaptation practices in agriculture	Climate resilience indicators	Implementation of climate adaptation measures in agriculture
Resource utilisation efficiency	Efficient use of natural resources	Resource use efficiency in agriculture	Resource productivity indicators	Efficiency of resource use in agriculture
Soil acidification	Degree of soil acidification and its causes	Soil acidification levels	Soil pH indicators	Impact of acidification on agricultural soils
Soil salinisation	Level of soil salinisation and its effects	Soil salinisation rates	Soil salinity indicators	Effects of salinisation on agricultural productivity
Utilisation of renewable energies	Share of renewable energies in agriculture	Renewable energy use in agricultural practices	Share of renewable energy in agriculture	Use of renewable energy sources in farming
Environmentally friendly cultivation methods	Spreading environmentally friendly cultivation methods	Adoption of eco-friendly farming practices	Eco-friendly agricultural practices	Implementation of environmentally friendly farming methods
Economic sustainability	Economic viability of farms	Economic sustainability of agricultural holdings	Economic viability indicators	Economic sustainability of farms
Social sustainability	Social aspects of agricultural practice	Social sustainability in agriculture	Social indicators in rural areas	Social impacts of agricultural practices
Productivity per unit area	Productivity of agricultural land	Land productivity indicators	Productivity of agricultural land	Output per unit of agricultural area
Water quality indicators	Impact of agriculture on water quality	Impact of agriculture on water quality	Water quality in agricultural areas	Effects of agricultural runoff on water quality
Infrastructure for agriculture	Availability and quality of agricultural infrastructure	Agricultural infrastructure development	Infrastructure investment in agriculture	Quality and accessibility of agricultural infrastructure
Innovation in agriculture	Implementation of new technologies and processes	Agricultural innovation and technology adoption	Innovation indicators in agriculture	Adoption of new agricultural techn

Table A2. High spatial resolution satellite missions, sensor/type, spatial resolution, spectral bands/type, availability, launch date and operator.

Satellite/Mission	Sensor/Type	Spatial Resolution	Spectral Bands/Sensor Type	Availability	Start Date	Operator of the Satellite Mission
WorldView-3	Visible (PAN+MS+SWIR)	0.31 m (PAN), 1.24 m (MS)	Panchromatic Multispectral SWIR	Commercial	2014	Maxar
WorldView-2	Optically	0.46 m (PAN), 1.84 m (MS)	Panchromatic Multispectral	Commercial	2009	Maxar
GeoEye-1	Optically	0.41 m (PAN), 1.65 m (MS)	Panchromatic Multispectral	Commercial	2008	Maxar
Pleiades Neo	Optically	0.3 m (PAN), 1.2 m (MS)	Panchromatic Multispectral	Commercial	2021+	Airbus

Pleiades 1A/1B	Optically	0.5 m (PAN), 2.0 m (MS)	Panchromatic Multispectral	Commercial	2011/2012	Airbus
SkySat	Optically + Video	0.5–0.8 m (PAN), 1–2 m (MS)	RGB, NIR, Video	Commercial	2013+	Planet
BJ-3B (Super-View-2)	Optically	0.3 m (PAN), 1.2 m (MS)	Panchromatic Multispectral	Commercial	2022	21AT (China)
Capella Space	RADAR (X-Band SAR)	0.3–0.5 m (Spotlight)	SAR	Commercial	2018+	Capella Space (USA)
ICEYE	RADAR (X-Band SAR)	0.25–1 m	SAR	Commercial	2018+	ICEYE (Finland)
TerraSAR-X	RADAR (X-Band SAR)	bis 1 m (Spot-light-Modus)	SAR	Commercial/Sci-entifically free	2007	DLR/Airbus
PAZ	RADAR (SAR)	1 m	SAR (X-Band)	Commercial	2018	Hisdesat (Spain)
Sentinel-1A/B	RADAR (C-Band SAR)	10 m	SAR	Freely available	2014/2016	ESA/Copernicus
Drohnen/UAV	Optically + Multispectral	<0.1 m	RGB, Multispectral, Hyperspectral, Li-DAR	Own operation		User-based
Aerial photos	Optically	0.20 cm	Orthophotos (DOP) True Orthophotos, RGB, CIR	Commercial/Au-thorities and partly scientific free		Federal states, Federal Agency for Cartography and Geodesy

Table A3. Linking key challenges of monitoring agricultural land use intensity (A-LUI) with RS to the proposed indicator framework categories and potential RS/AI-based solutions.

Challenge	Relevant Frame-work Category	Possible RS/AI Solution	Example Application
Distinguishing intensive vs. extensive cultivation (e.g., organic vs. conventional)	Trait indicators	Hyperspectral indices (red-edge, SIF) combined with AI crop classification	Separation of organic vs. conventional wheat fields using Sentinel-2 red-edge indices
Seasonal dynamics and multiple harvests	Genesis indicators	Multi-temporal analysis (Sentinel-1/2, SAR–optical fusion); AI-based phenology detection	Identification of double-cropping sys-tems in India
Irrigation and water man-agement	Functional indica-tors	Radar-derived soil moisture (Sentinel-1), thermal RS for evapotranspiration, AI sepa-ration of natural vs. man-aged water stress	Mapping irrigation events in Mediterra-nean orchards
Fertiliser and pesticide ap-plication (not directly visi-ble in RS)	Trait and func-tional indicators	Indirect proxies: leaf N con-tent, chlorophyll indices, stress detection; ML calibra-tion with in situ records	Estimating nitrogen application in maize with UAV hyperspectral imaging
Small-scale heterogeneous fields	Structural indica-tors	High-resolution UAV/Planet imagery; OBIA; deep learn-ing for parcel boundary de-lineation	Smallholder mapping in Sub-Saharan Africa using PlanetScope + CNN
Agroforestry and mixed cropping	Taxonomic indica-tors	Hyperspectral UAV imag-ing and AI spectral unmix-ing	Differentiating coffee under shade trees in agroforestry systems

Limited spectral resolution of standard satellites	Trait and functional indicators	Integration of hyperspectral missions (EnMAP, PRISMA, CHIME); AI-based spectral downscaling	Improved stress detection in crops using EnMAP data
Climate and topographic confounding effects	Genesis & Functional indicators	AI domain adaptation, topographic correction, normalisation with weather/soil data	Adjusting RS-based yield intensity estimates in mountainous regions

Table A4. Various indicators for measuring A-LUI that can be detected using RS. Here is a comprehensive table summarising the various indicators for measuring A-LUI and landscape structure that can be measured using RS.

Indicators	Satellites	References
Trait diversity of A-LUI		
Chlorophyll-a/b Content Leaf chlorophyll content (LCC) Chlorophyllgehalt (Cab) Canopy Chlorophyll Content (CCC) Carotinoide, anthocyanin Anthocyanin reflectance index (ARI) Carotenoid reflectance index (CRI)	Sentinel-1 [1], Sentinel-2 [1], Landsat 8 [1], CRIME [1], EnMAP[1], Airborne hyperspectral CASI [2], Airborne Visible/Infrared Imaging Spectrometer AVIRIS [2], Airborne HyMap [2], UAV-(HSP,MSP) [3], Handheld portable hyperspectral camera (Specim IQ) ASD [4], Laboratory spectroscopy [5]	[86,96,102,105,118,239–251]
Foliar Nitrogen, Phosphorus, Potassium—NPK	UAV (LiDAR, MSP) [3], SVC HR-1024i spectrometer ASD [4]	[86,252,253]
Solar-induced chlorophyll fluorescence (SIF), Photosynthesis activity	Sentinel-3 [1], GOSIF data [1], AS-SpecFOM (ground-based) [6], FluoSpec2 system (ground-based)	[72,107,254–257]
Leaf nitrogen content (LNC) Nitrogen use efficiency, Nitrogen nutrition index	Sentinel-2 [1], CRIME [1], PRISMA [1],Airborne micro-hyperspec NIR-100 camera [2], UAV	[86,96,98,119,120,258,259]
Plant water content Leaf water content Plant water stress Cropland water-use efficiency Crop Water Productivity	GLASS [1], Landsat [1], Sentinel-2 [1], UAV (MSP, HSP) [3], mmWave RADAR (Tower) [6], Cropland ecosystem flux sites [6], Local TIR Sensor [6],	[260–268]
Land Surface Temperature Crop surface temperature	Landsat [1], High Spatio-Temporal Resolution Land Surface Temperature Monitoring (LSTM) Mission [1], UAV (TIR, RGB, MSP) [3]	[264,269–273]
Evapotranspriration (ET) Crop evapotranspiration (ETc)	MODIS [1], DEIMOS-1 is a commercial tasking EO satellite [1], Landsat [1], Sentinel-2 [1], SuperDove satellites (PlanetScope) [1], UAV-(RGB, MSP, TIR) [3]	[274–282]
Soil moisture	MODIS-Terra [1], Landsat [1], AMSR-2 [1], AMSR-E [1], NISAR [1], Sentinel-1 [1], Sentinel-2 [1], SMAP [1], Airborne hyperspectral (DAIS) [2], Airborne hyperspectral (AISA Eagle, Hawk) [2]	[283–291]
Irrigation Irrigation Efficiency Water Productivity and Efficiency Irrigation patterns	MODIS [1], Landsat [1], Sentinel-2 [1], UAV (MSP) [3], ASD [4],	[292–303]

Water-Ferilizer use efficency Water Stress Soil Water Deficit Soil water stress		
LAI (Leaf Area Index)	MODIS [1], Landsat [1], Sentinel-2 [1], UAV-(HSP, TIR, LiDAR) [3], Ocean Optics USB2000 (Tower) [6]	[247,248,304–306]
Genesis Trait Diversity of A-LUI		
Subsurface drainage systems, Drainage density	RADAR (SAR) [1], Landsat [1], Senitnel-2 [1], Airborne LiDAR [2], Airborne data [2], UAV–RGB, CIR, TIR [3]	[132–136,307,308]
Terrace mapping	Landsat [1], Sentinel-1 [1], Sentinel-2 [1], GF-2 satellite image [1], WorldView-1 [1], WorldView-3 [1], Airborne LiDAR [2], UAV-LiDAR [3]	[87,137,138,143–145]
Allmenden	Airborne LiDAR [3]	[146,147]
Deforestation	MODIS [1], ALOS PALSAR data [1], RADARSAT-2 [1], Landsat [1], Sentinel-1 [1], Sentinel-2 [1], UAV (RGB, NIR, IRT) [3]	[150–154,309–312]
Polder and single-polder systems	Google Earth RS data [1], Corona spy satellite imagery [1]	[313,314]
DEM (Digital Elevation Model) DSM (Digital Surface Model)	SRTM [1], TerraSAR-X [1], TanDEM-X [1], Sentinel-1 [1], Sentinel-3 [1], ALOS-2 PALSAR-2 [1], ALOS PRISM [1], Terra ASTER [1], ICESat GLAS [1], Airborne LiDAR [2], UAV (SAR, RGB) [3]	[61,315–327]
Soil Topography Farmland microtopography feature	Landsat [1], Sentinel-1 [1], Sentinel-2 [1], CORONA KH-4B [1], Gaofen-7 satellite [1], Airborne LiDAR [2]	[171,328–332]
Soil metagenomics data	UAV (MSP, LiDAR) [3]	[333]
Structural traits of A-LUI		
Soil, crop vegetation composition and configuration (e.g., patch size, distribution Field size, Interspersion and Juxtaposition Index, Proximity Index, Edge Density, Edge Contrast Index, Contagion Index, Core Area Index, Shape Index, Cropland Extent, Fragmentation, Homogeneity, Isolation, land use intensity patterns, Canopy structure Farmland Boundary Extraction, Cropland extent, Cropland area, Harvested Area Fraction, Structural Connectivity Index, Vegetation Coherence Index, Crop Richness, Crop Evenness, Crop Simpson's Diversity Index, Fractal Dimension Index, Entropy Index, Clumping Index, Grassland plant species diversity Plant density	MODIS [1], Landsat [1], Spot [1], Sentinel-2 [1], WorldView-2/-3 [1], QuickBird [1], Pleiades [1], GeoEye [1], GF-2 [1], RapidEye [1], PlanetScope [1], Airborne Hyperspectral AVIRIS and HYDICE [2], Airborne data [2], UAV (RGB, MSP, HSP) [3]	[31,33,67,88,161,162,258,334–349]
Vertical Vegetation Structure, Vegetation height, Plant height	GEDI LiDAR [1], ICESat-2 [1], UAV (RGB, LiDAR)	[350–355]

3D-structures, 3D mapping	Phenotyping robot "MARS-PhenoBot" [6], 6-DOT robot [6], RGB-Camera [6], Terrestrial Li-DAR [6]	
Surface roughness Canopy roughness	Sentinel-1 [1], MODIS [1], UAV (RGB) [3]	[167–169]
Spektraler Heterogenität, Rao's Q diversity index, Plant Species Richness Spatiotemporal variability	MODIS [1], Landsat [1], Sentinel-2 [1]	[165,166,356]
Homogeneity Index, Grassland Homogeneity Index Crop homogeneity	Sentinel-1 [1], Sentinel-2 [1], GF-2 [1]	[357–359]
Soil Roughness, Soil texture, Farmland microtopography	Landsat [1], Sentinel-1 [1], Sentinel-2 [1], AHSI/ZY1-02D satellite [1], SRTM [1], Airborne LiDAR [2], ASD Handspectometer [4], Smartphone-captured digital images [6]	[171,172,332,360–368]
Taxonomic A-LUI		
Cropping patterns (single cropping, multiple cropping, sequential cropping, inter-cropping)	MODIS [1], Spot [1], Landsat [1], Sentinel-1 [1], Sentinel-2 [1], IRS [1], WiFS [1], Airborne AVIRIS [2], RADARSAT-2 [1], Airborne LiDAR [2]	[155,173–183,186,369,370]
Crop classification, Crop type classification Crop type mapping	MODIS [1], Landsat [1], Sentinel-1 [1], Sentinel-2 [1], Sentinel-3 [1], Airborne AVIRIS [2], UAV (HSP) [3]	[90,142,156,371–377]
Classification of grassland community types	Landsat [1], Sentinel-1 [1], Sentinel-2 [1]	[378–380]
Cropping frequency (single cropping/double cropping/triple cropping) Crop rotation Multi-cropping frequency (MCF) Cropping intensity Cropping intensity index Change Detection crops	MODIS [1], Gaofen-1 [1], GF-1 [1], Landsat [1], Sentinel-1 [1], Sentinel-2 [1]	[174,187,341,370,381–390]
Crop residue cover mapping	Landsat [1], Sentinel-2 [1], Google Earth Engine [1], UAV [3], FieldSpec Pro [4], Photo analysis surveys [6]	[391–396]
Crop burning residue	MODIS [1], AVHRR [1], LISS-III [1], LISS-IV [1], UAV [3]	[397–399]
Classification between cultivated and fallow fields	MODIS [1], Landsat [1], Sentinel-2 [1]	[369,381,400–402]
Organic, conventional farming Organic and non-organic farming	Landsat [1], Spot [1], Sentinel-2 [1], KOMPSAT-2 [1], WorldView-2 [1], UAV (RGB) [3], Hyperspectral ASD [4]	[403–406]
Phenotyping, Phenology, Phenology-Stadien (BBCH-Scale)	UAV (RGB, MSP, HSP, TIR, LiDAR) [3], UAV (RGB, VIS, NIR, TIR, LiDAR) [3], Labour-Hyperspectral–AISA-EAGLE [5]	[244,304,327,407–412]
Crop growth duration (GDa),	MODIS [1], Landsat [1], Gaofen-1 [1], Sentinel-2 [1], RapidEye [1], UAV (SAR) [2]	[387,413–416]
Hedgerow map classifications, Hedgerows and field margins	TerraSAR-X [1], Spot [1], IKONOS [1], Airborne MSP [2], Aerial photographs [2], UAV (RGB, MSP) [3]	[89,417–421]

Flower strip mapping Flower Mapping	Airborne Hyperspectral (HySPEX, RGB, TIR) [2], Airborne Hyperspectral (AISA-Eagle) [2], Airborne MSP [2], UAV (MSP, HSP) [3]	[421–426]
Buffer Zone Efficiency Agricultural Pesticides Drift zones	Landsat [1], Sentinel-2 [1]	[427]
Classification of agroforestry systems	RapidEye [1], PlantetScope [1], LISS IV [1], Sentinel-2 [1]	[428–432]
Plastic-covered greenhouses Plasticulture detection Plastic greenhouses (PGs) and Plastic-mulched farmland (PMF)	Landsat [1], Sentinel-1 [1], Sentinel-2 [1], GF-2	[433–437]
Crop yield predictions Grain Yield, Protein estimation	MODIS [1], Landsat [1], Sentinel-2 [1], UAV–(MSP, HSP) [3]	[258,438–447]
Hop cultivation classification	UAV (MSP) [3], Mobile phone camera [6]	[448,449]
Functional traits of A-LUI		
Crop biomass, Aboveground biomass (AGB), Relative biomass potential (rel. BMP)	MODIS [1], Landsat [1], Sentinel-1 [1], Sentinel-2 [1], PlanetScope [1], UAV (MSP, RGB) [3], Smartphone [6]	[191–197,293,450]
Plant Nitrogen Concentration (PNC) Leaf Nitrogen Content Fertilisation Gradient	Sentinel-2 [1], UAV (MSP, TIR) [3]	[102,205–207,451–453]
Soil organic carbon (SOC) Soil organic matter (SOM)	ALOS-2 [1], PALSAR-2 [1], Landsat [1], Spot 4/5 [1], GF-1 [1], RADAR (PLAS) [1], Sentinel-1 [1], Sentinel-2 [1], Sentinel-3 [1], Airborne hyperspectral (DAIS) [2], Airborne hyperspectral (AISA Eagle, Hawk) [2], Hyperspectral APEX [2], UAV (SAR) [3], VIS–NIR spectroscopy (Field) [1],	[93,210,215,216,221,223,291,454–466]
Clay content	Landsat [1], Aster [1], Sentinel-2 [1], Airborne hyperspectral (AISA Eagle, Hawk) [2]	[368,467–473]
Soil total nitrogen (TN) N-Monitoring Total soil nitrogen (TSN) Nutritional Status Soil Total Nitrogen Soil Nutrients Contents	Sentinel-1 [1], Sentinel-2 [1], GF-1 [1], UAV (HSP, MSP, TIR) [3], ASD (Field) [4]	[208,215,461,472,474–480]
C:N ratio soil	Landsat [1], Sentinel-1 [1], Sentinel-2 [1], Sentinel-3 [1]	[93,460,481–484]
Carbon use efficiency (CUE)	MODIS [1], Landsat [1], Sentinel-2 [1]	[485–488]
Silt content	GF-1 [1], Airborne hyperspectral (AISA Eagle, Hawk) [2],	[368,489]
Sand content	Landsat [1], Sentinel-2 [1], Aster [1], GF-1 [1], Planet/NICFI [1], Airborne hyperspectral (AISA Eagle, Hawk) [2]	[368,473,489–493]
Potassium content	PRISMA [1], UAV (MSP) [3]	[476,477]
Phosphorus content (P)	MODIS [1], Landsat [1], Sentinel-2 [1], PRISMA [1], UAV (MSP, LiDAR) [3], ASD [4]	[333,476–479,494]
Pestizide, Herbizide, Fungizide Pest management	Sentinel-2 [1], UAV [3], Local hyperspectral camera [6], ASD—LeafSpec hyperspectral images [4]	[198–203,495,496]

Plant Disease Detection, Crop vegetation health Plant health	Sentinel-1 [1], Sentinel-2 [1], UAV (RGB, MSP, VIS, NIR, TIR, LiDAR) [3], ASD FieldSpec Pro FR [4]	[92,105,404,409,497–508]
CSR-Plant Strategy Types Plant functional groups (PFGs) Ellenberg Indicator Species	Landsat [1], Sentinel-2 [1], Airborne hyperspectral data (AISA dual) [2], Airborne AISA Fenix [2], Airborne imaging spectrometer APEX [2], Airborne hyperspectral HySpex [2]	[509–516]
Gross Primary Production (GPP) Dynamic of carbon emissions, Carbon Fluxes	MODIS [1], Meris [1], Landsat [1], Sentinel-1 [1], Sentinel-2 [1], Sentinel-3 [1], Hyperspectral Ocean Optics USB2000 (Tower) [6], LEDAPS-Aerosol Robotic Network (AERONET) [6]	[246,485,517–524]
Cropland NPP	MODIS [1], Landsat [1], UAV (MSP) [3]	[306,347,485,525–530]
HANPP (Human Appropriation of Net Primary Production)	MODIS [1], Landsat [1], Sentinel-2 [1]	[531–535]
Water use efficiency (WUE)	MODIS [1], Landsat [1], Sentinel-1 [1], Sentinel-2 [1]	[485,536–540]
Yield and Quality	Landsat [1], Sentinel-1 [1], Sentinel-2 [1], UAV (MSP) [3]	[196,523,541–548]
Harvest Index	MODIS [1], HJ-1 satellite [1], Sentinel-2 [1], UAV (HSP) [3], FieldSpec HandHeld Spectroradiometer (ASD) [4]	[549–552]
Soil quality index (SQI)	Landsat [1], Sentinel-2 [1], Airborne hyperspectral (AISA) [2]	[330,553,554]
Soil productivity potential	MODIS [1], Landsat [1], Sentinel-2 [1], ASD FieldSpec [4]	[302,472,555–557]
Soil Crust	KOMPSAT-2 satellite [1], Airborne hyperspectral (DAIS) [2], Airborne hyperspectral (AISA Eagle, Hawk) [2], UAV (RGB, MSP, HSP) [3], ASD Fieldspec [4]	[291,558–564]
Soil infiltration	Airborne hyperspectral (DAIS) [2], Airborne hyperspectral (AISA Eagle, Hawk) [2], Airborne CASI-1500 [2], SASI-600 [2], Airborne TASI-600 hyperspectral sensors [2], UAV (HSP, Cubert UHD-185) [3]	[291,565,566]
Soil pH value	PALSAR-1/2 [1], SRTM [1], Landsat [1], PlantetScope [1], Sentinel-1 [1], Sentinel-2 [1], UAV (MSP) [3], ASD FieldSpec [4]	[290,361,547,567–577]
Soil salinity Soil salinisation	Landsat [1], RADAR [1], Airborne LiDAR [2], HJ-1 Hyperspectral Imager Data [2]	[290,578–585]
Land degradation, Soil degradation, Soil erosion Desertification	Landsat [1], SRTM [1], Sentinel-1 [1], Sentinel-2 [1], RapidEye [1], Airborne hyperspectral (DAIS) [2], Airborne hyperspectral (AISA Eagle, Hawk) [2], UAV (RGB) [3]	[291,586–591]
Soil compaction Soil Compaction Index Soil aggregation Soil penetration resistance	Landsat [1], GoogleEarth aerial imagery [1], Sentinel-2 [1], RapidEye [1], Airborne hyperspectral (CASI) [2], UAV (RGB, SAR, LiDAR, MSP, TIR) [3]	[587,592–599]
Cattle intensification, Spatial distribution of cattle	Sentinel-1 [1], Sentinel-2 [1]	[600]
Grassland use intensity Grassland management intensity	Landsat [1], Sentinel-1 [1], Sentinel-2 [1], RapidEye [1],	[91,188,601–605]
Grassland fire	MODIS [1], Sentinel-1 [1], Sentinel-2 [1], GF-6 WFV [1], UAV [3]	[606–610]

Grassland cut detection	SAR [1], Sentinel-1 [1], Sentinel-2 [1]	[611–613]
Different Water quality indicators	All RS Sensors with all RS characteristics (MSP, HSP, TIR, RADAR, LiDAR)	[63]

The sensor is used on the RS platform: [1]—spaceborne RS platforms, [2]—airborne RS platform, [3]—UAV, [4]—Handheld portable hyperspectral camera (Specim IQ) ASD, [5]—Laboratory spectroscopy, [6]—Tower, Smartphone, ground-based.

Table A5. Illustrative examples linking plant and soil traits to RS observables, intensity signals, and key confounders.

Trait/Process	RS Sensor/Modality	Directionality with Intensity	Key Confounders (Non-Management)
Leaf N/chlorophyll content	Red-edge indices (Sentinel-2), hyperspectral (EnMAP, CHIME), solar-induced fluorescence (FLEX)	↑ with higher fertilisation and improved management	Cultivar-specific pigment traits; background soil reflectance; cloud/shadow effects
Canopy structure (LAI, height, biomass)	Multispectral VIs (NDVI, EVI), LiDAR metrics (GEDI, UAV-LiDAR), SAR backscatter (Sentinel-1)	↑ with higher input intensity, dense sowing, irrigation	Natural soil fertility; precipitation regime; lodging events
Phenology (timing, cropping frequency)	Time series (Sentinel-1 coherence for tillage/harvest; Sentinel-2 optical indices; PlanetScope)	More frequent harvests or longer growing season → ↑ intensity	Climate-driven shifts in growing season; interannual weather variability
Root traits (water/nutrient uptake)	Thermal (ET proxies), SAR soil moisture (Sentinel-1), hyperspectral water stress proxies	Intensive irrigation/fertilisation → ↑ water use efficiency or altered root activity	Soil texture; groundwater availability; drought stress independent of management
Canopy temperature/water status	Thermal sensors (ECOSTRESS, UAV-TIR), ET modelling with optical+thermal fusion	↓ canopy temperature and ↑ ET with irrigation intensity	Heat waves, VPD variability, soil hydraulic properties
Structural diversity (field size, edges, hedgerows)	High-res optical (PlanetScope, UAV), LiDAR for vertical structure, OBIA	↑ intensity often linked to larger fields, reduced edge density	Historical land consolidation, topography, land tenure
Crop type diversity (taxonomic composition)	Multi-temporal Sentinel-2/Landsat, hyperspectral UAV, classification algorithms	↑ intensity often → ↓ diversity, monocropping	Regional crop rotations, policy incentives, cultural practices
Soil organic matter/C:N ratio	Hyperspectral reflectance (VNIR-SWIR), SAR + optical fusion, regression models	↓ SOM with long-term intensive use, ↑ mineral N inputs → altered C:N	Parent material, drainage, climate-driven decomposition
Harvest/tillage events	SAR coherence (Sentinel-1), time-series change detection, UAV imagery	↑ intensity = more frequent disturbance signals per season	Weather-induced soil roughness, cloud cover gaps
Pest/disease stress signals	Hyperspectral indices (red-edge, PRI), fluorescence (SIF), UAV multispectral	Intensive management may ↓ visible stress due to pesticide control	Pathogen pressure, local outbreak dynamics, cultivar resistance

Table A6. Integrative framework linking management practices, traits, RS proxies, A-LUI indicator categories, validation needs, and policy relevance. The table highlights how RS-derived observables can serve as bridges between field management, biophysical processes, and policy-relevant indicators of agricultural land use intensity.

Management Practice	Trait/Process Affected	RS Proxy/Observable	A-LUI Indicator Category	Validation Needs	Policy Relevance
Fertiliser application	Leaf nitrogen, canopy chlorophyll	Red-edge indices (Sentinel-2), hyperspectral retrievals	Trait/Functional	Ground sampling, cultivar comparisons	Nutrient efficiency, sustainability reporting
Irrigation	Soil moisture, evapotranspiration	SAR backscatter (Sentinel-1), thermal RS, ET models	Functional	Flux tower data, lysimeter validation	Water use efficiency, water policy compliance
Tillage/harvest	Soil disturbance, residue cover	SAR coherence, optical time series	Genesis/Structural	In situ soil disturbance surveys	Soil conservation, monitoring sustainable practices
Crop rotation	Temporal diversity, phenology	Multi-temporal NDVI/EVI, crop classification	Genesis/Taxonomic	Farm records, phenological ground obs.	Agri-environmental schemes, crop diversification targets
Field consolidation	Landscape heterogeneity, field size	High-res optical imagery, LiDAR boundaries	Structural	Field surveys, cadastral data	Land consolidation monitoring, biodiversity impacts
Intensified cropping cycles	Aboveground biomass, multiple harvests	Time series (MODIS, Sentinel-2), SIF (FLEX, OCO-2)	Genesis/Functional	Yield data, harvest records	Productivity vs. sustainability trade-offs
Hedgerow removal/addition	Semi-natural habitat, species richness	High-res imagery (UAV, Planet), landscape metrics	Structural/Taxonomic	Biodiversity field surveys	CAP greening measures, landscape conservation

Table A7. Sensors and emerging technologies for A-LUI monitoring.

Technology/Approach	Example Missions or Tools	Indicator Categories Addressed	Spatial/Temporal Resolution	Development Stage	Added Value
Multispectral optical	Landsat, Sentinel-2, PlanetScope	Trait (NDVI, chlorophyll, phenology)	10–30 m/5–16 d	Operational	Long time series, global coverage
Hyperspectral	EnMAP, CHIME, PRISMA	Trait (chlorophyll, N, stress proxies)	20–30 m/<30 d	Operational/new	Detailed biochemical information
Thermal infrared	ECOSTRESS, Landsat TIRS, MODIS	Functional (evapotranspiration, irrigation)	70–1000 m/daily–16 d	Operational	Direct link to water/energy fluxes
Radar (SAR)	Sentinel-1, RADARSAT, ALOS PALSAR	Structure (tillage, harvest, soil moisture)	10–30 m/6–12 d	Operational	All-weather, soil and canopy penetration
LiDAR	GEDI, ICESat-2, airborne LiDAR	Structure (canopy height, biomass, terraces)	1–25 m/campaign-based	Operational/campaign	3D structure, fine-scale terrain

UAV-based platforms	Multispectral & thermal drones	Trait & Structure (field scale)	cm–dm/flexible	Operational	Ultra-high resolution, flexible timing
Solar-Induced Fluorescence (SIF)	OCO-2, FLEX (upcoming)	Functional (photosynthesis, GPP)	300 m–2 km/daily	Research/upcoming	Direct proxy for photosynthesis
Multi-sensor fusion	Sentinel-1 + Sentinel-2, optical + thermal	All categories	Depends on data	Research & operational	Improves robustness & accuracy
AI/ML approaches	Deep learning, data fusion methods	All categories	Depends on training data	Research & early operational	Enhanced pattern recognition
Semantic web and linked data	RDF/OWL/SPARQL ontologies	Data integration	N/A	Conceptual	Harmonisation across datasets

References

1. Diogo, V.; Helfenstein, J.; Mohr, F.; Varghese, V.; Debonne, N.; Levers, C.; Swart, R.; Sonderegger, G.; Nemecek, T.; Schader, C.; et al. Developing context-specific frameworks for integrated sustainability assessment of agricultural intensity change: An application for Europe. *Environ. Sci. Policy* **2022**, *137*, 128–142.
2. Tripathi, S.; Srivastava, P.; Devi, R.S.; Bhadouria, R. Influence of synthetic fertilizers and pesticides on soil health and soil microbiology. In *Agrochemicals Detection, Treatment and Remediation*; Elsevier: Amsterdam, The Netherlands, 2020; pp. 25–54.
3. Yahaya, S.M.; Mahmud, A.A.; Abdullahi, M.; Haruna, A. Recent advances in the chemistry of nitrogen, phosphorus and potassium as fertilizers in soil: A review. *Pedosphere* **2023**, *33*, 385–406.
4. Shah, A.N.; Tanveer, M.; Shahzad, B.; Yang, G.; Fahad, S.; Ali, S.; Bukhari, M.A.; Tung, S.A.; Hafeez, A.; Souliyanonh, B. Soil compaction effects on soil health and cropproductivity: An overview. *Environ. Sci. Pollut. Res.* **2017**, *24*, 10056–10067.
5. Ingrao, C.; Strippoli, R.; Lagioia, G.; Huisingh, D. Water scarcity in agriculture: An overview of causes, impacts and approaches for reducing the risks. *Heliyon* **2023**, *9*, e18507.
6. Scanlon, B.R.; Jolly, I.; Sophocleous, M.; Zhang, L. Global impacts of conversions from natural to agricultural ecosystems on water resources: Quantity versus quality. *Water Resour. Res.* **2007**, *43*, W03437.
7. Sharma, K.; Rajan, S.; Nayak, S.K. Water pollution: Primary sources and associated human health hazards with special emphasis on rural areas. In *Water Resources Management for Rural Development*; Elsevier: Amsterdam, The Netherlands, 2024; pp. 3–14.
8. Pannard, A.; Souchu, P.; Chauvin, C.; Delabuis, M.; Gascuel-Odoux, C.; Jeppesen, E.; Le Moal, M.; Ménesguen, A.; Pinay, G.; Rabalais, N.N.; et al. Why are there so many definitions of eutrophication? *Ecol. Monogr.* **2024**, *94*, e1616.
9. Zabel, F.; Delzeit, R.; Schneider, J.M.; Seppelt, R.; Mauser, W.; Václavík, T. Global impacts of future cropland expansion and intensification on agricultural markets and biodiversity. *Nat. Commun.* **2019**, *10*, 2844.
10. Mupepele, A.C.; Bruelheide, H.; Brühl, C.; Dauber, J.; Fenske, M.; Freibauer, A.; Gerowitt, B.; Krüß, A.; Lakner, S.; Plieninger, T.; et al. Biodiversity in European agricultural landscapes: Transformative societal changes needed. *Trends Ecol. Evol.* **2021**, *36*, 1067–1070.
11. Burian, A.; Kremen, C.; Wu, J.S.T.; Beckmann, M.; Bulling, M.; Garibaldi, L.A.; Krisztin, T.; Mehrabi, Z.; Ramankutty, N.; Seppelt, R. Biodiversity–production feedback effects lead to intensification traps in agricultural landscapes. *Nat. Ecol. Evol.* **2024**, *8*, 752–760.
12. Le Provost, G.; Thiele, J.; Westphal, C.; Penone, C.; Allan, E.; Neyret, M.; van der Plas, F.; Ayasse, M.; Bardgett, R.D.; Birkhofer, K.; et al. Contrasting responses of above-and belowground diversity to multiple components of land-use intensity. *Nat. Commun.* **2021**, *12*, 3918.
13. Beckmann, M.; Gerstner, K.; Akin-Fajiye, M.; Ceauşu, S.; Kambach, S.; Kinlock, N.L.; Phillips, H.R.P.; Verhagen, W.; Gurevitch, J.; Klotz, S.; et al. Conventional land-use intensification reduces species richness and increases production: A global meta-analysis. *Glob. Change Biol.* **2019**, *25*, 1941–1956.
14. Felipe-Lucia, M.R.; Soliveres, S.; Penone, C.; Fischer, M.; Ammer, C.; Boch, S.; Boeddinghaus, R.S.; Bonkowski, M.; Buscot, F.; Fiore-Donno, A.M.; et al. Land-use intensity alters networks between biodiversity, ecosystem functions, and services. *Proc. Natl. Acad. Sci.* **2020**, *117*, 28140–28149.
15. Gossner, M.M.; Lewinsohn, T.M.; Kahl, T.; Grassein, F.; Boch, S.; Prati, D.; Birkhofer, K.; Renner, S.C.; Sikorski, J.; Wubet, T.; et al. Land-use intensification causes multitrophic homogenization of grassland communities. *Nature* **2016**, *540*, 266–269.
16. Millard, J.; Outhwaite, C.L.; Kinnersley, R.; Freeman, R.; Gregory, R.D.; Adedoja, O.; Gavini, S.; Kioko, E.; Kuhlmann, M.; Ollerton, J.; et al. Global effects of land-use intensity on local pollinator biodiversity. *Nat. Commun.* **2021**, *12*, 2902.

17. Suarez, A.; Gwozdz, W. On the relation between monocultures and ecosystem services in the Global South: A review. *Biol. Conserv.* **2023**, *278*, 109870.
18. Cheng, C.; Liu, Z.; Song, W.; Chen, X.; Zhang, Z.; Li, B.; van Kleunen, M.; Wu, J. Biodiversity increases resistance of grasslands against plant invasions under multiple environmental changes. *Nat. Commun.* **2024**, *15*, 4506.
19. Scanes, C.G. Human Activity and Habitat Loss: Destruction, Fragmentation, and Degradation. In *Animals and Human Society*; Elsevier: Amsterdam, The Netherlands, 2018; pp. 451–482, ISBN 9780128052471.
20. Oliver, T.H.; Marshall, H.H.; Morecroft, M.D.; Brereton, T.; Prudhomme, C.; Huntingford, C. Interacting effects of climate change and habitat fragmentation on drought-sensitive butterflies. *Nat. Clim. Change* **2015**, *5*, 941–946.
21. Peters, M.K.; Hemp, A.; Appelhans, T.; Becker, J.N.; Behler, C.; Classen, A.; Detsch, F.; Ensslin, A.; Ferger, S.W.; Frederiksen, S.B.; et al. Climate–land-use interactions shape tropical mountain biodiversity and ecosystem functions. *Nature* **2019**, *568*, 88–92.
22. Schneider, J.M.; Delzeit, R.; Neumann, C.; Heimann, T.; Seppelt, R.; Schuenemann, F.; Söder, M.; Mauser, W.; Zabel, F. Effects of profit-driven cropland expansion and conservation policies. *Nat. Sustain.* **2024**, *7*, 1335–1347.
23. Kaur, R.; Choudhary, D.; Bali, S.; Bandral, S.S.; Singh, V.; Ahmad, M.A.; Rani, N.; Singh, T.G.; Chandrasekaran, B. Pesticides: An alarming detrimental to health and environment. *Sci. Total Environ.* **2024**, *915*, 170113.
24. Bava, R.; Castagna, F.; Lupia, C.; Poerio, G.; Liguori, G.; Lombardi, R.; Naturale, M.D.; Mercuri, C.; Bulotta, R.M.; Britti, D.; et al. Antimicrobial Resistance in Livestock: A Serious Threat to Public Health. *Antibiotics* **2024**, *13*, 551.
25. Khmaissa, M.; Zouari-Mechichi, H.; Sciara, G.; Record, E.; Mechichi, T. Pollution from livestock farming antibiotics an emerging environmental and human health concern: A review. *J. Hazard. Mater. Adv.* **2024**, *13*, 100410.
26. Turner, B.L.; Doolittle, W.E. The Concept and Measure of Agricultural Intensity. *Prof. Geogr.* **1978**, *30*, 297–301.
27. Herzog, F.; Steiner, B.; Bailey, D.; Baudry, J.; Billeter, R.; Bukácek, R.; De Blust, G.; De Cock, R.; Dirksen, J.; Dormann, C.F.; et al. Assessing the intensity of temperate European agriculture at the landscape scale. *Eur. J. Agron.* **2006**, *24*, 165–181.
28. Lüscher, G.; Jeanneret, P.; Schneider, M.K.; Turnbull, L.A.; Arndorfer, M.; Balázs, K.; Báldi, A.; Bailey, D.; Bernhardt, K.G.; Choisis, J.P.; et al. Responses of plants, earthworms, spiders and bees to geographic location, agricultural management and surrounding landscape in European arable fields. *Agric. Ecosyst. Environ.* **2014**, *186*, 124–134.
29. Helfenstein, J.; Hepner, S.; Kreuzer, A.; Achermann, G.; Williams, T.; Bürgi, M.; Debonne, N.; Dimopoulos, T.; Diogo, V.; Fjellstad, W.; et al. Divergent agricultural development pathways across farm and landscape scales in Europe: Implications for sustainability and farmer satisfaction. *Glob. Environ. Change* **2024**, *86*, 102855.
30. Canisius, F.; Turral, H.; Molden, D. Fourier analysis of historical NOAA time series data to estimate bimodal agriculture. *Int. J. Remote Sens.* **2007**, *28*, 5503–5522.
31. Kuemmerle, T.; Hostert, P.; St-Louis, V.; Radeloff, V.C. Using image texture to map farmland field size: A case study in Eastern Europe. *J. Land Use Sci.* **2009**, *4*, 85–107.
32. Verburg, P.H.; Neumann, K.; Nol, L. Challenges in using land use and land cover data for global change studies. *Glob. Change Biol.* **2011**, *17*, 974–989.
33. Kuemmerle, T.; Erb, K.; Meyfroidt, P.; Müller, D.; Verburg, P.H.; Estel, S.; Haberl, H.; Hostert, P.; Jepsen, M.R.; Kastner, T.; et al. Challenges and opportunities in mapping land use intensity globally. *Curr. Opin. Environ. Sustain.* **2013**, *5*, 484–493.
34. Wellmann, T.; Haase, D.; Knapp, S.; Salbach, C.; Selsam, P.; Lausch, A. Urban land use intensity assessment: The potential of spatio-temporal spectral traits with remote sensing. *Ecol. Indic.* **2018**, *85*, 190–203.
35. Weber, D.; Schwieder, M.; Ritter, L.; Koch, T.; Psomas, A.; Huber, N.; Ginzler, C.; Boch, S. Grassland-use intensity maps for Switzerland based on satellite time series: Challenges and opportunities for ecological applications. *Remote Sens. Ecol. Conserv.* **2024**, *10*, 312–327.
36. Liu, H.; Zhou, Z.; Wen, Q.; Chen, J.; Kojima, S. Spatiotemporal Land Use/Land Cover Changes and Impact on Urban Thermal Environments: Analyzing Cool Island Intensity Variations. *Sustainability* **2024**, *16*, 3205.
37. Qiu, B.; Liu, B.; Tang, Z.; Dong, J.; Xu, W.; Liang, J.; Chen, N.; Chen, J.; Wang, L.; Zhang, C.; et al. National-scale 10-m maps of cropland use intensity in China during 2018–2023. *Sci. Data* **2024**, *11*, 691.
38. Hank, T.B.; Berger, K.; Bach, H.; Clevers, J.G.P.W.; Gitelson, A.; Zarco-Tejada, P.; Mauser, W. *Spaceborne Imaging Spectroscopy for Sustainable Agriculture: Contributions and Challenges*; Springer Netherlands: Dordrecht, The Netherlands, 2019; Volume 40, ISBN 0123456789.
39. Wulder, M.A.; Coops, N.C. Make Earth observations open access. *Nature* **2014**, *513*, 30–31.
40. Wulder, M.A.; Roy, D.P.; Radeloff, V.C.; Loveland, T.R.; Anderson, M.C.; Johnson, D.M.; Healey, S.; Zhu, Z.; Scambos, T.A.; Pahlevan, N.; et al. Fifty years of Landsat science and impacts. *Remote Sens. Environ.* **2022**, *280*, 113195.

41. Malenovský, Z.; Rott, H.; Cihlar, J.; Schaepman, M.E.; García-Santos, G.; Fernandes, R.; Berger, M. Sentinels for science: Potential of Sentinel-1, -2, and -3 missions for scientific observations of ocean, cryosphere, and land. *Remote Sens. Environ.* **2012**, *120*, 91–101.
42. Guanter, L.; Kaufmann, H.; Segl, K.; Foerster, S.; Rogass, C.; Chabrillat, S.; Kuester, T.; Hollstein, A.; Rossner, G.; Chlebek, C.; et al. The EnMAP Spaceborne Imaging Spectroscopy Mission for Earth Observation. *Remote Sens.* **2015**, *7*, 8830–8857.
43. Nieke, J.; Rast, M. Towards the Copernicus Hyperspectral Imaging Mission For The Environment (CHIME). In Proceedings of the IGARSS 2018—2018 IEEE International Geoscience and Remote Sensing Symposium, Valencia, Spain, 22–27 July 2018; pp. 157–159.
44. Dubayah, R.; Blair, J.B.; Goetz, S.; Fatoyinbo, L.; Hansen, M.; Healey, S.; Hofton, M.; Hurtt, G.; Kellner, J.; Luthcke, S.; et al. The Global Ecosystem Dynamics Investigation: High-resolution laser ranging of the Earth's forests and topography. *Sci. Remote Sens.* **2020**, *1*, 100002.
45. Lee, C.M.; Cable, M.L.; Hook, S.J.; Green, R.O.; Ustin, S.L.; Mandl, D.J.; Middleton, E.M. An introduction to the NASA Hyperspectral InfraRed Imager (HyspIRI) mission and preparatory activities. *Remote Sens. Environ.* **2015**, *167*, 6–19.
46. Kraft, S.; Del Bello, U.; Bouvet, M.; Drusch, M.; Moreno, J. FLEX: ESA's Earth Explorer 8 candidate mission. In Proceedings of the 2012 IEEE International Geoscience and Remote Sensing Symposium, Munich, Germany, 22–27 July 2012; pp. 7125–7128.
47. Omia, E.; Bae, H.; Park, E.; Kim, M.S.; Baek, I.; Kabenge, I.; Cho, B.K. Remote Sensing in Field Crop Monitoring: A Comprehensive Review of Sensor Systems, Data Analyses and Recent Advances. *Remote Sens.* **2023**, *15*, 354.
48. Sethy, P.K.; Pandey, C.; Sahu, Y.K.; Behera, S.K. *Hyperspectral Imagery Applications for Precision Agriculture—A Systemic Survey*; Springer US: New York, NY, USA, 2022; Volume 81, ISBN 0123456789.
49. Maes, W.H.; Steppe, K. Perspectives for Remote Sensing with Unmanned Aerial Vehicles in Precision Agriculture. *Trends Plant Sci.* **2019**, *24*, 152–164.
50. Khanal, S.; Fulton, J.; Shearer, S. An overview of current and potential applications of thermal remote sensing in precision agriculture. *Comput. Electron. Agric.* **2017**, *139*, 22–32.
51. Segarra, J.; Buchaillot, M.L.; Araus, J.L.; Kefauver, S.C. Remote Sensing for Precision Agriculture: Sentinel-2 Improved Features and Applications. *Agronomy* **2020**, *10*, 641.
52. Barbosa Júnior, M.R.; de Almeida Moreira, B.R.; Carreira, V.D.S.; Brito Filho, A.L.d.; Trentin, C.; Souza, F.L.P.d.; Tedesco, D.; Setiyono, T.; Flores, J.P.; Ampatzidis, Y.; et al. Precision agriculture in the United States: A comprehensive meta-review inspiring further research, innovation, and adoption. *Comput. Electron. Agric.* **2024**, *221*, 108993.
53. Marques, P.; Pádua, L.; Sousa, J.J.; Fernandes-Silva, A. Advancements in Remote Sensing Imagery Applications for Precision Management in Olive Growing: A Systematic Review. *Remote Sens.* **2024**, *16*, 1324.
54. Bonfanti, J.; Langridge, J.; Avadí Ef, A.; Casajus, N.; Chaudhary, A.; Damour Hi, G.; Estrada-Carmona, N.; Jones, S.K.; Makowski, D.; Mitchell, M.; et al. Global review of meta-analyses reveals key data gaps in agricultural impact studies on biodiversity in croplands. *BioRxiv* **2024**. Doi: https://doi.org/10.1101/2024.04.19.590051
55. Khanal, S.; Kushal, K.C.; Fulton, J.P.; Shearer, S.; Ozkan, E. Remote sensing in agriculture—Accomplishments, limitations, and opportunities. *Remote Sens.* **2020**, *12*, 3783.
56. Lu, B.; Dao, P.D.; Liu, J.; He, Y.; Shang, J. Recent advances of hyperspectral imaging technology and applications in agriculture. *Remote Sens.* **2020**, *12*, 2659.
57. Lausch, A.; Selsam, P.; Pause, M.; Bumberger, J. Monitoring vegetation- and geodiversity with remote sensing and traits. *Philos. Trans. R. Soc. A Math. Phys. Eng. Sci.* **2024**, *382*, 20230058.
58. Cavender-Bares, J.; Gamon, J.A.; Townsend, P.A. *Remote Sensing of Plant Biodiversity*; Cavender-Bares, J., Gamon, J.A., Townsend, P.A., Eds.; Springer International Publishing: Cham, Switzerland, 2020; ISBN 978-3-030-33156-6.
59. Lausch, A.; Bastian, O.; Klotz, S.; Leitão, P.J.; Jung, A.; Rocchini, D.; Schaepman, M.E.; Skidmore, A.K.; Tischendorf, L.; Knapp, S. Understanding and assessing vegetation health by in situ species and remote-sensing approaches. *Methods Ecol. Evol.* **2018**, *9*, 1799–1809.
60. Lausch, A.; Baade, J.; Bannehr, L.; Borg, E.; Bumberger, J.; Chabrilliat, S.; Dietrich, P.; Gerighausen, H.; Glässer, C.; Hacker, J.; et al. Linking Remote Sensing and Geodiversity and Their Traits Relevant to Biodiversity—Part I: Soil Characteristics. *Remote Sens.* **2019**, *11*, 2356.
61. Lausch, A.; Schaepman, M.E.; Skidmore, A.K.; Truckenbrodt, S.C.; Hacker, J.M.; Baade, J.; Bannehr, L.; Borg, E.; Bumberger, J.; Dietrich, P.; et al. Linking the Remote Sensing of Geodiversity and Traits Relevant to Biodiversity—Part II: Geomorphology, Terrain and Surfaces. *Remote Sens.* **2020**, *12*, 3690.

62. Lausch, A.; Schaepman, M.E.; Skidmore, A.K.; Catana, E.; Bannehr, L.; Bastian, O.; Borg, E.; Bumberger, J.; Dietrich, P.; Glässer, C.; et al. Remote Sensing of Geomorphodiversity Linked to Biodiversity—Part III: Traits, Processes and Remote Sensing Characteristics. *Remote Sens.* **2022**, *14*, 2279.
63. Lausch, A.; Bannehr, L.; Berger, S.A.; Borg, E.; Bumberger, J. Monitoring Water Diversity and Water Quality with Remote Sensing and Traits. *Remote Sens.* **2024**, *16*, 2425.
64. Andersson, E.; Haase, D.; Anderson, P.; Cortinovis, C.; Goodness, J.; Kendal, D.; Lausch, A.; McPhearson, T.; Sikorska, D.; Wellmann, T. What are the traits of a social-ecological system: Towards a framework in support of urban sustainability. *Npj Urban Sustain.* **2021**, *1*, 14.
65. Wellmann, T.; Lausch, A.; Andersson, E.; Knapp, S.; Cortinovis, C.; Jache, J.; Scheuer, S.; Kremer, P.; Mascarenhas, A.; Kraemer, R.; et al. Remote sensing in urban planning: Contributions towards ecologically sound policies? *Landsc. Urban Plan.* **2020**, *204*, 103921.
66. Xie, C.; Wang, J.; Haase, D.; Wellmann, T.; Lausch, A. Measuring spatio-temporal heterogeneity and interior characteristics of green spaces in urban neighborhoods: A new approach using gray level co-occurrence matrix. *Sci. Total Environ.* **2023**, *855*, 158608.
67. Roilo, S.; Paulus, A.; Alarcón-Segura, V.; Kock, L.; Beckmann, M.; Klein, N.; Cord, A.F. Quantifying agricultural land-use intensity for spatial biodiversity modelling: Implications of different metrics and spatial aggregation methods. *Landsc. Ecol.* **2024**, *39*, 55.
68. Erb, K.H.; Haberl, H.; Jepsen, M.R.; Kuemmerle, T.; Lindner, M.; Müller, D.; Verburg, P.H.; Reenberg, A. A conceptual framework for analysing and measuring land-use intensity. *Curr. Opin. Environ. Sustain.* **2013**, *5*, 464–470.
69. Çakmakçı, R.; Salık, M.A.; Çakmakçı, S. Assessment and Principles of Environmentally Sustainable Food and Agri-culture Systems. Agriculture 2023, 13, 1073.
70. Dullinger, I.; Essl, F.; Moser, D.; Erb, K.; Haberl, H.; Dullinger, S. Biodiversity models need to represent land-use intensity more comprehensively. *Glob. Ecol. Biogeogr.* **2021**, *30*, 924–932.
71. Rascher, U.; Alonso, L.; Burkart, A.; Cilia, C.; Cogliati, S.; Colombo, R.; Damm, A.; Drusch, M.; Guanter, L.; Hanus, J.; et al. Sun-induced fluorescence—A new probe of photosynthesis: First maps from the imaging spectrometer HyPlant. *Glob. Change Biol.* **2015**, *21*, 4673–4684.
72. Mohammed, G.H.; Colombo, R.; Middleton, E.M.; Rascher, U.; van der Tol, C.; Nedbal, L.; Goulas, Y.; Pérez-Priego, O.; Damm, A.; Meroni, M.; et al. Remote sensing of solar-induced chlorophyll fluorescence (SIF) in vegetation: 50 years of progress. *Remote Sens. Environ.* **2019**, *231*, 111177.
73. Anderson, J.R.; Hardy, E.E.; Roach, J.T.; Witmer, R.E. *A Land Use and Land Cover Classification System for Use with Remote Sensor Data*; US Government Printing Office: Washington, DC, USA, 1976; Volume 964.
74. Adewumi, J.R.; Akomolafe, J.K.; Ajibade, F.O.; Fabeku, B.B. Application of GIS and Remote Sensing Technique to Change Detection in Land Use/Land Cover Mapping of Igbokoda, Ondo State, Nigeria. *J. Appl. Sci. Process Eng.* **1970**, *3*, 34–54.
75. Matthews, E. Global Vegetation and Land Use: New High-Resolution Data Bases for Climate Studies. *J. Clim. Appl. Meteorol.* **1983**, *22*, 474–487.
76. Masek, J.G.; Wulder, M.A.; Markham, B.; McCorkel, J.; Crawford, C.J.; Storey, J.; Jenstrom, D.T. Landsat 9: Empowering open science and applications through continuity. *Remote Sens. Environ.* **2020**, *248*, 111968.
77. Copernicus Copernicus the European Union's Earth Observation Programme. Available online: https://www.copernicus.eu (accessed on 2 August 2024).
78. Rocchini, D.; Santos, M.J.; Ustin, S.L.; Féret, J.; Asner, G.P.; Beierkuhnlein, C.; Dalponte, M.; Feilhauer, H.; Foody, G.M.; Geller, G.N.; et al. The Spectral Species Concept in Living Color. *J. Geophys. Res. Biogeosci.* **2022**, *127*, e2022JG007026.
79. Maudet, S.; Brusse, T.; Poss, B.; Caro, G.; Marrec, R. Estimating landscape intensity through farming practices: An integrative and flexible approach to modelling farming intensity from field to landscape. *Ecol. Modell.* **2025**, *501*, 110975.
80. Lausch, A.; Menz, G. Bedeutung der Integration linearer Elemente in Fernerkundungsdaten zur Berechnung von Landschaftsstrukturmaßen. *Photogramm. Fernerkund. Geoinf.* **1999**, *3*, 185–194.
81. Lausch, A.; Herzog, F. Applicability of landscape metrics for the monitoring of landscape change: Issues of scale, resolution and interpretability. *Ecol. Indic.* **2002**, *2*, 3–15.
82. Billeter, R.; Liira, J.; Bailey, D.; Bugter, R.; Arens, P.; Augenstein, I.; Aviron, S.; Baudry, J.; Bukacek, R.; Burel, F.; et al. Indicators for biodiversity in agricultural landscapes: A pan-European study. *J. Appl. Ecol.* **2008**, *45*, 141–150.

83. Mohr, F.; Diogo, V.; Helfenstein, J.; Debonne, N.; Dimopoulos, T.; Dramstad, W.; García-Martín, M.; Hernik, J.; Herzog, F.; Kizos, T.; et al. Why has farming in Europe changed? A farmers' perspective on the development since the 1960s. *Reg. Environ. Change* **2023**, *23*, 156.
84. Martin, A.E.; Collins, S.J.; Crowe, S.; Girard, J.; Naujokaitis-Lewis, I.; Smith, A.C.; Lindsay, K.; Mitchell, S.; Fahrig, L. Effects of farmland heterogeneity on biodiversity are similar to—Or even larger than—The effects of farming practices. *Agric. Ecosyst. Environ.* **2020**, *288*, 106698.
85. Grenzdörffer, G. *Grundlagen der Landwirtschaftlichen Fernerkundung*; KTBL eV Kuratorium für Technik und Bauwesen in der Landwirtschaft: Darmstadt, Germany, 2022.
86. Picado, E.F.; Romero, K.F. Mapping Spatial Variability of Sugarcane Foliar Nitrogen, Phosphorus, Potassium and Chlorophyll Concentrations Using Remote Sensing. *Geomatics* **2025**, *5*, 3.
87. Yu, M.; Rui, X.; Xie, W.; Xu, X.; Wei, W. Research on Automatic Identification Method of Terraces on the Loess Plateau Based on Deep Transfer Learning. *Remote Sens.* **2022**, *14*, 2446.
88. Wang, X.; Shu, L.; Han, R.; Yang, F.; Gordon, T.; Wang, X.; Xu, H. A Survey of Farmland Boundary Extraction Technology Based on Remote Sensing Images. *Electronics* **2023**, *12*, 1156.
89. Betbeder, J.; Hubert-Moy, L.; Burel, F.; Corgne, S.; Baudry, J. Assessing ecological habitat structure from local to landscape scales using synthetic aperture radar. *Ecol. Indic.* **2015**, *52*, 545–557.
90. Griffiths, P.; Nendel, C.; Hostert, P. Intra-annual reflectance composites from Sentinel-2 and Landsat for national-scale crop and land cover mapping. *Remote Sens. Environ.* **2019**, *220*, 135–151.
91. Bartold, M.; Kluczek, M.; Wróblewski, K.; Dąbrowska-Zielińska, K.; Goliński, P.; Golińska, B. Mapping management intensity types in grasslands with synergistic use of Sentinel-1 and Sentinel-2 satellite images. *Sci. Rep.* **2024**, *14*, 32066.
92. Günder, M.; Yamati, F.R.I.; Alcántara, A.A.B.; Mahlein, A.-K.; Sifa, R.; Bauckhage, C. SugarViT—Multi-objective Regression of UAV Images with Vision Transformers and Deep Label Distribution Learning Demonstrated on Disease Severity Prediction in Sugar Beet. *PLoS ONE* **2023**, *20*, e0318097.
93. Zhou, T.; Geng, Y.; Ji, C.; Xu, X.; Wang, H.; Pan, J.; Bumberger, J.; Haase, D.; Lausch, A. Prediction of soil organic carbon and the C:N ratio on a national scale using machine learning and satellite data: A comparison between Sentinel-2, Sentinel-3 and Landsat-8 images. *Sci. Total Environ.* **2021**, *755*, 142661.
94. Díaz, S.; Kattge, J.; Cornelissen, J.H.C.; Wright, I.J.; Lavorel, S.; Dray, S.; Reu, B.; Kleyer, M.; Wirth, C.; Colin Prentice, I.; et al. The global spectrum of plant form and function. *Nature* **2016**, *529*, 167–171.
95. Joswig, J.S.; Wirth, C.; Schuman, M.C.; Kattge, J.; Reu, B.; Wright, I.J.; Sippel, S.D.; Rüger, N.; Richter, R.; Schaepman, M.E.; et al. Climatic and soil factors explain the two-dimensional spectrum of global plant trait variation. *Nat. Ecol. Evol.* **2022**, *6*, 36–50.
96. Candiani, G.; Tagliabue, G.; Panigada, C.; Verrelst, J.; Picchi, V.; Rivera Caicedo, J.P.; Boschetti, M. Evaluation of Hybrid Models to Estimate Chlorophyll and Nitrogen Content of Maize Crops in the Framework of the Future CHIME Mission. *Remote Sens.* **2022**, *14*, 1792.
97. Verrelst, J.; Rivera, J.P.; Veroustraete, F.; Muñoz-Marí, J.; Clevers, J.G.P.W.; Camps-Valls, G.; Moreno, J. Experimental Sentinel-2 LAI estimation using parametric, non-parametric and physical retrieval methods—A comparison. *ISPRS J. Photogramm. Remote Sens.* **2015**, *108*, 260–272.
98. Berger, K.; Verrelst, J.; Féret, J.-B.; Hank, T.; Wocher, M.; Mauser, W.; Camps-Valls, G. Retrieval of aboveground crop nitrogen content with a hybrid machine learning method. *Int. J. Appl. Earth Obs. Geoinf.* **2020**, *92*, 102174.
99. Loizzo, R.; Daraio, M.; Guarini, R.; Longo, F.; Lorusso, R.; Dini, L.; Lopinto, E. Prisma Mission Status and Perspective. In Proceedings of the IGARSS 2019—2019 IEEE International Geoscience and Remote Sensing Symposium, Yokohama, Japan, 28 July–2 August 2019; pp. 4503–4506.
100. Matsunaga, T.; Iwasaki, A.; Tachikawa, T.; Tanii, J.; Kashimura, O.; Mouri, K.; Inada, H.; Tsuchida, S.; Nakamura, R.; Yamamoto, H.; et al. Hyperspectral Imager Suite (HISUI): Its Launch and Current Status. In Proceedings of the IGARSS 2020–2020 IEEE International Geoscience and Remote Sensing Symposium, Waikoloa, HI, USA, 26 September–2 October 2020; pp. 3272–3273.
101. Feingersh, T.; Dor, E. Ben SHALOM—A Commercial Hyperspectral Space Mission. In *Optical Payloads for Space Missions*; Wiley: New York, NY, USA, 2015; pp. 247–263.
102. Delloye, C.; Weiss, M.; Defourny, P. Retrieval of the canopy chlorophyll content from Sentinel-2 spectral bands to estimate nitrogen uptake in intensive winter wheat cropping systems. *Remote Sens. Environ.* **2018**, *216*, 245–261.
103. Jacquemoud, S.; Verhoef, W.; Baret, F.; Bacour, C.; Zarco-Tejada, P.J.; Asner, G.P.; François, C.; Ustin, S.L. PROSPECT + SAIL models: A review of use for vegetation characterization. *Remote Sens. Environ.* **2009**, *113*, S56–S66.

104. Lhotáková, Z.; Neuwirthová, E.; Potůčková, M.; Červená, L.; Hunt, L.; Kupková, L.; Lukeš, P.; Campbell, P.; Albrechtová, J. Mind the leaf anatomy while taking ground truth with portable chlorophyll meters. *Sci. Rep.* **2025**, *15*, 1855.
105. Brewer, K.; Clulow, A.; Sibanda, M.; Gokool, S.; Naiken, V.; Mabhaudhi, T. Predicting the Chlorophyll Content of Maize over Phenotyping as a Proxy for Crop Health in Smallholder Farming Systems. *Remote Sens.* **2022**, *14*, 518.
106. Drusch, M.; Moreno, J.; Del Bello, U.; Franco, R.; Goulas, Y.; Huth, A.; Kraft, S.; Middleton, E.M.; Miglietta, F.; Mohammed, G.; et al. The FLuorescence EXplorer Mission Concept-ESA's Earth Explorer 8. *IEEE Trans. Geosci. Remote Sens.* **2017**, *55*, 1273–1284.
107. De Grave, C.; Verrelst, J.; Morcillo-Pallarés, P.; Pipia, L.; Rivera-Caicedo, J.P.; Amin, E.; Belda, S.; Moreno, J. Quantifying vegetation biophysical variables from the Sentinel-3/FLEX tandem mission: Evaluation of the synergy of OLCI and FLORIS data sources. *Remote Sens. Environ.* **2020**, *251*, 112101.
108. Ač, A.; Malenovský, Z.; Olejníčková, J.; Gallé, A.; Rascher, U.; Mohammed, G. Meta-analysis assessing potential of steady-state chlorophyll fluorescence for remote sensing detection of plant water, temperature and nitrogen stress. *Remote Sens. Environ.* **2015**, *168*, 420–436.
109. Moreno, J.F.; Goulas, Y.; Huth, A.; Middleton, E.; Miglietta, F.; Mohammed, G.; Nedbal, L.; Rascher, U.; Verhoef, W.; Drusch, M. Very high spectral resolution imaging spectroscopy: The Fluorescence Explorer (FLEX) mission. *Int. Geosci. Remote Sens. Symp.* **2016**, *2016*, 264–267.
110. Dong, N.; Prentice, I.C.; Wright, I.J.; Wang, H.; Atkin, O.K.; Bloomfield, K.J.; Domingues, T.F.; Gleason, S.M.; Maire, V.; Onoda, Y.; et al. Leaf nitrogen from the perspective of optimal plant function. *J. Ecol.* **2022**, *110*, 2585–2602.
111. Zheng, J.; Song, X.; Yang, G.; Du, X.; Mei, X.; Yang, X. Remote Sensing Monitoring of Rice and Wheat Canopy Nitrogen: A Review. *Remote Sens.* **2022**, *14*, 5712.
112. Silva, L.; Conceição, L.A.; Lidon, F.C.; Maçãs, B. Remote Monitoring of Crop Nitrogen Nutrition to Adjust Crop Models: A Review. *Agriculture* **2023**, *13*, 835.
113. Arogoundade, A.M.; Mutanga, O.; Odindi, J.; Naicker, R. The role of remote sensing in tropical grassland nutrient estimation: A review. *Environ. Monit. Assess.* **2023**, *195*, 954.
114. Xi, R.; Gu, Y.; Zhang, X.; Ren, Z. Nitrogen monitoring and inversion algorithms of fruit trees based on spectral remote sensing: A deep review. *Front. Plant Sci.* **2024**, *15*, 1489151.
115. Zhang, J.; Hu, Y.; Li, F.; Fue, K.G.; Yu, K. Meta-Analysis Assessing Potential of Drone Remote Sensing in Estimating Plant Traits Related to Nitrogen Use Efficiency. *Remote Sens.* **2024**, *16*, 838.
116. Ravikumar, S.; Vellingiri, G.; Sellaperumal, P.; Pandian, K.; Sivasankar, A.; Sangchul, H. Real-time nitrogen monitoring and management to augment N use efficiency and ecosystem sustainability—A review. *J. Hazard. Mater. Adv.* **2024**, *16*, 100466.
117. Chowdhury, M.; Kumar Khura, T.; Ahmad Parray, R.; Kushwaha, H.L.; Upadhyay, P.K.; Jha, A.; Patra, K.; Kushwah, A.; Kumar Prajapati, V. The use of destructive and nondestructive techniques in concrete nitrogen assessment in plants. *J. Plant Nutr.* **2024**, *47*, 2271–2294.
118. Tasnim, M.; Simic, A.; Verrelst, J.; Tian, Q.; Soleil, A.; Poku, H.; Rahman, A.; Processing, I.; Científic, P.; Val, U. De Optimizing Empirical and Hybrid Modeling for Advanced Canopy Chlorophyll and Nitrogen Retrieval Technique Using EnMAP Data. *Environ. Chall.* **2025**, *18*, 101114.
119. Verrelst, J.; Rivera-Caicedo, J.P.; Reyes-Muñoz, P.; Morata, M.; Amin, E.; Tagliabue, G.; Panigada, C.; Hank, T.; Berger, K. Mapping landscape canopy nitrogen content from space using PRISMA data. *ISPRS J. Photogramm. Remote Sens.* **2021**, *178*, 382–395.
120. Wang, Y.; Suarez, L.; Hornero, A.; Poblete, T.; Ryu, D.; Gonzalez-Dugo, V.; Zarco-Tejada, P.J. Assessing plant traits derived from Sentinel-2 to characterize leaf nitrogen variability in almond orchards: Modeling and validation with airborne hyperspectral imagery. *Precis. Agric.* **2025**, *26*, 13.
121. Zhang, X.; Han, L.; Sobeih, T.; Lappin, L.; Lee, M.A.; Howard, A.; Kisdi, A. The Self-Supervised Spectral–Spatial Vision Transformer Network for Accurate Prediction of Wheat Nitrogen Status from UAV Imagery. *Remote Sens.* **2022**, *14*, 1400.
122. Xu, S.; Xu, X.; Blacker, C.; Gaulton, R.; Zhu, Q.; Yang, M.; Yang, G.; Zhang, J.; Yang, Y.; Yang, M.; et al. Estimation of Leaf Nitrogen Content in Rice Using Vegetation Indices and Feature Variable Optimization with Information Fusion of Multiple-Sensor Images from UAV. *Remote Sens.* **2023**, *15*, 854.
123. Smith, D.R.; King, K.W.; Johnson, L.; Francesconi, W.; Richards, P.; Baker, D.; Sharpley, A.N. Surface Runoff and Tile Drainage Transport of Phosphorus in the Midwestern United States. *J. Environ. Qual.* **2015**, *44*, 495–502.
124. Valipour, M.; Krasilnikof, J.; Yannopoulos, S.; Kumar, R.; Deng, J.; Roccaro, P.; Mays, L.; Grismer, M.E.; Angelakis, A.N. The evolution of agricultural drainage from the earliest times to the present. *Sustainability* **2020**, *12*, 416.

125. Jepsen, M.R.; Kuemmerle, T.; Müller, D.; Erb, K.; Verburg, P.H.; Haberl, H.; Vesterager, J.P.; Andrič, M.; Antrop, M.; Austrheim, G.; et al. Transitions in European land-management regimes between 1800 and 2010. *Land Use Policy* **2015**, *49*, 53–64.
126. Davidson, N.C. How much wetland has the world lost? Long-term and recent trends in global wetland area. *Mar. Freshw. Res.* **2014**, *65*, 934–941.
127. Koch, J.; Elsgaard, L.; Greve, M.H.; Gyldenkærne, S.; Hermansen, C.; Levin, G.; Wu, S.; Stisen, S. Water-table-driven greenhouse gas emission estimates guide peatland restoration at national scale. *Biogeosciences* **2023**, *20*, 2387–2403.
128. Williamson, T.N.; Dobrowolski, E.G.; Meyer, S.M.; Frey, J.W.; Allred, B.J. Delineation of tile-drain networks using thermal and multispectral imagery—Implications for water quantity and quality differences from paired edge-of-field sites. *J. Soil Water Conserv.* **2018**, *74*, 1–11.
129. Carlsen, A.H.; Fensholt, R.; Looms, M.C.; Gominski, D.; Stisen, S.; Jepsen, M.R. Systematic review of the detection of subsurface drainage systems in agricultural fields using remote sensing systems. *Agric. Water Manag.* **2024**, *299*, 108892.
130. Karbs, H.H. Subsurface Drainage Mapping By Airborne Infrared. In Proceedings of the Oklahoma Academy of Science, Norman, Oklahoma, 31 August–4 September 1970; Volume 18, pp. 10–18.
131. Gökkaya, K.; Budhathoki, M.; Christopher, S.F.; Hanrahan, B.R.; Tank, J.L. Subsurface tile drained area detection using GIS and remote sensing in an agricultural watershed. *Ecol. Eng.* **2017**, *108*, 370–379.
132. Cho, E.; Jacobs, J.M.; Jia, X.; Kraatz, S. Identifying Subsurface Drainage using Satellite Big Data and Machine Learning via Google Earth Engine. *Water Resour. Res.* **2019**, *55*, 8028–8045.
133. Lai, Q.; Xin, Q.; Tian, Y.; Chen, X.; Li, Y.; Wu, R. Structural Analysis and 3D Reconstruction of Underground Pipeline Systems Based on LiDAR Point Clouds. *Remote Sens.* **2025**, *17*, 341.
134. Woo, D.K.; Ji, J.; Song, H. Subsurface drainage pipe detection using an ensemble learning approach and aerial images. *Agric. Water Manag.* **2023**, *287*, 108455.
135. Allred, B.; Eash, N.; Freeland, R.; Martinez, L.; Wishart, D.B. Effective and efficient agricultural drainage pipe mapping with UAS thermal infrared imagery: A case study. *Agric. Water Manag.* **2018**, *197*, 132–137.
136. Becker, A.M.; Becker, R.H.; Doro, K.O. Locating Drainage Tiles at a Wetland Restoration Site within the Oak Openings Region of Ohio, United States Using UAV and Land Based Geophysical Techniques. *Wetlands* **2021**, *41*, 116.
137. Liu, Z.; Chen, G.K.; Tang, B.; Wen, Q.; Tan, R.; Huang, Y. Regional scale terrace mapping in fragmented mountainous areas using multi-source remote sensing data and sample purification strategy. *Sci. Total Environ.* **2024**, *925*, 171366.
138. Lu, Y.; Li, X.; Xin, L.; Song, H.; Wang, X. Mapping the terraces on the Loess Plateau based on a deep learning-based model at 1.89 m resolution. *Sci. Data* **2023**, *10*, 115.
139. Ding, H.; Na, J.; Jiang, S.; Zhu, J.; Liu, K.; Fu, Y.; Li, F. Evaluation of three different machine learning methods for object-based artificial terrace mapping—A case study of the loess plateau, China. *Remote Sens.* **2021**, *13*, 1021.
140. Zhao, F.; Xiong, L.; Wang, C.; Wang, H.; Wei, H.; Tang, G. Terraces mapping by using deep learning approach from remote sensing images and digital elevation models. *Trans. GIS* **2021**, *25*, 2438–2454.
141. Zhai, D.; Dong, J.; Cadisch, G.; Wang, M.; Kou, W.; Xu, J.; Xiao, X.; Abbas, S. Comparison of pixel- and object-based approaches in phenology-based rubber plantation mapping in fragmented landscapes. *Remote Sens.* **2018**, *10*, 44.
142. Blickensdörfer, L.; Schwieder, M.; Pflugmacher, D.; Nendel, C.; Erasmi, S.; Hostert, P. Mapping of crop types and crop sequences with combined time series of Sentinel-1, Sentinel-2 and Landsat 8 data for Germany. *Remote Sens. Environ.* **2022**, *269*, 112831.
143. Godone, D.; Giordan, D.; Baldo, M. Rapid mapping application of vegetated terraces based on high resolution airborne lidar. *Geomat. Nat. Hazards Risk* **2018**, *9*, 970–985.
144. Le Vot, T.; Cohen, M.; Nowak, M.; Passy, P.; Sumera, F. Resilience of Terraced Landscapes to Human and Natural Impacts: A GIS-Based Reconstruction of Land Use Evolution in a Mediterranean Mountain Valley. *Land* **2024**, *13*, 592.
145. Garzón-Oechsle, A.; Johanson, E.; Nagarajan, S.; Martínez, V. In between the Sites: Understanding Late Holocene Manteño Agricultural Contexts in the Chongón-Colonche Mountains of Coastal Ecuador through UAV-Lidar and Excavation. *J. F. Archaeol.* **2025**, *50*, 42–59.
146. Lozić, E. Application of airborne lidar data to the archaeology of agrarian land use. The case study of the early medieval microregion of bled (Slovenia). *Remote Sens.* **2021**, *13*, 3228.
147. Masini, N.; Gizzi, F.T.; Biscione, M.; Fundone, V.; Sedile, M.; Sileo, M.; Pecci, A.; Lacovara, B.; Lasaponara, R. Medieval archaeology under the canopy with LiDAR. the (Re)discovery of a medieval fortified settlement in southern Italy. *Remote Sens.* **2018**, *10*, 1598.
148. Smith, C.; Baker, J.C.A.; Spracklen, D.V. Tropical deforestation causes large reductions in observed precipitation. *Nature* **2023**, *615*, 270–275.

149. Hansen, M.C.; Potapov, P.V.; Moore, R.; Hancher, M.; Turubanova, S.A.; Tyukavina, A.; Thau, D.; Stehman, S.V.; Goetz, S.J.; Loveland, T.R.; et al. High-Resolution Global Maps of 21st-Century Forest Cover Change. *Science* **2013**, *342*, 850–853.
150. Ponvert-Delisles Batista, D.R.; Estrada-Medina, H.; Gijón-Yescas, G.N.; Álvarez-Rivera, O.O. Land covers analyses during slash and burn agriculture by using multispectral imagery obtained with Unattended Aerial Vehicles (UAVs). *Trop. Subtrop. Agroecosystems* **2021**, *24*, 21.
151. Lechner, A.M.; Foody, G.M.; Boyd, D.S. Applications in Remote Sensing to Forest Ecology and Management. *One Earth* **2020**, *2*, 405–412.
152. Lehmann, E.A.; Caccetta, P.; Lowell, K.; Mitchell, A.; Zhou, Z.S.; Held, A.; Milne, T.; Tapley, I. SAR and optical remote sensing: Assessment of complementarity and interoperability in the context of a large-scale operational forest monitoring system. *Remote Sens. Environ.* **2015**, *156*, 335–348.
153. Ballère, M.; Bouvet, A.; Mermoz, S.; Le Toan, T.; Koleck, T.; Bedeau, C.; André, M.; Forestier, E.; Frison, P.L.; Lardeux, C. SAR data for tropical forest disturbance alerts in French Guiana: Benefit over optical imagery. *Remote Sens. Environ.* **2021**, *252*, 112159.
154. Tarazona, Y.; Mantas, V.M.; Pereira, A.J.S.C. Improving tropical deforestation detection through using photosynthetic vegetation time series–(PVts-β). *Ecol. Indic.* **2018**, *94*, 367–379.
155. Bégué, A.; Arvor, D.; Bellon, B.; Betbeder, J.; de Abelleyra, D.; Ferraz, R.P.D.; Lebourgeois, V.; Lelong, C.; Simões, M.; Verón, S.R. Remote sensing and cropping practices: A review. *Remote Sens.* **2018**, *10*, 99.
156. Preidl, S.; Lange, M.; Doktor, D. Introducing APiC for regionalised land cover mapping on the national scale using Sentinel-2A imagery. *Remote Sens. Environ.* **2020**, *240*, 111673.
157. Baessler, C.; Klotz, S. Effects of changes in agricultural land-use on landscape structure and arable weed vegetation over the last 50 years. *Agric. Ecosyst. Environ.* **2006**, *115*, 43–50.
158. Chapman, T. Calculating the Interspersion and Juxtaposition Rates for Saint Clair Flats State Wildlife Area. Ph.D. Thesis, University of Redlands, Redlands, CA, USA, 2022.
159. Uuemaa, E.; Antrop, M.; Roosaare, J.; Marja, R.; Mander, Ü. Landscape metrics and indices: An overview of their use in landscape research. *Living Rev. Landsc. Res.* **2009**, *3*, 1–28.
160. Oksanen, T. Shape-describing indices for agricultural field plots and their relationship to operational efficiency. *Comput. Electron. Agric.* **2013**, *98*, 252–259.
161. Griffel, L.M.; Vazhnik, V.; Hartley, D.S.; Hansen, J.K.; Roni, M. Agricultural field shape descriptors as predictors of field efficiency for perennial grass harvesting: An empirical proof. *Comput. Electron. Agric.* **2020**, *168*, 105088.
162. Salas, E.A.L.; Subburayalu, S.K. Correction: Modified shape index for object-based random forest image classification of agricultural systems using airborne hyperspectral datasets. *PLoS ONE* **2019**, *14*, e0222474.
163. Blüthgen, N.; Dormann, C.F.; Prati, D.; Klaus, V.H.; Kleinebecker, T.; Hölzel, N.; Alt, F.; Boch, S.; Gockel, S.; Hemp, A.; et al. A quantitative index of land-use intensity in grasslands: Integrating mowing, grazing and fertilization. *Basic Appl. Ecol.* **2012**, *13*, 207–220.
164. Rocchini, D.; Balkenhol, N.; Carter, G.A.; Foody, G.M.; Gillespie, T.W.; He, K.S.; Kark, S.; Levin, N.; Lucas, K.; Luoto, M.; et al. Remotely sensed spectral heterogeneity as a proxy of species diversity: Recent advances and open challenges. *Ecol. Inform.* **2010**, *5*, 318–329.
165. Rocchini, D.; Marcantonio, M.; Ricotta, C. Measuring Rao's Q diversity index from remote sensing: An open source solution. *Ecol. Indic.* **2017**, *72*, 234–238.
166. Rocchini, D.; Bacaro, G.; Chirici, G.; Da Re, D.; Feilhauer, H.; Foody, G.M.; Galluzzi, M.; Garzon-Lopez, C.X.; Gillespie, T.W.; He, K.S.; et al. Remotely sensed spatial heterogeneity as an exploratory tool for taxonomic and functional diversity study. *Ecol. Indic.* **2018**, *85*, 983–990.
167. Steele-Dunne, S.C.; McNairn, H.; Monsivais-Huertero, A.; Judge, J.; Liu, P.W.; Papathanassiou, K. Radar Remote Sensing of Agricultural Canopies: A Review. *IEEE J. Sel. Top. Appl. Earth Obs. Remote Sens.* **2017**, *10*, 2249–2273.
168. Howison, R.A.; Piersma, T.; Kentie, R.; Hooijmeijer, J.C.E.W.; Olff, H. Quantifying landscape–level land–use intensity patterns through radar–based remote sensing. *J. Appl. Ecol.* **2018**, *55*, 1276–1287.
169. Herrero-Huerta, M.; Bucksch, A.; Puttonen, E.; Rainey, K.M. Canopy roughness: A new phenotypic trait to estimate aboveground biomass from unmanned aerial system. *Plant Phenomics* **2020**, *2020*, 6735967.
170. Alfieri, J.G.; Kustas, W.P.; Nieto, H.; Prueger, J.H.; Hipps, L.E.; McKee, L.G.; Gao, F.; Los, S. Influence of wind direction on the surface roughness of vineyards. *Irrig. Sci.* **2019**, *37*, 359–373.
171. Singh, A.; Gaurav, K.; Rai, A.K.; Beg, Z. Machine learning to estimate surface roughness from satellite images. *Remote Sens.* **2021**, *13*, 3794.

172. Turner, R.; Panciera, R.; Tanase, M.A.; Lowell, K.; Hacker, J.M.; Walker, J.P. Estimation of soil surface roughness of agricultural soils using airborne LiDAR. *Remote Sens. Environ.* **2014**, *140*, 107–117.
173. Mahlayeye, M.; Darvishzadeh, R.; Nelson, A. Cropping Patterns of Annual Crops: A Remote Sensing Review. *Remote Sens.* **2022**, *14*, 2404.
174. Qiu, B.; Hu, X.; Chen, C.; Tang, Z.; Yang, P.; Zhu, X.; Yan, C.; Jian, Z. Maps of cropping patterns in China during 2015–2021. *Sci. Data* **2022**, *9*, 479.
175. El Hajj, M.; Bégué, A.; Guillaume, S.; Martiné, J.F. Integrating SPOT-5 time series, crop growth modeling and expert knowledge for monitoring agricultural practices—The case of sugarcane harvest on Reunion Island. *Remote Sens. Environ.* **2009**, *113*, 2052–2061.
176. Maponya, M.G.; van Niekerk, A.; Mashimbye, Z.E. Pre-harvest classification of crop types using a Sentinel-2 time-series and machine learning. *Comput. Electron. Agric.* **2020**, *169*, 105164.
177. Ahlawat, I.; Sheoran, H.S.; Roohi; Dahiya, G.; Sihag, P. Analysis of sentinel-1 data for regional crop classification: A multi-data approach for rabi crops of district Hisar (Haryana). *J. Appl. Nat. Sci.* **2020**, *12*, 165–170.
178. Orynbaikyzy, A.; Gessner, U.; Conrad, C. Crop type classification using a combination of optical and radar remote sensing data: A review. *Int. J. Remote Sens.* **2019**, *40*, 6553–6595.
179. Zhao, J.; Zhong, Y.; Hu, X.; Wei, L.; Zhang, L. A robust spectral-spatial approach to identifying heterogeneous crops using remote sensing imagery with high spectral and spatial resolutions. *Remote Sens. Environ.* **2020**, *239*, 111605.
180. Nigam, R.; Tripathy, R.; Dutta, S.; Bhagia, N.; Nagori, R.; Chandrasekar, K.; Kot, R.; Bhattacharya, B.K.; Ustin, S. Crop type discrimination and health assessment using hyperspectral imaging. *Curr. Sci.* **2019**, *116*, 1108–1123.
181. Prins, A.J.; Van Niekerk, A. Crop type mapping using LiDAR, Sentinel-2 and aerial imagery with machine learning algorithms. *Geo-Spat. Inf. Sci.* **2020**, *24*, 215–227.
182. He, T.; Zhang, M.; Xiao, W.; Zhai, G.; Fang, K.; Chen, Y.; Wu, C. Terend and potential enhancement of cropping intensity. *Comput. Electron. Agric.* **2025**, *229*, 109777.
183. Du, G.; Han, L.; Yao, L.; Faye, B. Spatiotemporal Dynamics and Evolution of Grain Cropping Patterns in Northeast China: Insights from Remote Sensing and Spatial Overlay Analysis. *Agriculture* **2024**, *14*, 1443.
184. Manjunath, K.R.; Kundu, N.; Ray, S.S.; Panigrahy, S.; Parihar, J.S. Cropping Systems Dynamics in the Lower Gangetic Plains of India using Geospatial Technologies. *Int. Arch. Photogramm. Remote Sens. Spat. Inf. Sci.* **2012**, *38*, 40–45.
185. Manjunath, K.R.; More, R.S.; Jain, N.K.; Panigrahy, S.; Parihar, J.S. Mapping of rice-cropping pattern and cultural type using remote-sensing and ancillary data: A case study for South and Southeast Asian countries. *Int. J. Remote Sens.* **2015**, *36*, 6008–6030.
186. Aduvukha, G.R.; Abdel-Rahman, E.M.; Sichangi, A.W.; Makokha, G.O.; Landmann, T.; Mudereri, B.T.; Tonnang, H.E.Z.; Dubois, T. Cropping pattern mapping in an agro-natural heterogeneous landscape using sentinel-2 and sentinel-1 satellite datasets. *Agric.* **2021**, *11*, 530.
187. Zhang, M.; Wu, B.; Zeng, H.; He, G.; Liu, C.; Tao, S.; Zhang, Q.; Nabil, M.; Tian, F.; Bofana, J.; et al. GCI30: A global dataset of 30m cropping intensity using multisource remote sensing imagery. *Earth Syst. Sci. Data* **2021**, *13*, 4799–4817.
188. Lange, M.; Feilhauer, H.; Kühn, I.; Doktor, D. Mapping land-use intensity of grasslands in Germany with machine learning and Sentinel-2 time series. *Remote Sens. Environ.* **2022**, *277*, 112888.
189. Griffiths, P.; Nendel, C.; Pickert, J.; Hostert, P. Towards national-scale characterization of grassland use intensity from integrated Sentinel-2 and Landsat time series. *Remote Sens. Environ.* **2020**, *238*, 111124.
190. Fischer, M.; Bossdorf, O.; Gockel, S.; Hänsel, F.; Hemp, A.; Hessenmöller, D.; Korte, G.; Nieschulze, J.; Pfeiffer, S.; Prati, D.; et al. Implementing large-scale and long-term functional biodiversity research: The Biodiversity Exploratories. *Basic Appl. Ecol.* **2010**, *11*, 473–485.
191. Sousa Júnior, V.d.P.; Sparacino, J.; Espindola, G.M.d.; Assis, R.J.S.d. Carbon Biomass Estimation Using Vegetation Indices in Agriculture–Pasture Mosaics in the Brazilian Caatinga Dry Tropical Forest. *ISPRS Int. J. Geo-Inf.* **2023**, *12*, 354.
192. Kumar, L.; Mutanga, O. Remote sensing of above-ground biomass. *Remote Sens.* **2017**, *9*, 935.
193. Zhang, P.; Lu, B.; Ge, J.; Wang, X.; Yang, Y.; Shang, J.; La, Z.; Zang, H.; Zeng, Z. Using UAV-based multispectral and RGB imagery to monitor above-ground biomass of oat-based diversified cropping. *Eur. J. Agron.* **2025**, *162*, 127422.
194. Da, H.; Li, Y.; Xu, L.; Wang, S.; Hu, L.; Hu, Z.; Wei, Q.; Zhu, R.; Chen, Q.; Xin, D.; et al. Advancing soybean biomass estimation through multi-source UAV data fusion and machine learning algorithms. *Smart Agric. Technol.* **2025**, *10*, 100778.

195. Breunig, F.M.; Dalagnol, R.; Galvão, L.S.; Bispo, P.d.C.; Liu, Q.; Berra, E.F.; Gaida, W.; Liesenberg, V.; Sampaio, T.V.M. Monitoring Cover Crop Biomass in Southern Brazil Using Combined PlanetScope and Sentinel-1 SAR Data. *Remote Sens.* **2024**, *16*, 2686.
196. Hagn, L.; Schuster, J.; Mittermayer, M.; Hülsbergen, K.J. A new method for satellite-based remote sensing analysis of plant-specific biomass yield patterns for precision farming applications. *Precis. Agric.* **2024**, *25*, 2801–2830.
197. Burger, R.; Aouizerats, B.; den Besten, N.; Guillevic, P.; Catarino, F.; van der Horst, T.; Jackson, D.; Koopmans, R.; Ridderikhoff, M.; Robson, G.; et al. The Biomass Proxy: Unlocking Global Agricultural Monitoring through Fusion of Sentinel-1 and Sentinel-2. *Remote Sens.* **2024**, *16*, 835.
198. Bloem, E.; Gerighausen, H.; Chen, X.; Schnug, E. The potential of spectral measurements for identifying glyphosate application to agricultural fields. *Agronomy* **2020**, *10*, 1409.
199. Niu, Z.; Rehman, T.; Young, J.; Johnson, W.G.; Yokoo, T.; Young, B.; Jin, J. Hyperspectral Analysis for Discriminating Herbicide Site of Action: A Novel Approach for Accelerating Herbicide Research. *Sensors* **2023**, *23*, 9300.
200. Zhang, T.; Huang, Y.; Reddy, K.N.; Yang, P.; Zhao, X.; Zhang, J. Using Machine Learning and Hyperspectral Images to Assess Damages to Corn Plant Caused by Glyphosate and to Evaluate Recoverability. *Agronomy* **2021**, *11*, 583.
201. Chu, H.; Zhang, C.; Wang, M.; Gouda, M.; Wei, X.; He, Y.; Liu, Y. Hyperspectral imaging with shallow convolutional neural networks (SCNN) predicts the early herbicide stress in wheat cultivars. *J. Hazard. Mater.* **2022**, *421*, 126706.
202. Xiao, T.; Yang, L.; He, X.; Wang, L.; Zhang, D.; Cui, T.; Zhang, K.; Bao, L.; An, S.; Zhang, X. A green and efficient method for detecting nicosulfuron residues in field maize using hyperspectral imaging and deep learning. *J. Hazard. Mater.* **2025**, *484*, 136724.
203. Pause, M.; Raasch, F.; Marrs, C.; Csaplovics, E. Csaplovics Monitoring Glyphosate-Based Herbicide Treatment Using Sentinel-2 Time Series—A Proof-of-Principle. *Remote Sens.* **2019**, *11*, 2541.
204. Pon Arasan, A.; Radhamani, S.; Pazhanivelan, S.; Kavitha, R.; Raja, R.; Kumaraperumal, R. Mapping and monitoring of weeds using unmanned aircraft systems and remote sensing. *Plant Prot. Sci.* **2024**, *61*, 44–55.
205. Li, J.; Ge, Y.; Puntel, L.A.; Heeren, D.M.; Bai, G.; Balboa, G.R.; Gamon, J.A.; Arkebauer, T.J.; Shi, Y. Devising optimized maize nitrogen stress indices in complex field conditions from UAV hyperspectral imagery. *Precis. Agric.* **2024**, *26*, 3.
206. Yin, H.; Li, F.; Yang, H.; Di, Y.; Hu, Y.; Yu, K. Mapping Plant Nitrogen Concentration and Aboveground Biomass of Potato Crops from Sentinel-2 Data Using Ensemble Learning Models. *Remote Sens.* **2024**, *16*, 349.
207. Almawazreh, A.; Buerkert, A.; Vazhacharickal, P.J.; Peth, S. Assessing canopy temperature responses to nitrogen fertilisation in South Indian crops using UAV -based thermal sensing. *Int. J. Remote Sens.* **2025**, *4*, 2389–2417.
208. Hossen, M.A.; Diwakar, P.K.; Ragi, S. Total nitrogen estimation in agricultural soils via aerial multispectral imaging and LIBS. *Sci. Rep.* **2021**, *11*, 12693.
209. Tiessen, H.; Cuevas, E.; Chacon, P. The role of soil organic matter in sustaining soil fertility. *Nature* **1994**, *371*, 783–785.
210. Castaldi, F.; Chabrillat, S.; Jones, A.; Vreys, K.; Bomans, B.; van Wesemael, B. Soil organic carbon estimation in croplands by hyperspectral remote APEX data using the LUCAS topsoil database. *Remote Sens.* **2018**, *10*, 153.
211. Wilcox, C.H.; Frazier, B.E.; Ball, S.T. Relationship between soil organic carbon and landsat tm data in eastern Washington. *Photogramm. Eng. Rem. Sens* **1994**, *60*, 777–781.
212. Batjes, N.H. Total carbon and nitrogen in the soils of the world. *Eur. J. Soil Sci.* **1996**, *47*, 151–163.
213. Basnyat, P.; McConkey, B.; Meinert, B.; Gatkze, C.; Noble, G. Agriculture Field Characterization Using Aerial Photograph and Satellite Imagery. *IEEE Geosci. Remote Sens. Lett.* **2004**, *1*, 7–10.
214. Nguyen, T.T.; Pham, T.D.; Nguyen, C.T.; Delfos, J.; Archibald, R.; Dang, K.B.; Hoang, N.B.; Guo, W.; Ngo, H.H. A novel intelligence approach based active and ensemble learning for agricultural soil organic carbon prediction using multispectral and SAR data fusion. *Sci. Total Environ.* **2022**, *804*, 150187.
215. Zhou, T.; Lv, W.; Geng, Y.; Xiao, S.; Chen, J.; Xu, X.; Pan, J.; Si, B.; Lausch, A. National-scale spatial prediction of soil organic carbon and total nitrogen using long-term optical and microwave satellite observations in Google Earth Engine. *Comput. Electron. Agric.* **2023**, *210*, 107928.
216. Castaldi, F.; Halil Koparan, M.; Wetterlind, J.; Žydelis, R.; Vinci, I.; Özge Savaş, A.; Kıvrak, C.; Tunçay, T.; Volungevičius, J.; Obber, S.; et al. Assessing the capability of Sentinel-2 time-series to estimate soil organic carbon and clay content at local scale in croplands. *ISPRS J. Photogramm. Remote Sens.* **2023**, *199*, 40–60.
217. Wang, X.; Zhang, Y.; Atkinson, P.M.; Yao, H. Predicting soil organic carbon content in Spain by combining Landsat TM and ALOS PALSAR images. *Int. J. Appl. Earth Obs. Geoinf.* **2020**, *92*, 102182.

218. Zhou, T.; Geng, Y.; Chen, J.; Pan, J.; Haase, D.; Lausch, A. High-resolution digital mapping of soil organic carbon and soil total nitrogen using DEM derivatives, Sentinel-1 and Sentinel-2 data based on machine learning algorithms. *Sci. Total Environ.* **2020**, *729*, 138244.
219. Li, H.; Zhang, C.; Zhang, S.; Atkinson, P.M. Full year crop monitoring and separability assessment with fully-polarimetric L-band UAVSAR: A case study in the Sacramento Valley, California. *Int. J. Appl. Earth Obs. Geoinf.* **2019**, *74*, 45–56.
220. Ottinger, M.; Kuenzer, C. Spaceborne L-Band Synthetic Aperture Radar Data for Geoscientific Analyses in Coastal Land Applications: A Review. *Remote Sens.* **2020**, *12*, 2228.
221. Shafizadeh-Moghadam, H.; Minaei, F.; Talebi-khiavi, H.; Xu, T.; Homaee, M. Synergetic use of multi-temporal Sentinel-1, Sentinel-2, NDVI, and topographic factors for estimating soil organic carbon. *Catena* **2022**, *212*, 106077.
222. Wang, L.; Wang, X.; Wang, D.; Qi, B.; Zheng, S.; Liu, H.; Luo, C.; Li, H.; Meng, L.; Meng, X.; et al. Spatiotemporal Changes and Driving Factors of Cultivated Soil Organic Carbon in Northern China's Typical Agro-Pastoral Ecotone in the Last 30 Years. *Remote Sens.* **2021**, *13*, 3607.
223. Odebiri, O.; Mutanga, O.; Odindi, J.; Naicker, R. Modelling soil organic carbon stock distribution across different land-uses in South Africa: A remote sensing and deep learning approach. *ISPRS J. Photogramm. Remote Sens.* **2022**, *188*, 351–362.
224. Wang, X.; Zeng, H.; Yang, X.; Shu, J.; Wu, Q.; Que, Y.; Yang, X.; Yi, X.; Khalil, I.; Zomaya, A.Y. Remote sensing revolutionizing agriculture: Toward a new frontier. *Futur. Gener. Comput. Syst.* **2025**, *166*, 107691.
225. Zhu, X.; Cai, F.; Tian, J.; Williams, T.K.A. Spatiotemporal fusion of multisource remote sensing data: Literature survey, taxonomy, principles, applications, and future directions. *Remote Sens.* **2018**, *10*, 527.
226. Wang, D.; Cao, W.; Zhang, F.; Li, Z.; Xu, S.; Wu, X. A Review of Deep Learning in Multiscale Agricultural Sensing. *Remote Sens.* **2022**, *14*, 559.
227. Osco, L.P.; Junior, J.M.; Ramos, A.P.M.; Furuya, D.E.G.; Santana, D.C.; Teodoro, L.P.R.; Gonçalves, W.N.; Baio, F.H.R.; Pistori, H.; Junior, C.A. da S.; et al. Leaf nitrogen concentration and plant height prediction for maize using UAV-based multispectral imagery and machine learning techniques. *Remote Sens.* **2020**, *12*, 3237.
228. Reda, R.; Saffaj, T.; Ilham, B.; Saidi, O.; Issam, K.; Brahim, L.; El Hadrami, E.M. A comparative study between a new method and other machine learning algorithms for soil organic carbon and total nitrogen prediction using near infrared spectroscopy. *Chemom. Intell. Lab. Syst.* **2019**, *195*, 103873.
229. Castaldi, F.; Hueni, A.; Chabrillat, S.; Ward, K.; Buttafuoco, G.; Bomans, B.; Vreys, K.; Brell, M.; Wesemael, B. Van ISPRS Journal of Photogrammetry and Remote Sensing Evaluating the capability of the Sentinel 2 data for soil organic carbon prediction in croplands. *ISPRS J. Photogramm. Remote Sens.* **2019**, *147*, 267–282.
230. Shi, P.; Wang, Y.; Xu, J.; Zhao, Y.; Yang, B.; Yuan, Z.; Sun, Q. Rice nitrogen nutrition estimation with RGB images and machine learning methods. *Comput. Electron. Agric.* **2021**, *180*, 105860.
231. Sahabiev, I.; Smirnova, E.; Giniyatullin, K. Spatial prediction of agrochemical properties on the scale of a single field using machine learning methods based on remote sensing data. *Agronomy* **2021**, *11*, 2266.
232. Wolanin, A.; Mateo-Garciá, G.; Camps-Valls, G.; Gómez-Chova, L.; Meroni, M.; Duveiller, G.; Liangzhi, Y.; Guanter, L. Estimating and understanding crop yields with explainable deep learning in the Indian Wheat Belt. *Environ. Res. Lett.* **2020**, *15*, 024019.
233. Ferentinos, K.P. Deep learning models for plant disease detection and diagnosis. *Comput. Electron. Agric.* **2018**, *145*, 311–318.
234. Jaihuni, M.; Khan, F.; Lee, D.; Basak, J.K.; Bhujel, A.; Moon, B.E.; Park, J.; Kim, H.T. Determining Spatiotemporal Distribution of Macronutrients in a Cornfield Using Remote Sensing and a Deep Learning Model. *IEEE Access* **2021**, *9*, 30256–30266.
235. Gebbers, R.; Adamchuk, V.I. Precision Agriculture and Food Security. *Science* **2010**, *327*, 828–831.
236. Jiang, H.; Zhang, C.; Qiao, Y.; Zhang, Z.; Zhang, W.; Song, C. CNN feature based graph convolutional network for weed and crop recognition in smart farming. *Comput. Electron. Agric.* **2020**, *174*, 105450.
237. Khusro, S.; Jabeen, F.; Mashwani, S.R.; Alam, I. Linked open data: Towards the realization of semantic web-A review. *Indian J. Sci. Technol.* **2014**, *7*, 745–764.
238. Lausch, A.; Schmidt, A.; Tischendorf, L. Data mining and linked open data—New perspectives for data analysis in environmental research. *Ecol. Modell.* **2015**, *295*, 5–17.
239. Zhou, X.; Zhang, J.; Chen, D.; Huang, Y.; Kong, W.; Yuan, L.; Ye, H.; Huang, W. Assessment of Leaf Chlorophyll Content Models for Winter Wheat Using Landsat-8 Multispectral Remote Sensing Data. *Remote Sens.* **2020**, *12*, 2574.
240. Zolotukhina, A.; Machikhin, A.; Guryleva, A.; Gresis, V.; Kharchenko, A.; Dekhkanova, K.; Polyakova, S.; Fomin, D.; Nesterov, G.; Pozhar, V. Evaluation of Leaf Chlorophyll Content from Acousto-Optic Hyperspectral Data: A Multi-Crop Study. *Remote Sens.* **2024**, *16*, 1073.

241. Cheng, J.; Yang, H.; Qi, J.; Sun, Z.; Han, S.; Feng, H.; Jiang, J.; Xu, W.; Li, Z.; Yang, G.; et al. Estimating canopy-scale chlorophyll content in apple orchards using a 3D radiative transfer model and UAV multispectral imagery. *Comput. Electron. Agric.* **2022**, *202*, 107401.
242. Haboudane, D.; Miller, J.R.; Tremblay, N.; Zarco-Tejada, P.J.; Dextraze, L. Integrated narrow-band vegetation indices for prediction of crop chlorophyll content for application to precision agriculture. *Remote Sens. Environ.* **2002**, *81*, 416–426.
243. Qian, B.; Ye, H.; Huang, W.; Xie, Q.; Pan, Y.; Xing, N.; Ren, Y.; Guo, A.; Jiao, Q.; Lan, Y. A sentinel-2-based triangular vegetation index for chlorophyll content estimation. *Agric. For. Meteorol.* **2022**, *322*, 109000.
244. Holtgrave, A.K.; Röder, N.; Ackermann, A.; Erasmi, S.; Kleinschmit, B. Comparing Sentinel-1 and -2 data and indices for agricultural land use monitoring. *Remote Sens.* **2020**, *12*, 2919.
245. Wu, Q.; Zhang, Y.; Zhao, Z.; Xie, M.; Hou, D. Estimation of Relative Chlorophyll Content in Spring Wheat Based on Multi-Temporal UAV Remote Sensing. *Agronomy* **2023**, *13*, 211.
246. Gitelson, A.A.; Viña, A.; Solovchenko, A. Spectral response of gross primary production to in situ canopy light absorption coefficient of chlorophyll. *Photosynth. Res.* **2025**, *163*, 20.
247. Gitelson, A.; Arkebauer, T.; Solovchenko, A.; Nguy-Robertson, A.; Inoue, Y. An insight into spectral composition of light available for photosynthesis via remotely assessed absorption coefficient at leaf and canopy levels. *Photosynth. Res.* **2022**, *151*, 47–60.
248. Abdelbaki, A.; Schlerf, M.; Retzlaff, R.; Machwitz, M.; Verrelst, J.; Udelhoven, T. Comparison of crop trait retrieval strategies using UAV-based VNIR hyperspectral imaging. *Remote Sens.* **2021**, *13*, 1748.
249. Blackburn, G.A. Hyperspectral remote sensing of plant pigments. *J. Exp. Bot.* **2007**, *58*, 855–867.
250. Lee, S.; Ghimire, A.; Kim, Y.; Lee, J.D. Automatic optimization of regions of interest in hyperspectral images for detecting vegetative indices in soybeans. *Front. Plant Sci.* **2025**, *16*, 1511646.
251. Gitelson, A.; Solovchenko, A.; Viña, A. Foliar absorption coefficient derived from reflectance spectra: A gauge of the efficiency of in situ light-capture by different pigment groups. *J. Plant Physiol.* **2020**, *254*, 153277.
252. Shen, J.; Huang, Y.; Chen, W.; Li, M.; Tan, W.; Wang, R.; Deng, Y.; Gong, Y.; Ai, S.; Liu, N. Assessing the Transferability of Models for Predicting Foliar Nutrient Concentrations Across Maize Cultivars. *Remote Sens.* **2025**, *17*, 652.
253. Kharel, T.P.; Tyler, H.L.; Mubvumba, P.; Huang, Y.; Bhandari, A.B.; Fletcher, R.S.; Anapalli, S.; Joshi, D.R.; Mengistu, A.; Birru, G.; et al. Machine learning on multi-spectral imagery to estimate nutrient yield of mixed-species cover crops. *Agric. Environ. Lett.* **2025**, *10*, e70009.
254. Geng, G.; Gu, Q.; Zhou, H.; Zhang, B.; He, Z.; Zheng, R. Random forest model that incorporates solar-induced chlorophyll fluorescence data can accurately track crop yield variations under drought conditions. *Ecol. Inform.* **2025**, *85*, 102972.
255. Wu, Y.; Zhang, Z.; Wu, L.; Zhang, Y. Solar-induced chlorophyll fluorescence and its relationship with photosynthesis during waterlogging in a maize field. *Agric. For. Meteorol.* **2025**, *363*, 110404.
256. Li, Z.; Zhang, Q.; Li, J.; Yang, X.; Wu, Y.; Zhang, Z.; Wang, S.; Wang, H.; Zhang, Y. Solar-induced chlorophyll fluorescence and its link to canopy photosynthesis in maize from continuous ground measurements. *Remote Sens. Environ.* **2020**, *236*, 111420.
257. Song, L.; Cai, J.; Wu, K.; Li, Y.; Hou, G.; Du, S.; Duan, J.; He, L.; Guo, T.; Feng, W. Early diagnosis of wheat powdery mildew using solar-induced chlorophyll fluorescence and hyperspectral reflectance. *Eur. J. Agron.* **2025**, *162*, 127427.
258. Jin, X.; Zarco-Tejada, P.J.; Schmidhalter, U.; Reynolds, M.P.; Hawkesford, M.J.; Varshney, R.K.; Yang, T.; Nie, C.; Li, Z.; Ming, B.; et al. High-Throughput Estimation of Crop Traits: A Review of Ground and Aerial Phenotyping Platforms. *IEEE Geosci. Remote Sens. Mag.* **2021**, *9*, 200–231.
259. Camino, C.; González-Dugo, V.; Hernández, P.; Sillero, J.C.; Zarco-Tejada, P.J. Improved nitrogen retrievals with airborne-derived fluorescence and plant traits quantified from VNIR-SWIR hyperspectral imagery in the context of precision agriculture. *Int. J. Appl. Earth Obs. Geoinf.* **2018**, *70*, 105–117.
260. Gerhards, M.; Schlerf, M.; Mallick, K.; Udelhoven, T. Challenges and future perspectives of multi-/Hyperspectral thermal infrared remote sensing for crop water-stress detection: A review. *Remote Sens.* **2019**, *11*, 1240.
261. Abbas, T.; Farooq, N.; Nadeem, M.A. Application of leaf water content measurement to improve herbicide efficacy for effective weed management in a changing climate—A review. *Crop Prot.* **2025**, *191*, 107138.
262. Cardamis, M.; Jia, H.; Qian, H.; Chen, W.; Yan, Y.; Ghannoum, O.; Quigley, A.; Chou, C.T.; Hu, W. Leafeon: Towards Accurate Sensing of Leaf Water Content for Protected Cropping, with mmWave Radar. *IEEE Internet Things J.* **2025**, *12*, 19646–19659.
263. Dong, H.; Dong, J.; Sun, S.; Bai, T.; Zhao, D.; Yin, Y.; Shen, X.; Wang, Y.; Zhang, Z.; Wang, Y. Crop water stress detection based on UAV remote sensing systems. *Agric. Water Manag.* **2024**, *303*, 109059.

264. Ahmad, U.; Alvino, A.; Marino, S. A Review of Crop Water Stress Assessment Using Remote Sensing. *Remote Sens.* **2021**, *13*, 4155.
265. Romero-Trigueros, C.; Bayona Gambín, J.M.; Nortes Tortosa, P.A.; Alarcón Cabañero, J.J.; Nicolás, E.N. Determination of Crop Water Stress index by infrared thermometry in grapefruit trees irrigated with saline reclaimed water combined with deficit irrigation. *Remote Sens.* **2019**, *11*, 757.
266. Jiang, M.; Zheng, C.; Jia, L.; Chen, J. A 20-year dataset (2001—2020) of global cropland water-use efficiency at 1-km grid resolution. *Sci. Data* **2025**, *12*, 574.
267. Cheng, M.; Yin, D.; Wu, W.; Cui, N.; Nie, C.; Shi, L.; Liu, S.; Yu, X.; Bai, Y.; Liu, Y.; et al. A review of remote sensing estimation of crop water productivity: Definition, methodology, scale, and evaluation. *Int. J. Remote Sens.* **2023**, *44*, 5033–5068.
268. Safi, A.R.; Karimi, P.; Mul, M.; Chukalla, A.; de Fraiture, C. Translating open-source remote sensing data to crop water productivity improvement actions. *Agric. Water Manag.* **2022**, *261*, 107373.
269. Koetz, B.; Bastiaanssen, W.; Berger, M.; Defourney, P.; Del Bello, U.; Drusch, M.; Drinkwater, M.; Duca, R.; Fernandez, V.; Ghent, D.; et al. High spatio-temporal resolution land surface temperature mission—A copernicus candidate mission in support of agricultural monitoring. In Proceedings of the IEEE International Geoscience and Remote Sensing Symposium, Valencia, Spain, 22–27 July 2018; pp. 8160–8162.
270. Heinemann, S.; Siegmann, B.; Thonfeld, F.; Muro, J.; Jedmowski, C.; Kemna, A.; Kraska, T.; Muller, O.; Schultz, J.; Udelhoven, T.; et al. Land surface temperature retrieval for agricultural areas using a novel UAV platform equipped with a thermal infrared and multispectral sensor. *Remote Sens.* **2020**, *12*, 1075.
271. Lee, J. Estimating Near-Surface Air Temperature from Satellite-Derived Land Surface Temperature Using Temporal Deep Learning: A Comparative Analysis. *IEEE Access* **2025**, *13*, 28935–28945.
272. Majumder, A.; Kingra, P.K.; Setia, R.; Singh, S.P.; Pateriya, B. Influence of land use/land cover changes on surface temperature and its effect on crop yield in different agro-climatic regions of Indian Punjab. *Geocarto Int.* **2020**, *35*, 663–686.
273. Barai, K.; Wallhead, M.; Hall, B.; Rahimzadeh-Bajgiran, P.; Meireles, J.; Herrmann, I.; Zhang, Y.J. Detecting spatial variation in wild blueberry water stress using UAV-borne thermal imagery: Distinct temporal and reference temperature effects. *Precis. Agric.* **2025**, *26*, 25.
274. García-Santos, V.; Sánchez, J.M.; Cuxart, J. Evapotranspiration Acquired with Remote Sensing Thermal-Based Algorithms: A State-of-the-Art Review. *Remote Sens.* **2022**, *14*, 3440.
275. El Hazdour, I.; Le Page, M.; Hanich, L.; Chakir, A.; Lopez, O.; Jarlan, L. A GEE TSEB workflow for daily high-resolution fully remote sensing evapotranspiration: Validation over four crops in semi-arid conditions and comparison with the SSEBop experimental product. *Environ. Model. Softw.* **2025**, *187*, 106365.
276. Bhattarai, N.; Wagle, P. Recent advances in remote sensing of evapotranspiration. *Remote Sens.* **2021**, *13*, 4260.
277. Pelosi, A.; Villani, P.; Bolognesi, S.F.; Chirico, G.B.; D'urso, G. Predicting crop evapotranspiration by integrating ground and remote sensors with air temperature forecasts. *Sensors* **2020**, *20*, 1740.
278. Ippolito, M.; De Caro, D.; Ciraolo, G.; Minacapilli, M.; Provenzano, G. Estimating crop coefficients and actual evapotranspiration in citrus orchards with sporadic cover weeds based on ground and remote sensing data. *Irrig. Sci.* **2023**, *41*, 5–22.
279. Wolff, W.; Francisco, J.P.; Flumignan, D.L.; Marin, F.R.; Folegatti, M.V. Optimized algorithm for evapotranspiration retrieval via remote sensing. *Agric. Water Manag.* **2022**, *262*, 107390.
280. Garofalo, S.P.; Ardito, F.; Sanitate, N.; De Carolis, G.; Ruggieri, S.; Giannico, V.; Rana, G.; Ferrara, R.M. Robustness of Actual Evapotranspiration Predicted by Random Forest Model Integrating Remote Sensing and Meteorological Information: Case of Watermelon (*Citrullus lanatus*, (Thunb.) Matsum. & Nakai, 1916). *Water* **2025**, *17*, 323.
281. Ratshiedana, P.E.; Elbasit, M.A.M.; Adam, E.; Chirima, G.J. Evaluation of remote sensing algorithms for estimating actual evapotranspiration in arid agricultural environments. *Hydrol. Earth Syst. Sci.* **2025**. doi: https://doi.org/10.5194/hess-2024-351
282. Liu, M.; Lei, H.; Wang, X.; Paredes, P. High-resolution mapping of evapotranspiration over heterogeneous cropland affected by soil salinity. *Agric. Water Manag.* **2025**, *308*, 109301.
283. Kaihotsu, I.; Asanuma, J.; Aida, K.; Oyunbaatar, D. Evaluation of the AMSR2 L2 soil moisture product of JAXA on the Mongolian Plateau over seven years (2012–2018). *SN Appl. Sci.* **2019**, *1*, 1477.
284. Kolassa, J.; Gentine, P.; Prigent, C.; Aires, F. Soil moisture retrieval from AMSR-E and ASCAT microwave observation synergy. Part 1: Satellite data analysis. *Remote Sens. Environ.* **2016**, *173*, 202–217.

285. NISAR NISAR: The NASA-ISRO SAR Mission. Water: Vital for Life and Civilization. © 2019 California Institute of Technology. Government Sponsorship Acknowledged. Available online: https://nisar.jpl.nasa.gov/system/documents/files/15_NISARApplications_SoilMoisture1.pdf (accessed on 19 October 2025).
286. Benninga, H.J.F.; van der Velde, R.; Su, Z. Sentinel-1 soil moisture content and its uncertainty over sparsely vegetated fields. *J. Hydrol. X* **2020**, *9*, 100066.
287. Abbaszadeh, P.; Moradkhani, H.; Gavahi, K.; Kumar, S.; Hain, C.; Zhan, X.; Duan, Q.; Peters-Lidard, C.; Karimiziarani, S. High-resolution smap satellite soil moisture product: Exploring the opportunities. *Bull. Am. Meteorol. Soc.* **2021**, *102*, 309–315.
288. Noory, H.; Khoshsima, M.; Tsunekawa, A.; Tsubo, M.; Haregeweyn, N.; Pashapour, S. Developing a method for root-zone soil moisture monitoring at the field scale using remote sensing and simulation modeling. *Agric. Water Manag.* **2025**, *308*, 109263.
289. Jalilvand, E.; Tajrishy, M.; Ghazi Zadeh Hashemi, S.A.; Brocca, L. Quantification of irrigation water using remote sensing of soil moisture in a semi-arid region. *Remote Sens. Environ.* **2019**, *231*, 111226.
290. Ghazali, M.F.; Wikantika, K.; Harto, A.B.; Kondoh, A. Generating soil salinity, soil moisture, soil pH from satellite imagery and its analysis. *Inf. Process. Agric.* **2020**, *7*, 294–306.
291. Chabrillat, S.; Ben-Dor, E.; Cierniewski, J.; Gomez, C.; Schmid, T.; van Wesemael, B. *Imaging Spectroscopy for Soil Mapping and Monitoring*; Springer: Dordrecht, The Netherlands, 2019; Volume 40, ISBN 0123456789.
292. Alvino, A.; Marino, S. Remote sensing for irrigation of horticultural crops. *Horticulturae* **2017**, *3*, 40.
293. Mpakairi, K.S.; Dube, T.; Sibanda, M.; Mutanga, O. Leveraging remote sensing for optimised national scale agricultural water management in South Africa. *Sci. Total Environ.* **2025**, *974*, 179199.
294. Zhou, D.; Zheng, C.; Jia, L.; Menenti, M.; Lu, J.; Chen, Q. Evaluating the Performance of Irrigation Using Remote Sensing Data and the Budyko Hypothesis: A Case Study in Northwest China. *Remote Sens.* **2025**, *17*, 1085.
295. Pitoro, V.S.J.; Franco, J.R.; de Souza Correa, L.R.; Manjate, M.J.; Román, R.M.S. Evaluating Water Productivity and Efficiency in Irrigated Fields Using Remote Sensing: A Case Study in Mozambique's Sugarcane Cultivation. *Water Conserv. Sci. Eng.* **2025**, *10*, 14.
296. Ahmad, U.; Sohel, F. Evaluating decision support systems for precision irrigation and water use efficiency. *Digit. Eng.* **2025**, *4*, 100038.
297. Akbar, M.U.; Mirchi, A.; Arshad, A.; Alian, S.; Mehata, M.; Taghvaeian, S.; Khodkar, K.; Kettner, J.; Datta, S.; Wagner, K. Multi-model ensemble mapping of irrigated areas using remote sensing, machine learning, and ground truth data. *Agric. Water Manag.* **2025**, *312*, 109416.
298. Zhai, W.; Cheng, Q.; Duan, F.; Huang, X.; Chen, Z. Remote sensing-based analysis of yield and water-fertilizer use efficiency in winter wheat management. *Agric. Water Manag.* **2025**, *311*, 109390.
299. Liu, Y.; Wang, Y.; Liao, Y.; Liao, R.; Šimůnek, J. Generating high-precision farmland irrigation pattern maps using remotely sensed ecological indices and machine learning algorithms. *Agric. Water Manag.* **2025**, *308*, 109302.
300. Ozdogan, M.; Yang, Y.; Allez, G.; Cervantes, C. Remote sensing of irrigated agriculture: Opportunities and challenges. *Remote Sens.* **2010**, *2*, 2274–2304.
301. Alordzinu, K.E.; Li, J.; Lan, Y.; Appiah, S.A.; Al Aasmi, A.; Wang, H.; Liao, J.; Sam-amoah, L.K.; Qiao, S. Ground-based hyperspectral remote sensing for estimating water stress in tomato growth in sandy loam and silty loam soils. *Sensors* **2021**, *21*, 5705.
302. Wang, X.; Guo, Z.; Zhang, K.; Fu, Z.; Lee, C.K.F.; Yang, D.; Detto, M.; Zhang, Y.; Wu, J. Can Large—Scale Satellite Products Track the Effects of Atmospheric Dryness and Soil Water Deficit on Ecosystem Productivity Under Droughts? *Geophys. Res. Lett.* **2025**, *52*, e2024GL110785.
303. Yu, J.; Wang, W.; Chen, Z.; Cao, M.; Qian, H. Disentangling the dominance of atmospheric and soil water stress on vegetation productivity in global drylands. *J. Hydrol.* **2025**, *657*, 133043.
304. Sankey, T.T. UAV hyperspectral-thermal-lidar fusion in phenotyping: Genetic trait differences among Fremont cottonwood populations. *Landsc. Ecol.* **2025**, *40*, 45.
305. Gitelson, A.; Arkebauer, T.; Viña, A.; Skakun, S.; Inoue, Y. Evaluating plant photosynthetic traits via absorption coefficient in the photosynthetically active radiation region. *Remote Sens. Environ.* **2021**, *258*, 112401.
306. Wang, X.; Lei, H.; Li, J.; Huo, Z.; Zhang, Y.; Qu, Y. Estimating evapotranspiration and yield of wheat and maize croplands through a remote sensing-based model. *Agric. Water Manag.* **2023**, *282*, 108294.
307. Koganti, T.; Ghane, E.; Martinez, L.R.; Iversen, B.V.; Allred, B.J. Mapping of agricultural subsurface drainage systems using unmanned aerial vehicle imagery and ground penetrating radar. *Sensors* **2021**, *21*, 2800. ISBN 4591732010.

308. Rahmani, S.R.; Schulze, D.G. Mapping subsurface tile lines on a research farm using aerial photography, paper maps, and expert knowledge. *Agrosystems Geosci. Environ.* **2023**, *6*, e20362.
309. Zhao, C.; Pan, Y.; Zhu, X.; Li, L.; Xia, X.; Ren, S.; Gao, Y. Monitoring of deforestation events in the tropics using multidimensional features of Sentinel 1 radar data. *Front. For. Glob. Change* **2023**, *6*, 1257806.
310. Tang, X.; Bratley, K.H.; Cho, K.; Bullock, E.L.; Olofsson, P.; Woodcock, C.E. Near real-time monitoring of tropical forest disturbance by fusion of Landsat, Sentinel-2, and Sentinel-1 data. *Remote Sens. Environ.* **2023**, *294*, 113626.
311. Zhao, F.; Sun, R.; Zhong, L.; Meng, R.; Huang, C.; Zeng, X.; Wang, M.; Li, Y.; Wang, Z. Monthly mapping of forest harvesting using dense time series Sentinel-1 SAR imagery and deep learning. *Remote Sens. Environ.* **2022**, *269*, 112822.
312. Bullock, E.L.; Woodcock, C.E.; Olofsson, P. Monitoring tropical forest degradation using spectral unmixing and Landsat time series analysis. *Remote Sens. Environ.* **2020**, *238*, 110968.
313. Li, Y.; Ye, Y.; Fang, X.; Zhang, C.; Zhao, Z. Loss of wetlands due to the expansion of polder in the Dongting Plain, China, AD 1368–1980. *Holocene* **2020**, *30*, 646–656.
314. Li, Y.; Dai, H.; Dai, Z.; Zhang, L. The polder systems legacies in the early twentieth century affect the contemporary landscape in the Jianghan Plain of Hubei, China. *Herit. Sci.* **2024**, *12*, 311.
315. Rosen, P.A.; Hensley, S.; Gurrola, E.; Rogez, F.; Chan, S.; Martin, J.; Rodriguez, E. SRTM C-band topographic data: Quality assessments and calibration activities. In Proceedings of the IGARSS 2001. Scanning the Present and Resolving the Future. Proceedings. IEEE 2001 International Geoscience and Remote Sensing Symposium (Cat. No.01CH37217), Sydney, NSW, Australia, 9–13 July 2001; Volume 2, pp. 739–741.
316. Wulder, M.A.; Loveland, T.R.; Roy, D.P.; Crawford, C.J.; Masek, J.G.; Woodcock, C.E.; Allen, R.G.; Anderson, M.C.; Belward, A.S.; Cohen, W.B.; et al. Current status of Landsat program, science, and applications. *Remote Sens. Environ.* **2019**, *225*, 127–147.
317. Zink, M.; Fiedler, H.; Hajnsek, I.; Krieger, G.; Moreira, A.; Werner, M. The TanDEM-X Mission Concept. In Proceedings of the 2006 IEEE International Symposium on Geoscience and Remote Sensing, Denver, CO, USA, 31 July–4 August 2006; pp. 1938–1941.
318. Wessel, B.; Huber, M.; Wohlfart, C.; Marschalk, U.; Kosmann, D.; Roth, A. Accuracy assessment of the global TanDEM-X Digital Elevation Model with GPS data. *ISPRS J. Photogramm. Remote Sens.* **2018**, *139*, 171–182.
319. Potin, P.; Rosich, B.; Roeder, J.; Bargellini, P. Sentinel-1 Mission operations concept. In Proceedings of the 2014 IEEE Geoscience and Remote Sensing Symposium, Munich, Germany, 22–27 July 2014; pp. 1465–1468.
320. Kankaku, Y.; Suzuki, S.; OSAWA, Y. ALOS-2 mission and development status. In Proceedings of the 2013 IEEE International Geoscience and Remote Sensing Symposium—IGARSS, Melbourne, VIC, Australia, 21–26 July 2013; pp. 2396–2399.
321. Hirano, A.; Welch, R.; Lang, H. Mapping from ASTER stereo image data: DEM validation and accuracy assessment. *ISPRS J. Photogramm. Remote Sens.* **2003**, *57*, 356–370.
322. Takaku, J.; Tadono, T. High resolution DSM generation from ALOS PRISM—Mosaic dataset-. In Proceedings of the 2012 IEEE International Geoscience and Remote Sensing Symposium, Munich, Germany, 22–27 July 2012; pp. 2687–2690.
323. Rosenqvist, A.; Shimada, M.; Ito, N.; Watanabe, M. ALOS PALSAR: A pathfinder mission for global-scale monitoring of the environment. *IEEE Trans. Geosci. Remote Sens.* **2007**, *45*, 3307–3316.
324. Schutz, B.E.; Zwally, H.J.; Shuman, C.A.; Hancock, D.; DiMarzio, J.P. Overview of the ICESat mission. *Geophys. Res. Lett.* **2005**, *32*, L21S01.
325. Roy, Y.L.; Deschaux-Beaume, M. Sral, A Radar Altime Ter Designed to Meas Ure A Wide Range of Surface Types. *Power* **2009**, *1*, 445–448.
326. Donnellan, A.; Parker, J.; Hensley, S.; Pierce, M.; Wang, J.; Rundle, J. UAVSAR observations of triggered slip on the Imperial, Superstition Hills, and East Elmore Ranch Faults associated with the 2010 M 7.2 El Mayor-Cucapah earthquake. *Geochem. Geophys. Geosyst.* **2014**, *15*, 815–829.
327. Dillner, R.P.; Wimmer, M.A.; Porten, M.; Udelhoven, T.; Retzlaff, R. Combining a Standardized Growth Class Assessment, UAV Sensor Data, GIS Processing, and Machine Learning Classification to Derive a Correlation with the Vigour and Canopy Volume of Grapevines. *Sensors* **2025**, *25*, 431.
328. Mulder, V.L.; de Bruin, S.; Schaepman, M.E.; Mayr, T.R. The use of remote sensing in soil and terrain mapping—A review. *Geoderma* **2011**, *162*, 1–19.
329. Kehoe, M.; Harding, A.; Pagdilao, S.J.; Appels, W.M. Effect of topographical and soil complexity on potato yields in irrigated fields. *Agric. Water Manag.* **2025**, *307*, 109216.

330. Perović, V.; Čakmak, D.; Jakšić, D.; Milanović, M.; Matić, M.; Pavlović, D.; Mitrović, M.; Pavlović, P. Development and evaluation approach of soil quality in agricultural soils: Integrated system for a more reliable delineation of homogeneous management zones. *Appl. Soil Ecol.* **2025**, *206*, 105860.
331. Tang, J.; Xie, Y.; Cheng, H.; Liu, G. Catena Impact of farmland landscape characteristics on gully erosion in the black soil region of Northeast China. *Catena* **2025**, *249*, 108623.
332. Liu, G.; Xia, J.; Zheng, K.; Cheng, J.; Wang, K.; Liu, Z.; Wei, Y.; Xie, D. Measurement and evaluation method of farmland microtopography feature information based on 3D LiDAR and inertial measurement unit. *Soil Tillage Res.* **2024**, *236*, 105921.
333. Ambaru, B.; Manvitha, R.; Madas, R. Synergistic integration of remote sensing and soil metagenomics data: Advancing precision agriculture through interdisciplinary approaches. *Front. Sustain. Food Syst.* **2024**, *8*, 1499973.
334. Wrbka, T.; Erb, K.H.; Schulz, N.B.; Peterseil, J.; Hahn, C.; Haberl, H. Linking pattern and process in cultural landscapes. An empirical study based on spatially explicit indicators. *Land Use Policy* **2004**, *21*, 289–306.
335. Sertel, E.; Topaloğlu, R.H.; Şallı, B.; Algan, I.Y.; Aksu, G.A. Comparison of landscape metrics for three different level land cover/land use maps. *ISPRS Int. J. Geo-Inf.* **2018**, *7*, 408.
336. Cai, Z.; Hu, Q.; Zhang, X.; Yang, J.; Wei, H.; He, Z.; Song, Q.; Wang, C.; Yin, G.; Xu, B. An Adaptive Image Segmentation Method with Automatic Selection of Optimal Scale for Extracting Cropland Parcels in Smallholder Farming Systems. *Remote Sens.* **2022**, *14*, 3067.
337. Wagner, M.P.; Oppelt, N. Extracting agricultural fields from remote sensing imagery using graph-based growing contours. *Remote Sens.* **2020**, *12*, 1205.
338. Watkins, B.; Van Niekerk, A. Automating field boundary delineation with multi-temporal Sentinel-2 imagery. *Comput. Electron. Agric.* **2019**, *167*, 105078.
339. Tieskens, K.F.; Schulp, C.J.E.; Levers, C.; Lieskovský, J.; Kuemmerle, T.; Plieninger, T.; Verburg, P.H. Characterizing European cultural landscapes: Accounting for structure, management intensity and value of agricultural and forest landscapes. *Land Use Policy* **2017**, *62*, 29–39.
340. Ye, S.; Ren, S.; Song, C.; Du, Z.; Wang, K.; Du, B.; Cheng, F.; Zhu, D. Spatial pattern of cultivated land fragmentation in mainland China: Characteristics, dominant factors, and countermeasures. *Land Use Policy* **2024**, *139*, 107070.
341. Erikstad, L.; Simensen, T.; Bakkestuen, V.; Halvorsen, R. Index Measuring Land Use Intensity—A Gradient-Based Approach. *Geomatics* **2023**, *3*, 188–204.
342. Meier, E.S.; Indermaur, A.; Ginzler, C.; Psomas, A. An effective way to map land-use intensity with a high spatial resolution based on habitat type and environmental data. *Remote Sens.* **2020**, *12*, 969.
343. Forkuor, G.; Conrad, C.; Thiel, M.; Zoungrana, B.J.B.; Tondoh, J.E. Multiscale remote sensing to map the spatial distribution and extent of cropland in the sudanian savanna of West Africa. *Remote Sens.* **2017**, *9*, 839.
344. Eckert, S.; Kiteme, B.; Njuguna, E.; Zaehringer, J.G. Agricultural expansion and intensification in the foothills of Mount Kenya: A landscape perspective. *Remote Sens.* **2017**, *9*, 784.
345. Knauer, K.; Gessner, U.; Fensholt, R.; Forkuor, G.; Kuenzer, C. Monitoring agricultural expansion in Burkina Faso over 14 years with 30 m resolution time series: The role of population growth and implications for the environment. *Remote Sens.* **2017**, *9*, 132.
346. Gilcher, M.; Udelhoven, T. Field geometry and the spatial and temporal generalization of crop classification algorithms—A randomized approach to compare pixel based and convolution based methods. *Remote Sens.* **2021**, *13*, 775.
347. Potapov, P.; Turubanova, S.; Hansen, M.C.; Tyukavina, A.; Zalles, V.; Khan, A.; Song, X.P.; Pickens, A.; Shen, Q.; Cortez, J. Global maps of cropland extent and change show accelerated cropland expansion in the twenty-first century. *Nat. Food* **2022**, *3*, 19–28.
348. Janus, J. Measuring land fragmentation considering the shape of transportation network: A method to increase the accuracy of modeling the spatial structure of agriculture with case study in Poland. *Comput. Electron. Agric.* **2018**, *148*, 259–271.
349. Wang, H.; Feng, C.; Li, X.; Yang, Y.; Zhang, Y.; Su, J.; Luo, D.; Wei, D.; He, Y. Plant Species Diversity Assessment in the Temperate Grassland Region of China Using UAV Hyperspectral Remote Sensing. *Diversity* **2024**, *16*, 775.
350. Xu, D.; Chen, H.; Ji, F.; Zhu, J.; Wang, Z.; Zhang, R.; Hou, M.; Huang, X.; Wang, D.; Lu, T.; et al. New insights on canopy heterogeneous analysis and light micro-climate simulation in Chinese solar greenhouse. *Comput. Electron. Agric.* **2025**, *233*, 110179.
351. Contreras, F.; Cayuela, M.L.; Sánchez-Monedero, M.Á.; Pérez-Cutillas, P. Multi-Source Remote Sensing for large-scale biomass estimation in mediterranean olive orchards using GEDI LiDAR and Machine Learning. *EGUsphere* **2025**.
352. Feng, H.; Fan, Y.; Yue, J.; Bian, M.; Liu, Y.; Chen, R.; Ma, Y.; Fan, J.; Yang, G.; Zhao, C. Estimation of potato above-ground biomass based on the VGC-AGB model and deep learning. *Comput. Electron. Agric.* **2025**, *232*, 110122.

353. Chen, M.; Tang, Y.; Zou, X.; Huang, Z.; Zhou, H.; Chen, S. 3D global mapping of large-scale unstructured orchard integrating eye-in-hand stereo vision and SLAM. *Comput. Electron. Agric.* **2021**, *187*, 106237.
354. Hadadi, M.; Saraeian, M.; Godbersen, J.; Jubery, T.; Li, Y.; Attigala, L.; Aditya Balu, S.S.; Schnable, P.S.; Krishnamurthy, A.; Ganapathysubramanian, B.; et al. Procedural Generation of 3D Maize Plant Architecture from LIDAR. *Comput. Sci.* **2025**, *236*, 110382.
355. Bao, Y.; Tang, L.; Srinivasan, S.; Schnable, P.S. ScienceDirect Field-based architectural traits characterisation of maize plant using time-of-flight 3D imaging. *Biosyst. Eng.* **2018**, *178*, 86–101.
356. Rocchini, D.; Dadalt, L.; Delucchi, L.; Neteler, M.; Palmer, M.W. Disentangling the role of remotely sensed spectral heterogeneity as a proxy for North American plant species richness. *Community Ecol.* **2014**, *15*, 37–43.
357. Yang, H.; Yang, Z.; Wu, Y.; Wang, C.; Wu, Y.; Zhang, P.; Wang, B. High-Resolution Remote Sensing Farmland Extraction Network Based on Dense-Feature Overlay Fusion and Information. *IEEE Geosci. Remote Sens. Lett.* **2025**, *22*, 1–5.
358. Pooya, M.R.; Hasankhani, A.; Fathololomi, S.; Karimi Firozjaei, M. A Spatial Multi-Criteria Decision-Making Approach to Evaluating Homogeneous Areas for Rainfed Wheat Yield Assessment. *Water* **2025**, *17*, 1045.
359. Fang, G.; Wang, C.; Dong, T.; Wang, Z.; Cai, C.; Chen, J.; Liu, M.; Zhang, H. A Landscape-Clustering Zoning Strategy to Map Multi-Crops in Fragmented Cropland Regions Using Sentinel-2 and Sentinel-1 Imagery with Feature Selection. *Agriculture* **2025**, *15*, 186.
360. Abdulraheem, M.I.; Zhang, W.; Li, S.; Moshayedi, A.J.; Farooque, A.A.; Hu, J. Advancement of Remote Sensing for Soil Measurements and Applications: A Comprehensive Review. *Sustain.* **2023**, *15*, 15444.
361. Yuzugullu, O.; Fajraoui, N.; Liebisch, F. Soil Texture and pH Mapping Using Remote Sensing and Support Sampling. *IEEE J. Sel. Top. Appl. Earth Obs. Remote Sens.* **2024**, *17*, 12685–12705.
362. Gao, L.; Zhang, Y.; Zang, D.; Yang, Q.; Liu, H.; Luo, C. Using Satellites to Monitor Soil Texture in Typical Black Soil Areas and Assess Its Impact on Crop Growth. *Agriculture* **2025**, *15*, 912.
363. Liu, F.; Zhang, G.L.; Song, X.; Li, D.; Zhao, Y.; Yang, J.; Wu, H.; Yang, F. High-resolution and three-dimensional mapping of soil texture of China. *Geoderma* **2020**, *361*, 114061.
364. Bahrami, A.; Danesh, M.; Bahrami, M. Studying sand component of soil texture using the spectroscopic method. *Infrared Phys. Technol.* **2022**, *122*, 104056.
365. Swetha, R.K.; Bende, P.; Singh, K.; Gorthi, S.; Biswas, A.; Li, B.; Weindorf, D.C.; Chakraborty, S. Predicting soil texture from smartphone-captured digital images and an application. *Geoderma* **2020**, *376*, 114562.
366. Taghizadeh-Mehrjardi, R.; Emadi, M.; Cherati, A.; Heung, B.; Mosavi, A.; Scholten, T. Bio-inspired hybridization of artificial neural networks: An application for mapping the spatial distribution of soil texture fractions. *Remote Sens.* **2021**, *13*, 1025.
367. Swain, S.R.; Chakraborty, P.; Panigrahi, N.; Vasava, H.B.; Reddy, N.N.; Roy, S.; Majeed, I.; Das, B.S. Estimation of soil texture using Sentinel-2 multispectral imaging data: An ensemble modeling approach. *Soil Tillage Res.* **2021**, *213*, 105134.
368. Shen, Q.; Shang, K.; Xiao, C.; Tang, H.; Wu, T.; Wang, C. A novel hyperspectral remote sensing estimation model for surface soil texture using AHSI/ZY1-02D satellite image. *Int. J. Appl. Earth Obs. Geoinf.* **2025**, *138*, 104453.
369. Tong, X.; Brandt, M.; Hiernaux, P.; Herrmann, S.M.; Tian, F.; Prishchepov, A.V.; Fensholt, R. Revisiting the coupling between NDVI trends and cropland changes in the Sahel drylands: A case study in western Niger. *Remote Sens. Environ.* **2017**, *191*, 286–296.
370. Tao, J.; Jiang, Q.; Zhang, X.; Huang, J.; Wang, Y.; Wu, W. From frequency to intensity—A new index for annual large-scale cropping intensity mapping. *Comput. Electron. Agric.* **2023**, *215*, 108428.
371. Estel, S.; Kuemmerle, T.; Levers, C.; Baumann, M.; Hostert, P. Mapping cropland-use intensity across Europe using MODIS NDVI time series. *Environ. Res. Lett.* **2016**, *11*, 024015.
372. Defourny, P.; Bontemps, S.; Bellemans, N.; Cara, C.; Dedieu, G.; Guzzonato, E.; Hagolle, O.; Inglada, J.; Nicola, L.; Rabaute, T.; et al. Near real-time agriculture monitoring at national scale at parcel resolution: Performance assessment of the Sen2-Agri automated system in various cropping systems around the world. *Remote Sens. Environ.* **2019**, *221*, 551–568.
373. Xu, F.; Yao, X.; Zhang, K.; Yang, H.; Feng, Q.; Li, Y.; Yan, S.; Gao, B.; Li, S.; Yang, J.; et al. Deep learning in cropland field identification: A review. *Comput. Electron. Agric.* **2024**, *222*, 109042.
374. Bouguettaya, A.; Zarzour, H.; Kechida, A.; Taberkit, A.M. Deep learning techniques to classify agricultural crops through UAV imagery: A review. *Neural Comput. Appl.* **2022**, *34*, 9511–9536.
375. Choukri, M.; Laamrani, A.; Chehbouni, A. Use of Optical and Radar Imagery for Crop Type Classification in Africa: A Review. *Sensors* **2024**, *24*, 3618.

376. Tan, Y.; Gu, J.; Lu, L.; Zhang, L.; Huang, J.; Pan, L.; Lv, Y.; Wang, Y.; Chen, Y. Hyperspectral Band Selection for Crop Identification and Mapping of Agriculture. *Remote Sens.* **2025**, *17*, 663.
377. Bourriz, M.; Hajji, H.; Laamrani, A.; Elbouanani, N.; Abdelali, H.A.; Bourzeix, F.; El-Battay, A.; Amazirh, A.; Chehbouni, A. Integration of Hyperspectral Imaging and AI Techniques for Crop Type Mapping: Present Status, Trends, and Challenges. *Remote Sens.* **2025**, *17*, 1574.
378. Muthoka, J.M.; Rowhani, P.; Salakpi, E.E.; Balzter, H.; Antonarakis, A.S. Classification of grassland community types and palatable pastures in semi-arid savannah grasslands of Kenya using multispectral Sentinel-2 imagery. *Front. Sustain. Food Syst.* **2025**, *9*, 1543491.
379. Li, Y.; Liu, T.; Wang, Y.; Duan, L.; Li, M.; Zhang, J.; Zhang, G. A more effective approach for species-level classifications using multi-source remote sensing data: Validation and application to an arid and semi-arid grassland. *Ecol. Indic.* **2024**, *160*, 111853.
380. Zhang, M.; Yu, W.; Chen, A.; Xu, C.; Guo, J.; Xing, X.; Yang, D.; Wang, Z.; Yang, X. Two-tier classification framework for mapping grassland types using multisource earth observation data. *GIScience Remote Sens.* **2024**, *61*, 2385170.
381. Liu, C.; Zhang, Q.; Tao, S.; Qi, J.; Ding, M.; Guan, Q.; Wu, B.; Zhang, M.; Nabil, M.; Tian, F.; et al. A new framework to map fine resolution cropping intensity across the globe: Algorithm, validation, and implication. *Remote Sens. Environ.* **2020**, *251*, 112095.
382. Krishna, G.; Biradar, C.M. Spatiotemporal mapping of rice fallows and soil moisture dynamics for sustainable intensification using time series geospatial big data. *J. Appl. Remote Sens.* **2025**, *19*, 014515.
383. Tao, J.; Wu, W.; Liu, W. Spatial-temporal dynamics of cropping frequency in hubei province over 2001–2015. *Sensors* **2017**, *17*, 2622.
384. Xiang, M.; Yu, Q.; Wu, W. From multiple cropping index to multiple cropping frequency: Observing cropland use intensity at a finer scale. *Ecol. Indic.* **2019**, *101*, 892–903.
385. Arjasakusuma, S.; Kusuma, S.S.; Mahendra, W.K.; Astriviany, N. Mapping paddy field extent and temporal pattern variation in a complex terrain area using sentinel 1-time series data: Case study of magelang district, indonesia. *Int. J. Geoinform.* **2021**, *17*, 79–88.
386. Pazhanivelan, S.; Kumaraperumal, R.; Vishnu Priya, M.; Rengabashyam, K.; Shankar, K.; Nivas Raj, M.; Yadav, M.K. Multi-Temporal Analysis of Cropping Patterns and Intensity Using Optical and SAR Satellite Data for Sustaining Agricultural Production in Tamil Nadu, India. *Sustainability* **2025**, *17*, 1613.
387. Yu, Q.; Xiang, M.; Sun, Z.; Wu, W. The complexity of measuring cropland use intensity: An empirical study. *Agric. Syst.* **2021**, *192*, 103180.
388. Conrad, C.; Schönbrodt-Stitt, S.; Löw, F.; Sorokin, D.; Paeth, H. Cropping intensity in the Aral Sea Basin and its dependency from the runoffformation 2000–2012. *Remote Sens.* **2016**, *8*, 630.
389. Rufin, P.; Levers, C.; Baumann, M.; Jägermeyr, J.; Krueger, T.; Kuemmerle, T.; Hostert, P. Global-scale patterns and determinants of cropping frequency in irrigation dam command areas. *Glob. Environ. Change* **2018**, *50*, 110–122.
390. Barbieri, P.; Pellerin, S.; Nesme, T. Comparing crop rotations between organic and conventional farming. *Sci. Rep.* **2017**, *7*, 13761.
391. Zheng, B.; Campbell, J.B.; de Beurs, K.M. Remote sensing of crop residue cover using multi-temporal Landsat imagery. *Remote Sens. Environ.* **2012**, *117*, 177–183.
392. Zhang, W.; Li, W.; Wang, C.; Yu, Q.; Tang, H.; Wu, W. A novel index for mapping crop residue covered cropland using remote sensing data. *Comput. Electron. Agric.* **2025**, *231*, 109995.
393. Du, J.; Jacinthe, P.-A.; Song, K.; Zhang, L.; Zhao, B.; Liu, H.; Wang, Y.; Zhang, W.; Zheng, Z.; Yu, W.; et al. Maize crop residue cover mapping using Sentinel-2 MSI data and random forest algorithms. *Int. Soil Water Conserv. Res.* **2025**, *13*, 189–202.
394. Yao, Y.; Ren, H.; Liu, Y. Remote sensing estimation of winter wheat residue cover with dry and wet soil background. *Agric. Water Manag.* **2025**, *307*, 109227.
395. Williams, F.; Gelder, B.; Presley, D.A.; Pape, B.; Einck, A. Estimation of Crop Residue Cover Utilizing Multiple Ground Truth Survey Techniques and Multi-Satellite Regression Models. *Remote Sens.* **2024**, *16*, 4185.
396. Kavoosi, Z.; Raoufat, M.H.; Dehghani, M.; Abdolabbas, J.; Kazemeini, S.A.; Nazemossadat, M.J. Feasibility of satellite and drone images for monitoring soil residue cover. *J. Saudi Soc. Agric. Sci.* **2020**, *19*, 56–64.
397. Singh, G.; Kant, Y.; Dadhwal, V.K. Remote sensing of crop residue burning in Punjab (India): A study on burned area estimation using multi-sensor approach. *Geocarto Int.* **2009**, *24*, 273–292.
398. Sharma, A.; Kumar Singh, P. Applicability of UAVs in detecting and monitoring burning residue of paddy crops with IoT Integration: A step towards greener environment. *Comput. Ind. Eng.* **2023**, *184*, 109524.
399. Walker, K. Overcoming Common Pitfalls to Improve the Accuracy of Crop Residue Burning Measurement Based on Remote Sensing Data. *Remote Sens.* **2024**, *16*, 342.

400. Xie, Z.; Zhao, Y.; Jiang, R.; Zhang, M.; Hammer, G.; Chapman, S.; Brider, J.; Potgieter, A.B. Seasonal dynamics of fallow and cropping lands in the broadacre cropping region of Australia. *Remote Sens. Environ.* **2024**, *305*, 114070.
401. Oliphant, A.J.; Thenkabail, P.S.; Teluguntla, P.G.; Aneece, I.P.; Foley, D.J.; McCormick, R.L. Automated Cropland Fallow Algorithm (ACFA) for the Northern Great Plains of USA. *Int. J. Digit. Earth* **2024**, *17*, 2337221.
402. Tong, X.; Brandt, M.; Hiernaux, P.; Herrmann, S.; Rasmussen, L.V.; Rasmussen, K.; Tian, F.; Tagesson, T.; Zhang, W.; Fensholt, R. The forgotten land use class: Mapping of fallow fields across the Sahel using Sentinel-2. *Remote Sens. Environ.* **2020**, *239*, 111598.
403. Denis, A.; Desclee, B.; Migdall, S.; Hansen, H.; Bach, H.; Ott, P.; Kouadio, A.L.; Tychon, B. Multispectral remote sensing as a tool to support organic crop certification: Assessment of the discrimination level between organic and conventional maize. *Remote Sens.* **2021**, *13*, 117.
404. Atanasova, D.; Bozhanova, V.; Biserkov, V.; Maneva, V. Distinguishing areas of organic, biodynamic and conventional farming by means of multispectral images. A pilot study. *Biotechnol. Biotechnol. Equip.* **2021**, *35*, 977–993.
405. Denis, A.; Tychon, B. Remote sensing enables high discrimination between organic and non-organic cotton for organic cotton certification in West Africa. *Agron. Sustain. Dev.* **2015**, *35*, 1499–1510.
406. Serrano-Grijalva, L.; Ochoa-Hueso, R.; Veen, G.F.; Repeto-Deudero, I.; Van Rijssel, S.Q.; Koorneef, G.J.; Van der Putten, W.H. Normalized difference vegetation index analysis reveals increase of biomass production and stability during the conversion from conventional to organic farming. *Glob. Change Biol.* **2024**, *30*, e17461.
407. Cheng, T.; Zhang, D.; Zhang, G.; Wang, T.; Ren, W.; Yuan, F.; Liu, Y.; Wang, Z.; Zhao, C. High-throughput phenotyping techniques for forage: Status, bottleneck, and challenges. *Artif. Intell. Agric.* **2025**, *15*, 98–115.
408. Lausch, A.; Salbach, C.; Schmidt, A.; Doktor, D.; Merbach, I.; Pause, M. Deriving phenology of barley with imaging hyperspectral remote sensing. *Ecol. Modell.* **2015**, *295*, 123–135.
409. Ispizua Yamati, F.R.; Bömer, J.; Noack, N.; Linkugel, T.; Paulus, S.; Mahlein, A.K. Configuration of a multisensor platform for advanced plant phenotyping and disease detection: Case study on Cercospora leaf spot in sugar beet. *Smart Agric. Technol.* **2025**, *10*, 100740.
410. Grubinger, S.; Coops, N.C.; O'Neill, G.A.; Degner, J.C.; Wang, T.; Waite, O.J.M.; Riofrío, J.; Koch, T.L. Seasonal vegetation dynamics for phenotyping using multispectral drone imagery: Genetic differentiation, climate adaptation, and hybridization in a common-garden trial of interior spruce (*Picea engelmannii* × *glauca*). *Remote Sens. Environ.* **2025**, *317*, 114512.
411. Peng, Y.; Solovchenko, A.; Zhang, C.; Shurygin, B.; Liu, X.; Wu, X.; Gong, Y.; Fang, S.; Gitelson, A. Remote sensing of rice phenology and physiology via absorption coefficient derived from unmanned aerial vehicle imaging. *Precis. Agric.* **2024**, *25*, 285–302.
412. Zheng, C.; Abd-elrahman, A.; Whitaker, V. Remote sensing and machine learning in crop phenotyping and management, with an emphasis on applications in strawberry farming. *Remote Sens.* **2021**, *13*, 531.
413. French, A.; Sanchez, C.A.; Wirth, T.; Scott, A.T.; Shields, J.; Bautista, E.; Saber, M.N.; Wisniewski, E. Estimating Fao-56 Crop Growth Stage Lengths with Sentinel 2. *SSRN Electron. J.* **2022**, 4068442.
414. Xiang, M.; Yu, Q.; Li, Y.; Shi, Z.; Wu, W. Increasing multiple cropping for land use intensification: The role of crop choice. *Land Use Policy* **2022**, *112*, 105846.
415. Bahrami, H.; Homayouni, S.; Safari, A.; Mirzaei, S.; Mahdianpari, M.; Reisi-Gahrouei, O. Deep learning-based estimation of crop biophysical parameters using multi-source and multi-temporal remote sensing observations. *Agronomy* **2021**, *11*, 1363.
416. Mokhtari, A.; Noory, H.; Vazifedoust, M.; Palouj, M.; Bakhtiari, A.; Barikani, E.; Zabihi Afrooz, R.A.; Fereydooni, F.; Sadeghi Naeni, A.; Pourshakouri, F.; et al. Evaluation of single crop coefficient curves derived from Landsat satellite images for major crops in Iran. *Agric. Water Manag.* **2019**, *218*, 234–249.
417. Pirbasti, M.A.; Mcardle, G.; Akbari, V. Hedgerows Monitoring in Remote Sensing: A Comprehensive Review. *IEEE Access* **2024**, *12*, 156184–156207.
418. Ahlswede, S.; Asam, S.; Röder, A. Hedgerow object detection in very high-resolution satellite images using convolutional neural networks. *J. Appl. Remote Sens.* **2021**, *15*, 018501.
419. Wolstenholme, J.M.; Cooper, F.; Thomas, R.E.; Ahmed, J.; Parsons, K.J.; Parsons, D.R. Automated identification of hedgerows and hedgerow gaps using deep learning. *Remote Sens. Ecol. Conserv.* **2025**, *11*, 411–424.
420. Smigaj, M.; Gaulton, R. Capturing hedgerow structure and flowering abundance with UAV remote sensing. *Remote Sens. Ecol. Conserv.* **2021**, *7*, 521–533.
421. Barnsley, S.L.; Lovett, A.A.; Dicks, L.V. Mapping nectar-rich pollinator floral resources using airborne multispectral imagery. *J. Environ. Manag.* **2022**, *313*, 114942.

422. Prokoph, S.; Cheema, J.; Kirmer, A.; Lausch, A.; Bannehr, L. Monitoring von blütenreichen Flächen mittels Fernerkundung. *DGPF* **2022**, *30*, 220–236.
423. Abdel-Rahman, E.M.; Makori, D.M.; Landmann, T.; Piiroinen, R.; Gasim, S.; Pellikka, P.; Raina, S.K. The utility of AISA eagle hyperspectral data and random forest classifier for flower mapping. *Remote Sens.* **2015**, *7*, 13298–13318.
424. Gallmann, J.; Schüpbach, B.; Jacot, K.; Albrecht, M.; Winizki, J.; Kirchgessner, N.; Aasen, H. Flower Mapping in Grasslands With Drones and Deep Learning. *Front. Plant Sci.* **2022**, *12*, 774965
425. Gonzales, D.; Hempel de Ibarra, N.; Anderson, K. Remote Sensing of Floral Resources for Pollinators—New Horizons From Satellites to Drones. *Front. Ecol. Evol.* **2022**, *10*, 869751.
426. Schnalke, M.; Funk, J.; Wagner, A. Bridging technology and ecology: Enhancing applicability of deep learning and UAV-based flower recognition. *Front. Plant Sci.* **2025**, *16*, 1498913.
427. El Afandi, G.; Ismael, H.; Fall, S.; Ankumah, R. Effectiveness of Utilizing Remote Sensing and GIS Techniques to Estimate the Exposure to Organophosphate Pesticides Drift over Macon, Alabama. *Agronomy* **2023**, *13*, 1759.
428. Bolívar-Santamaría, S.; Reu, B. Detection and characterization of agroforestry systems in the Colombian Andes using sentinel-2 imagery. *Agrofor. Syst.* **2021**, *95*, 499–514.
429. Koralewicz, A.; Vlcek, J.; Menor, I.O.; Hirons, M.; Akinyugha, A.; Olowoyo, O.S.; Ajayi-Ebenezer, M.; Owen, O. Mapping the extent and exploring the drivers of cocoa agroforestry in Nigeria, insights into trends for climate change adaptation. *Agrofor. Syst.* **2025**, *99*, 38.
430. Yang, W.; Ortiz-Gonzalo, D.; Tong, X.; Gominski, D.; Fensholt, R. Mapping forest-agroforest frontiers in the Peruvian Amazon with deep learning and PlanetScope satellite data. *Ecol. Inform.* **2025**, *86*, 103034.
431. Ahmad, T.; Sahoo, P.M.; Jally, S.K. Estimation of area under agroforestry using high resolution satellite data. *Agrofor. Syst.* **2016**, *90*, 289–303.
432. Brandt, M.; Gominski, D.; Reiner, F.; Kariryaa, A.; Guthula, V.B.; Ciais, P.; Tong, X.; Zhang, W.; Govindarajulu, D.; Ortiz-Gonzalo, D.; et al. Severe decline in large farmland trees in India over the past decade. *Nat. Sustain.* **2024**, *7*, 860–868.
433. Veettil, B.K.; Van, D.D.; Quang, N.X.; Hoai, P.N. Remote sensing of plastic-covered greenhouses and plastic-mulched farmlands: Current trends and future perspectives. *Land Degrad. Dev.* **2023**, *34*, 591–609.
434. Niu, B.; Feng, Q.; Qiu, B.; Su, S.; Zhang, X.; Cui, R.; Zhang, X.; Sun, F.; Yan, W.; Zhao, S.; et al. Global-PCG-10: A 10-m global map of plastic-covered greenhouses derived from Sentinel-2 in 2020. *Earth Syst. Sci. Data* **2025**, *17*, 5065–5088.
435. Zhang, M.; Dong, J.; Ge, Q.; Hasituya; Hao, P. A Review of Agricultural Film Mapping: Current Status, Challenges, and Future Directions. *J. Remote Sens.* **2025**, *5*, 0395.
436. Wu, Y.; Dai, J.; Zhu, Y.; Zhang, T. Intelligent Agricultural Greenhouse Extraction Method Based on Multi-Feature Modeling: Fusion of Geometric, Spatial, and Spectral Characteristics. *IEEE J. Sel. Top. Appl. Earth Obs. Remote Sens.* **2025**, *18*, 5568–5581.
437. Zhang, X.; Li, J.; Li, H.; Guo, Z.; Chang, C.; Xu, X.; Zhen, T.; Yu, K.; Li, P. Identification Of Plastic Film Mulched Farmland in the Core Area of the Beijing-Tianjin Sand Source Region Using Multi-Temporal Remote Sensing Features. *Remote Sens. Appl. Soc. Environ.* **2025**, *38*, 101600.
438. Shafi, U.; Mumtaz, R.; Anwar, Z.; Ajmal, M.M.; Khan, M.A.; Mahmood, Z.; Qamar, M.; Jhanzab, H.M. Tackling Food Insecurity Using Remote Sensing and Machine Learning-Based Crop Yield Prediction. *IEEE Access* **2023**, *11*, 108640–108657.
439. Haseeb, M.; Tahir, Z.; Mahmood, S.A.; Tariq, A. Winter wheat yield prediction using linear and nonlinear machine learning algorithms based on climatological and remote sensing data. *Inf. Process. Agric.* 2025, *in press*.
440. Fita, D.; Rubio, C.; Franch, B.; Castiñeira-Ibáñez, S.; Tarrazó-Serrano, D.; San Bautista, A. Improving harvester yield maps postprocessing leveraging remote sensing data in rice crop. *Precis. Agric.* **2025**, *26*, 33.
441. Hou, X.; Zhang, J.; Luo, X.; Zeng, S.; Lu, Y.; Wei, Q.; Liu, J.; Feng, W.; Li, Q. Peanut yield prediction using remote sensing and machine learning approaches based on phenological characteristics. *Comput. Electron. Agric.* **2025**, *232*, 110084.
442. Liu, Y.; Feng, H.; Fan, Y.; Yue, J.; Yang, F.; Fan, J.; Ma, Y.; Chen, R.; Bian, M.; Yang, G. Utilizing UAV-based hyperspectral remote sensing combined with various agronomic traits to monitor potato growth and estimate yield. *Comput. Electron. Agric.* **2025**, *231*, 109984.
443. Abdul-Jabbar, T.S.; Ziboon, A.T.; Albayati, M.M. Crop yield estimation using different remote sensing data: Literature review. *IOP Conf. Ser. Earth Environ. Sci.* **2023**, *1129*, 012004.
444. Badagliacca, G.; Messina, G.; Presti, E.L.; Preiti, G.; Di Fazio, S.; Monti, M.; Modica, G.; Praticò, S. Durum Wheat (*Triticum durum* Desf.) Grain Yield and Protein Estimation by Multispectral UAV Monitoring and Machine Learning Under Mediterranean Conditions. *AgriEngineering* **2025**, *7*, 99.

445. Raza, A.; Shahid, M.A.; Zaman, M.; Miao, Y.; Huang, Y.; Safdar, M.; Maqbool, S.; Muhammad, N.E. Improving Wheat Yield Prediction with Multi-Source Remote Sensing Data and Machine Learning in Arid Regions. *Remote Sens.* **2025**, *17*, 774.
446. Mena, F.; Pathak, D.; Najjar, H.; Sanchez, C.; Helber, P.; Bischke, B.; Habelitz, P.; Miranda, M.; Siddamsetty, J.; Nuske, M.; et al. Adaptive fusion of multi-modal remote sensing data for optimal sub-field crop yield prediction. *Remote Sens. Environ.* **2025**, *318*, 114547.
447. Dhillon, M.S.; Kübert-Flock, C.; Dahms, T.; Rummler, T.; Arnault, J.; Steffan-Dewenter, I.; Ullmann, T. Evaluation of MODIS, Landsat 8 and Sentinel-2 Data for Accurate Crop Yield Predictions: A Case Study Using STARFM NDVI in Bavaria, Germany. *Remote Sens.* **2023**, *15*, 1830.
448. Řeřicha, J.; Kohútek, M.; Vandírková, V.; Krofta, K.; Kumhála, F.; Kumhálová, J. Assessment of UAV Imageries for Estimating Growth Vitality, Yield and Quality of Hop (*Humulus lupulus* L.) Crops. *Remote Sens.* **2025**, *17*, 970.
449. Brito, L.G.d.; Jorge, R.C.; Oliveira, V.C.d.; Cassemiro, P.F.; Dal Pai, A.; Sarnighausen, V.C.R.; Rodrigues, S.A. Classification Models for Nitrogen Concentration in Hop Leaves Using Digital Image Processing. *Appl. Sci.* **2025**, *15*, 4799.
450. Dietrich, P.; Elias, M.; Dietrich, P.; Harpole, S.; Roscher, C.; Bumberger, J. Advancing plant biomass measurements: Integrating smartphone-based 3D scanning techniques for enhanced ecosystem monitoring. *Methods Ecol. Evol.* **2025**, *2025*, 1723–1732.
451. Zhang, H.; Zhang, L.; Wu, H.; Wang, D.; Ma, X.; Shao, Y.; Jiang, M.; Chen, X. Unmanned-Aerial-Vehicle-Based Multispectral Monitoring of Nitrogen Content in Canopy Leaves of Processed Tomatoes. *Agriculture* **2025**, *15*, 309.
452. Acharya, B.; Dodla, S.; Tubana, B.; Gentimis, T.; Rontani, F.; Adhikari, R.; Duron, D.; Bortolon, G.; Setiyono, T. Characterizing Optimum N Rate in Waterlogged Maize (*Zea mays* L.) with Unmanned Aerial Vehicle (UAV) Remote Sensing. *Agronomy* **2025**, *15*, 434.
453. Segarra, J.; Buchaillot, M.L.; Stefani, U.; Araus, J.L.; Kefauver, S.C. Sentinel-2 Responsiveness to Fertilization Gradients in Wheat at Field Level in Córdoba Province, Argentina. In Proceedings of the 2020 Mediterranean and Middle-East Geoscience and Remote Sensing Symposium (M2GARSS), Tunis, Tunisia, 9–11 March 2020; pp. 322–325.
454. Zhou, T.; Geng, Y.; Lv, W.; Xiao, S.; Zhang, P.; Xu, X.; Chen, J.; Wu, Z.; Pan, J.; Si, B.; et al. Effects of optical and radar satellite observations within Google Earth Engine on soil organic carbon prediction models in Spain. *J. Environ. Manag.* **2023**, *338*, 117810.
455. Zhou, T.; Geng, Y.; Chen, J.; Liu, M.; Haase, D.; Lausch, A. Mapping soil organic carbon content using multi-source remote sensing variables in the Heihe River Basin in China. *Ecol. Indic.* **2020**, *114*, 106288.
456. Suleymanov, A.; Gabbasova, I.; Suleymanov, R.; Abakumov, E.; Polyakov, V.; Liebelt, P. Mapping soil organic carbon under erosion processes using remote sensing. *Hung. Geogr. Bull.* **2021**, *70*, 49–64.
457. Yuzugullu, O.; Fajraoui, N.; Don, A.; Liebisch, F. Satellite-based soil organic carbon mapping on European soils using available datasets and support sampling. *Sci. Remote Sens.* **2024**, *9*, 100118.
458. Radočaj, D.; Gašparović, M.; Jurišić, M. Open Remote Sensing Data in Digital Soil Organic Carbon Mapping: A Review. *Agric.* **2024**, *14*, 1005.
459. Qian, J.; Yang, J.; Sun, W.; Zhao, L.; Shi, L.; Shi, H.; Liao, L.; Dang, C. Soil Organic Carbon Estimation and Transfer Framework in Agricultural Areas Based on Spatiotemporal Constraint Strategy Combined with Active and Passive Remote Sensing. *Remote. Sens.* **2025**, *17*, 333.
460. Geng, J.; Tan, Q.; Lv, J.; Fang, H. Assessing spatial variations in soil organic carbon and C:N ratio in Northeast China's black soil region: Insights from Landsat-9 satellite and crop growth information. *Soil Tillage Res.* **2024**, *235*, 105897.
461. Xu, D.; Chen, S.; Zhou, Y.; Ji, W.; Shi, Z. Spatial Estimation of Soil Organic Matter and Total Nitrogen by Fusing Field Vis–NIR Spectroscopy and Multispectral Remote Sensing Data. *Remote Sens.* **2025**, *17*, 729.
462. Zhang, Y.; Luo, C.; Zhang, W.; Wu, Z.; Zang, D. Mapping Soil Organic Matter in Black Soil Cropland Areas Using Remote Sensing and Environmental Covariates. *Agriculture* **2025**, *15*, 339.
463. Zhang, J.; Gan, S.; Yang, P.; Zhou, J.; Huang, X.; Chen, H.; He, H.; Saintilan, N.; Sanders, C.J.; Wang, F. A global assessment of mangrove soil organic carbon sources and implications for blue carbon credit. *Nat. Commun.* **2024**, *15*, 8994.
464. Chen, X.; Yuan, F.; Ata-Ul-Karim, S.T.; Liu, X.; Tian, Y.; Zhu, Y.; Cao, W.; Cao, Q. A bibliometric analysis of research on remote sensing-based monitoring of soil organic matter conducted between 2003 and 2023. *Artif. Intell. Agric.* **2025**, *15*, 26–38.
465. Van Wasmael, B. A European soil organic carbon monitoring system leveraging Sentinel 2 imagery and the LUCAS soil data base. *Geoderma* **2024**, *452*, 117113.
466. Petropoulos, T.; Benos, L.; Busato, P.; Kyriakarakos, G.; Kateris, D.; Aidonis, D.; Bochtis, D. Soil Organic Carbon Assessment for Carbon Farming: A Review. *Agriculture* **2025**, *15*, 567.

467. Gomez, C.; Oltra-carrió, R.; Bacha, S.; Lagacherie, P.; Briottet, X. Evaluating the sensitivity of clay content prediction to atmospheric effects and degradation of image spatial resolution using Hyperspectral VNIR/SWIR imagery. *Remote Sens. Environ.* **2015**, *164*, 1–15.
468. Shabou, M.; Mougenot, B.; Chabaane, Z.L.; Walter, C.; Boulet, G.; Aissa, N.B.; Zribi, M. Soil clay content mapping using a time series of Landsat TM data in semi-arid lands. *Remote Sens.* **2015**, *7*, 6059–6078.
469. Gomez, C.; Adeline, K.; Bacha, S.; Driessen, B.; Gorretta, N.; Lagacherie, P.; Roger, J.M.; Briottet, X. Sensitivity of clay content prediction to spectral configuration of VNIR/SWIR imaging data, from multispectral to hyperspectral scenarios. *Remote Sens. Environ.* **2018**, *204*, 18–30.
470. Paul, S.S.; Coops, N.C.; Johnson, M.S.; Krzic, M.; Chandna, A.; Smukler, S.M. Mapping soil organic carbon and clay using remote sensing to predict soil workability for enhanced climate change adaptation. *Geoderma* **2020**, *363*, 114177.
471. Gasmi, A.; Gomez, C.; Lagacherie, P.; Zouari, H. Surface soil clay content mapping at large scales using multispectral (VNIR–SWIR) ASTER data. *Int. J. Remote Sens.* **2019**, *40*, 1506–1533.
472. Franz, A.; Sowiński, J.; Głogowski, A.; Fiałkiewicz, W. A Preliminary Study on the Use of Remote Sensing Techniques to Determine the Nutritional Status and Productivity of Oats on Spatially Variable Sandy Soils. *Agronomy* **2025**, *15*, 616.
473. Fongaro, C.T.; Demattê, J.A.M.; Rizzo, R.; Safanelli, J.L.; Mendes, W.d.S.; Dotto, A.C.; Vicente, L.E.; Franceschini, M.H.D.; Ustin, S.L. Improvement of clay and sand quantification based on a novel approach with a focus on multispectral satellite images. *Remote Sens.* **2018**, *10*, 1555.
474. Cerasola, V.A.; Orsini, F.; Pennisi, G.; Moretti, G.; Bona, S.; Mirone, F.; Verrelst, J.; Berger, K.; Gianquinto, G. Hyperspectral imaging for precision nitrogen management: A comparative exploration of two methodological approaches to estimate optimal nitrogen rate in processing tomato. *Smart Agric. Technol.* **2025**, *10*, 100802.
475. Wang, J.; Wang, W.; Liu, S.; Hui, X.; Zhang, H.; Yan, H.; Maes, W.H. UAV-Based Multiple Sensors for Enhanced Data Fusion and Nitrogen Monitoring in Winter Wheat Across Growth Seasons. *Remote Sens.* **2025**, *17*, 498.
476. Misbah, K.; Laamrani, A.; Khechba, K.; Dhiba, D.; Chehbouni, A. Multi-sensors remote sensing applications for assessing, monitoring, and mapping npk content in soil and crops in african agricultural land. *Remote Sens.* **2022**, *14*, 81.
477. Peng, X.; Chen, D.; Zhou, Z.; Zhang, Z.; Xu, C.; Zha, Q.; Wang, F.; Hu, X. Prediction of the Nitrogen, Phosphorus and Potassium Contents in Grape Leaves at Different Growth Stages Based on UAV Multispectral Remote Sensing. *Remote Sens.* **2022**, *14*, 2659.
478. Zhang, W.; Zhu, L.; Zhuang, Q.; Chen, D.; Sun, T. Mapping Cropland Soil Nutrients Contents Based on Multi-Spectral Remote Sensing and Machine Learning. *Agriculture* **2023**, *13*, 1592.
479. Lin, C.; Ma, R.; Zhu, Q.; Li, J. Using hyper-spectral indices to detect soil phosphorus concentration for various land use patterns. *Environ. Monit. Assess.* **2015**, *187*, 4130.
480. Guo, C.; Zhang, L.; Zhou, X.; Zhu, Y.; Cao, W.; Qiu, X.; Cheng, T.; Tian, Y. Integrating remote sensing information with crop model to monitor wheat growth and yield based on simulation zone partitioning. *Precis. Agric.* **2018**, *19*, 55–78.
481. Wang, S.; Adhikari, K.; Wang, Q.; Jin, X.; Li, H. Role of environmental variables in the spatial distribution of soil carbon (C), nitrogen (N), and C:N ratio from the northeastern coastal agroecosystems in China. *Ecol. Indic.* **2018**, *84*, 263–272.
482. Wang, X.; Geng, Y.; Zhou, T.; Zhao, Y.; Li, H.; Liu, Y.; Li, H.; Ren, R.; Zhang, Y.; Xu, X.; et al. Mapping the soil C:N ratio at the European scale by combining multi-year Sentinel radar and optical data via cloud computing. *Soil Tillage Res.* **2025**, *245*, 106311.
483. Rapiya, M.; Ramoelo, A.; Truter, W. Seasonal monitoring of forage C:N:ADF ratio in natural rangeland using remote sensing data. *Environ. Monit. Assess.* **2025**, *197*, 137.
484. Wang, Y.; Chen, S.; Hong, Y.; Hu, B.; Peng, J.; Shi, Z. A comparison of multiple deep learning methods for predicting soil organic carbon in Southern Xinjiang, China. Comput. Electron. Agric. 2023, 212, 108067.
485. Lei, S.; Zhou, P.; Lin, J.; Tan, Z.; Huang, J.; Yan, P.; Chen, H. Spatiotemporal Variation in Carbon and Water Use Efficiency and Their Influencing Variables Based on Remote Sensing Data in the Nanling Mountains Region. Remote Sens. 2025, 17, 648.
486. Yue, F.; Liu, D.; Xiong, L.; Chen, J.; Chen, H.; Yin, J. Understanding the roles of climate change, land use and land cover change and water diversion project in modulating water- and carbon-use efficiency in Han River Basin. *J. Environ. Manag.* **2025**, *373*, 123445.
487. Xu, C.; Chen, X.; Yu, Q.; Avirmed, B.; Zhao, J.; Liu, W.; Sun, W. Relationship between ecological spatial network and vegetation carbon use efficiency in the Yellow River Basin, China. *GISci. Remote Sens.* **2024**, *61*, 2318070.
488. Nair, R.; Luo, Y.; El-Madany, T.; Rolo, V.; Pacheco-Labrador, J.; Caldararu, S.; Morris, K.A.; Schrumpf, M.; Carrara, A.; Moreno, G.; et al. Nitrogen availability and summer drought, but not N:P imbalance, drive carbon use efficiency of a Mediterranean tree-grass ecosystem. *Glob. Change Biol.* **2024**, *30*, e17486.

489. Wu, J.; Gao, Z.; Liu, Q.; Li, Z.; Zhong, B. Methods for sandy land detection based on multispectral remote sensing data. *Geoderma* **2018**, *316*, 89–99.
490. Di Raimo, L.A.D.L.; Couto, E.G.; Poppiel, R.R.; Mello, D.C.d.; Amorim, R.S.S.; Torres, G.N.; Bocuti, E.D.; Veloso, G.V.; Fernandes-Filho, E.I.; Francelino, M.R.; et al. Sand subfractions by proximal and satellite sensing: Optimizing agricultural expansion in tropical sandy soils. *Catena* **2024**, *234*, 107604.
491. Secu, C.V.; Stoleriu, C.C.; Lesenciuc, C.D.; Ursu, A. Normalized Sand Index for Identification of Bare Sand Areas in Temperate Climates Using Landsat Images, Application to the South of Romania. *Remote Sens.* **2022**, *14*, 3802.
492. Meng, J.; Chu, N.; Luo, C.; Liu, H.; Li, X. High-Resolution Mapping of Topsoil Sand Content in Planosol Regions Using Temporal and Spectral Feature Optimization. *Remote Sens.* **2025**, *17*, 553.
493. Espinoza, N.S.; Piedade, M.T.F.; Demarchi, L.O.; Lima, G.R.; Resende, A.F.; Ferreira, R.R.; Silva, F.A.G.; Machado, L.A.T.; Schörgart, J. Detection of white sand patches in central Amazonia using remote sensing and meteorological data. *Int. J. Remote Sens.* **2025**, *46*, 3446–3465.
494. Lou, H.; Yang, S.; Zhao, C.; Shi, L.; Wu, L.; Wang, Y.; Wang, Z. Detecting and analyzing soil phosphorus loss associated with critical source areas using a remote sensing approach. *Sci. Total Environ.* **2016**, *573*, 397–408.
495. Aziz, D.; Rafiq, S.; Saini, P.; Ahad, I.; Gonal, B.; Rehman, S.A.; Rashid, S.; Saini, P.; Rohela, G.K.; Aalum, K.; et al. Remote sensing and artificial intelligence: Revolutionizing pest management in agriculture. *Front. Sustain. Food Syst.* **2025**, *9*, 1551460.
496. Bautista, A.S.; Tarrazó-Serrano, D.; Uris, A.; Blesa, M.; Estruch-Guitart, V.; Castiñeira-Ibáñez, S.; Rubio, C. Remote Sensing Evaluation Drone Herbicide Application Effectiveness for Controlling *Echinochloa* spp. in Rice Crop in Valencia (Spain). *Sensors* **2024**, *24*, 804.
497. Mahlein, A.-K. Present and Future Trends in Plant Disease Detection. *Plant Dis* **2016**, *100*, 1–11.
498. Okole, N.; Yamati, F.R.I.; Hossain, R.; Varrelmann, M.; Mahlein, A.K.; Heim, R.H.J. Hyperspectral signatures and betalain indicator for beet mosaic virus infection in sugar beet. In Proceedings of the 2023 IEEE International Workshop on Metrology for Agriculture and Forestry (MetroAgriFor), Pisa, Italy, 6–8 November 2023; pp. 506–511.
499. Okole, N.; Ispizua Yamati, F.R.; Hossain, R.; Varrelmann, M.; Mahlein, A.K.; Heim, R.H.J. Aerial low-altitude remote sensing and deep learning for in-field disease incidence scoring of virus yellows in sugar beet. *Plant Pathol.* **2024**, *73*, 2310–2324.
500. Hossain, R.; Ispizua Yamati, F.R.; Barreto, A.; Savian, F.; Varrelmann, M.; Mahlein, A.K.; Paulus, S. Elucidation of turnip yellows virus (TuYV) spectral reflectance pattern in Nicotiana benthamiana by non-imaging sensor technology. *J. Plant Dis. Prot.* **2023**, *130*, 35–43.
501. Barreto, A.; Ispizua Yamati, F.R.; Varrelmann, M.; Paulus, S.; Mahlein, A.K. Disease Incidence and Severity of Cercospora Leaf Spot in Sugar Beet Assessed by Multispectral Unmanned Aerial Images and Machine Learning. *Plant Dis.* **2023**, *107*, 188–200.
502. Isip, M.F.; Alberto, R.T.; Biagtan, A.R. Exploring vegetation indices adequate in detecting twister disease of onion using Sentinel-2 imagery. *Spat. Inf. Res.* **2020**, *28*, 369–375.
503. Navrozidis, L.; Alexandridis, T.K.; Moshou, D.; Pantazi, X.E.; Alexandra Tamouridou, A.; Kozhukh, D.; Castef, F.; Lagopodi, A.; Zartaloudis, Z.; Mourelatos, S.; et al. Olive Trees Stress Detection Using Sentinel-2 Images. In Proceedings of the 2019 IEEE International Geoscience and Remote Sensing Symposium, Yokohama, Japan, 28 July–2 August 2019; pp. 7220–7223.
504. Safari, M.M.; Malian, A. Plant disease mapping in paddy growing stages using remotely sensed data. *Environ. Earth Sci.* **2025**, *84*, 1.
505. Taneja, A.; Rani, S. Target localization and communication for remote sensing with use case of self-supervised learning in plant disease detection. *Int. J. Remote Sens.* **2025**, 1–22. doi: 10.1080/01431161.2024.2448310
506. Zhu, H.; Lin, C.; Liu, G.; Wang, D.; Qin, S.; Li, A.; Xu, J.L.; He, Y. Intelligent agriculture: Deep learning in UAV-based remote sensing imagery for crop diseases and pests detection. *Front. Plant Sci.* **2024**, *15*, 1435016.
507. Zheng, Q.; Huang, W.; Xia, Q.; Dong, Y.; Ye, H.; Jiang, H.; Chen, S.; Huang, S. Remote Sensing Monitoring of Rice Diseases and Pests from Different Data Sources: A Review. *Agronomy* **2023**, *13*, 1851.
508. Zhang, T.; Cai, Y.; Zhuang, P.; Li, J. Remotely Sensed Crop Disease Monitoring by Machine Learning Algorithms: A Review. *Unmanned Syst.* **2024**, *12*, 161–171.
509. Schmidtlein, S. Imaging spectroscopy as a tool for mapping Ellenberg indicator values. *J. Appl. Ecol.* **2005**, *42*, 966–974.
510. Schmidt, J.; Fassnacht, F.E.; Lausch, A.; Schmidtlein, S. Assessing the functional signature of heathland landscapes via hyperspectral remote sensing. *Ecol. Indic.* **2017**, *73*, 505–512.
511. Schmidtlein, S.; Feilhauer, H.; Bruelheide, H. Mapping plant strategy types using remote sensing. *J. Veg. Sci.* **2012**, *23*, 395–405.
512. Cushnahan, T.A.; Grafton, M.C.E.; Pearson, D.; Ramilan, T. Hyperspectral Data Can Classify Plant Functional Groups Within New Zealand Hill Farm Pasture. *Remote Sens.* **2025**, *17*, 1120.

513. Kanta, C.; Kumar, A.; Chauhan, A.; Singh, H.; Sharma, I.P. *The Interplay Between Plant Functional Traits and Climate Change*; Springer: Berlin/Heidelberg, Germany, 2024; ISBN 9789819715107.
514. Schweiger, A.K.; Schütz, M.; Risch, A.C.; Kneubühler, M.; Haller, R.; Schaepman, M.E. How to predict plant functional types using imaging spectroscopy: Linking vegetation community traits, plant functional types and spectral response. *Methods Ecol. Evol.* **2017**, *8*, 86–95.
515. Möckel, T.; Löfgren, O.; Prentice, H.C.; Eklundh, L.; Hall, K. Airborne hyperspectral data predict Ellenberg indicator values for nutrient and moisture availability in dry grazed grasslands within a local agricultural landscape. *Ecol. Indic.* **2016**, *66*, 503–516.
516. Klinke, R.; Kuechly, H.; Frick, A.; Förster, M.; Schmidt, T.; Holtgrave, A.K.; Kleinschmit, B.; Spengler, D.; Neumann, C. Indicator-Based Soil Moisture Monitoring of Wetlands by Utilizing Sentinel and Landsat Remote Sensing Data. *PFG-J. Photogramm. Remote Sens. Geoinf. Sci.* **2018**, *86*, 71–84.
517. Peng, Y.; Kira, O.; Nguy-Robertson, A.; Suyker, A.; Arkebauer, T.; Sun, Y.; Gitelson, A.A. Gross primary production estimation in crops using solely remotely sensed data. *Agron. J.* **2019**, *111*, 2981–2990.
518. Reeves, M.C.; Zhao, M.; Running, S.W. Usefulness and limits of MODIS GPP for estimating wheat yield. *Int. J. Remote Sens.* **2005**, *26*, 1403–1421.
519. Maleki, M.; Arriga, N.; Barrios, J.M.; Wieneke, S.; Liu, Q.; Peñuelas, J.; Janssens, I.A.; Balzarolo, M. Estimation of Gross Primary Productivity (GPP) Phenology of a Short-Rotation Plantation Using Remotely Sensed Indices Derived from Sentinel-2 Images. *Remote Sens.* **2020**, *12*, 2104.
520. Celis, J.; Xiao, X.; White, P.M.; Cabral, O.M.R.; Freitas, H.C. Improved Modeling of Gross Primary Production and Transpiration of Sugarcane Plantations with Time-Series Landsat and Sentinel-2 Images. *Remote Sens.* **2023**, *16*, 46.
521. Shirkey, G.; John, R.; Chen, J.; Dahlin, K.; Abraha, M.; Sciusco, P.; Lei, C.; Reed, D.E. Fine resolution remote sensing spectra improves estimates of gross primary production of croplands. *Agric. For. Meteorol.* **2022**, *326*, 109175.
522. Cicuéndez, V.; Inclán, R.; Sánchez-Cañete, E.P.; Román-Cascón, C.; Sáenz, C.; Yagüe, C. Modeling Gross Primary Production (GPP) of a Mediterranean Grassland in Central Spain Using Sentinel-2 NDVI and Meteorological Field Information. *Agronomy* **2024**, *14*, 1243.
523. He, L.; Mostovoy, G. Cotton yield estimate using Sentinel-2 data and an ecosystem model over the southern US. *Remote Sens.* **2019**, *11*, 2000.
524. Wang, T.; Zhang, Y.; Yue, C.; Wang, Y.; Wang, X.; Lyu, G.; Wei, J.; Yang, H.; Piao, S. Progress and challenges in remotely sensed terrestrial carbon fluxes. *Geo-Spat. Inf. Sci.* **2024**, *28*, 1–21.
525. Yan, Y.; Xu, X.; Liu, X.; Wen, Y.; Ou, J. Assessing the contributions of climate change and human activities to cropland productivity by means of remote sensing. *Int. J. Remote Sens.* **2020**, *41*, 2004–2021.
526. Feng, X.; Liu, G.; Chen, J.M.; Chen, M.; Liu, J.; Ju, W.M.; Sun, R.; Zhou, W. Net primary productivity of China's terrestrial ecosystems from a process model driven by remote sensing. *J. Environ. Manag.* **2007**, *85*, 563–573.
527. Li, C.; Han, W.; Peng, M. Improving the spatial and temporal estimating of daytime variation in maize net primary production using unmanned aerial vehicle-based remote sensing. *Int. J. Appl. Earth Obs. Geoinf.* **2021**, *103*, 102467.
528. Niedertscheider, M.; Kastner, T.; Fetzel, T.; Haberl, H.; Kroisleitner, C.; Plutzar, C.; Erb, K.H. Mapping and analysing cropland use intensity from a NPP perspective. *Environ. Res. Lett.* **2016**, *11*, 014008.
529. Xu, L.; Zhao, Z.; Wang, C.; Wang, H.; Ma, C. Quantitative estimation of net primary productivity by an improved tCASA model using Landsat time series data: A case study of Central Plains, China. *IEEE J. Sel. Top. Appl. Earth Obs. Remote Sens.* **2025**, *18*, 10403–10418.
530. Li, J.; Xu, D.; Xu, Z.; Wang, Y.; Yang, J. Analysis of Spatio-Temporal Variation of Vegetation Npp and its Driving Factors in Tianshan Mountains Based on Casa Model. *SSRN* **2025**.
531. Baeza, S.; Paruelo, J.M. Spatial and temporal variation of human appropriation of net primary production in the Rio de la Plata grasslands. *ISPRS J. Photogramm. Remote Sens.* **2018**, *145*, 238–249.
532. Liu, Y.; Song, W. Mapping human appropriation of net primary production in agroecosystems in the Heihe River Basin, China. *Agric. Ecosyst. Environ.* **2022**, *335*, 107996.
533. Paudel, S.; Mueller, K.; Ovando-Montejo, G.; Tango, L.; Rushforth, R.; Lant, C. A dataset cataloging product-specific human appropriation of net primary production (HANPP) in US counties. *Data Br.* **2023**, *50*, 109530.
534. Matej, S.; Weidinger, F.; Kaufmann, L.; Roux, N.; Gingrich, S.; Haberl, H.; Krausmann, F.; Erb, K.H. A global land-use data cube 1992–2020 based on the Human Appropriation of Net Primary Production. *Sci. Data* **2025**, *12*, 511.
535. Zhao, J.; Sun, X.; Wang, M.; Li, G.; Hou, X. Crop mapping and quantitative evaluation of cultivated land use intensity in Shandong Province, 2018–2022. *L. Degrad. Dev.* **2024**, *35*, 4648–4665.

536. Cai, W.; Ullah, S.; Yan, L.; Lin, Y. Remote sensing of ecosystem water use efficiency: A review of direct and indirect estimation methods. *Remote Sens.* **2021**, *13*, 2393.
537. Yu, X.; Yin, Q.; Zhao, T.; Chen, K.; Qian, L.; Wang, W.; Hu, X.; Zhang, B. Detecting ecosystem water use efficiency responses to drought from long-term remote sensing data. *Ecol. Indic.* **2025**, *177*, 113734.
538. Rao, S.; Kisekka, I. Science of the Total Environment Carbon—Water coupling in California almond orchards: A multi-scale assessment of ecosystem water use efficiency using eddy covariance and remote sensing. *Sci. Total Environ.* **2025**, *990*, 179914.
539. Jiang, L.; Zhang, F.; Chi, J.; Yan, P.; Bu, X.; He, Y.; Bai, T. Evaluation of pear orchard yield and water use efficiency at the field scale by assimilating remotely sensed LAI and SM into the WOFOST model. *Comput. Electron. Agric.* **2025**, *233*, 110145.
540. He, J.; Zhou, Y.; Liu, X.; Duan, W.; Pan, N. Spatiotemporal Changes in Water-Use Efficiency of China's Terrestrial Ecosystems During 2001–2020 and the Driving Factors. *Remote Sens.* **2025**, *17*, 136.
541. Ali, A.; Kaul, H.P. Monitoring Yield and Quality of Forages and Grassland in the View of Precision Agriculture Applications—A Review. *Remote Sens.* **2025**, *17*, 279.
542. Guillevic, P.C.; Aouizerats, B.; Burger, R.; Den Besten, N.; Jackson, D.; Ridderikhoff, M.; Zajdband, A.; Houborg, R.; Franz, T.E.; Robertson, G.P.; et al. Planet's Biomass Proxy for monitoring aboveground agricultural biomass and estimating crop yield. *F. Crop. Res.* **2024**, *316*, 109511.
543. Reinermann, S.; Boos, C.; Kaim, A.; Schucknecht, A.; Asam, S.; Annuth, S.H.; Schmitt, T.M.; Koellner, T.; Kiese, R. Grassland yield estimations-potentials and limitations of remote sensing, process-based modelling and field measurements. *EGUsphere* **2025**.
544. Åström, O.; Månsson, S.; Lazar, I.; Nilsson, M.; Ekelöf, J.; Oxenstierna, A.; Sopasakis, A. Predicting Intra-Field Yield Variations for Winter Wheat Using Remote Sensing and Graph Attention Networks. *SSRN Electron. J.* **2025**, *237*, 110499.
545. Muruganantham, P.; Wibowo, S.; Grandhi, S.; Samrat, N.H.; Islam, N. A Systematic Literature Review on Crop Yield Prediction with Deep Learning and Remote Sensing. *Remote Sens.* **2022**, *14*, 1990.
546. Luo, L.; Sun, S.; Xue, J.; Gao, Z.; Zhao, J.; Yin, Y.; Gao, F.; Luan, X. Crop yield estimation based on assimilation of crop models and remote sensing data: A systematic evaluation. *Agric. Syst.* **2023**, *210*, 103711.
547. Filippi, P.; Jones, E.J.; Ginns, B.J.; Whelan, B.M.; Roth, G.W.; Bishop, T.F.A. Mapping the depth-to-soil pH constraint, and the relationship with cotton and grain yield at the within-field scale. *Agronomy* **2019**, *9*, 251.
548. Li, M.; Wang, J.; Li, K.; Liu, Y.; Ochir, A.; Davaasuren, D. Assessment of grazing livestock balance on the Eastern Mongolian Plateau based on remote sensing monitoring and grassland carrying capacity evaluation. *Sci. Rep.* **2024**, *14*, 32151.
549. Ren, J.; Zhang, N.; Liu, X.; Wu, S.; Li, D. Dynamic Harvest Index Estimation of Winter Wheat Based on UAV Hyperspectral Remote Sensing Considering Crop Aboveground Biomass Change and the Grain Filling Process. *Remote Sens.* **2022**, *14*, 1955.
550. Xu, J.; Meng, J.; Quackenbush, L.J. Use of remote sensing to predict the optimal harvest date of corn. *F. Crop. Res.* **2019**, *236*, 1–13.
551. Li, H.; Luo, Y.; Xue, X.; Zhao, Y.; Zhao, H.; Li, F. A comparison of harvest index estimation methods of winter wheat based on field measurements of biophysical and spectral data. *Biosyst. Eng.* **2011**, *109*, 396–403.
552. Yue, J.; Yao, Y.; Shen, J.; Li, T.; Xu, N.; Feng, H.; Wei, Y.; Xu, X.; Lin, Y.; Guo, W.; et al. Winter wheat harvest detection via Sentinel-2 MSI images. *Int. J. Remote Sens.* **2025**, *46*, 2482–2500.
553. Paz-Kagan, T.; Zaady, E.; Salbach, C.; Schmidt, A.; Lausch, A.; Zacharias, S.; Notesco, G.; Ben-Dor, E.; Karnieli, A. Mapping the spectral soil quality index (SSQI) using airborne imaging spectroscopy. *Remote Sens.* **2015**, *7*, 15748–15781.
554. Baroudy, A.A.E.; Ali, A.M.; Mohamed, E.S.; Moghanm, F.S.; Shokr, M.S.; Savin, I.; Poddubsky, A.; Ding, Z.; Kheir, A.M.S.; Aldosari, A.A.; et al. Modeling Land Suitability for Rice Crop Using Remote Sensing and Soil Quality Indicators: The Case Study of the Nile Delta. *Sustainability* **2020**, *12*, 9653.
555. Kumar, U.S.; Kapali, B.S.C.; Nageswaran, A.; Umapathy, K.; Jangir, P.; Swetha, K.; Begum, M.A. Fusion of MobileNet and GRU: Enhancing Remote Sensing Applications for Sustainable Agriculture and Food Security. *Remote Sens. Earth Syst. Sci.* **2024**, *8*, 118–131.
556. Dedeoğlu, M.; Başayiğit, L.; Yüksel, M.; Kaya, F. Assessment of the vegetation indices on Sentinel-2A images for predicting the soil productivity potential in Bursa, Turkey. *Environ. Monit. Assess.* **2020**, *192*, 16.
557. Fadl, M.E.; AbdelRahman, M.A.E.; El-Desoky, A.I.; Sayed, Y.A. Assessing soil productivity potential in arid region using remote sensing vegetation indices. *J. Arid Environ.* **2024**, *222*, 105166.
558. Rieser, J.; Veste, M.; Thiel, M.; Schönbrodt-stitt, S. Coverage and rainfall response of biological soil crusts using multi-temporal sentinel-2 data in a central european temperate dry acid grassland. *Remote Sens.* **2021**, *13*, 3093.
559. Crucil, G.; Van Oost, K. Towards mapping of soil crust using multispectral imaging. *Sensors* **2021**, *21*, 1850.

560. Weber, B.; Hill, J. Remote Sensing of Biological Soil Crusts at Different Scales. In *Biological soil crusts: An organizing principle in drylands*; Springer: Berlin/Heidelberg, Germany, 2016; pp. 215–234.
561. Crucil, G. Characterizing soil Physical Crusts in Loamy Soils Using Spectral Data Processing Techniques from Proximal and Remote Sensing. Ph.D. Thesis, UCL-Université Catholique de Louvain, Ottignies-Louvain-la-Neuve, Belgique, 2022.
562. Han, H.Q.; Yin, C.Y.; Wang, K.; Zhou, H.Y. Progress and Prospects of Research on Karst Ecosystem Services. *Appl. Ecol. Environ. Res.* **2025**, *23*, 507–529.
563. Wu, C.; Wu, Z.; Wang, Y.; Yang, Y. Effect of soil crust on the prediction of soil organic matter based on soil colour. *Catena* **2025**, *251*, 108818.
564. Beaugendre, N.; Malam Issa, O.; Choné, A.; Cerdan, O.; Desprats, J.F.; Rajot, J.L.; Sannier, C.; Valentin, C. Developing a predictive environment-based model for mapping biological soil crust patterns at the local scale in the Sahel. *Catena* **2017**, *158*, 250–265.
565. Brom, J.; Duffková, R.; Haberle, J.; Zajíček, A.; Nedbal, V.; Bernasová, T.; Křováková, K. Identification of infiltration features and hydraulic properties of soils based on crop water stress derived from remotely sensed data. *Remote Sens.* **2021**, *13*, 4127.
566. Francos, N.; Romano, N.; Nasta, P.; Zeng, Y.; Szabó, B.; Manfreda, S.; Ciraolo, G.; Mészáros, J.; Zhuang, R.; Su, B.; et al. Mapping water infiltration rate using ground and uav hyperspectral data: A case study of alento, italy. *Remote Sens.* **2021**, *13*, 2606.
567. Geng, Y.; Zhou, T.; Zhang, Z.; Cui, B.; Sun, J.; Zeng, L.; Yang, R.; Wu, N.; Liu, T.; Pan, J.; et al. Continental-scale mapping of soil pH with SAR-optical fusion based on long-term earth observation data in google earth engine. *Ecol. Indic.* **2024**, *165*, 112246.
568. Zhang, Y.; Sui, B.; Shen, H.; Wang, Z. Estimating temporal changes in soil pH in the black soil region of Northeast China using remote sensing. *Comput. Electron. Agric.* **2018**, *154*, 204–212.
569. Jia, P.; Shang, T.; Zhang, J.; Sun, Y. Inversion of soil pH during the dry and wet seasons in the Yinbei region of Ningxia, China, based on multi-source remote sensing data. *Geoderma Reg.* **2021**, *25*, e00399.
570. Webb, H.; Barnes, N.; Powell, S.; Jones, C. Does drone remote sensing accurately estimate soil pH in a spring wheat field in southwest Montana? *Precis. Agric.* **2021**, *22*, 1803–1815.
571. Wang, Z.; Wu, W.; Liu, H. Comparing Soil pH Mapping from Multi-Temporal PlanetScope and Sentinel-2 Data Across Land Use Types. *Remote Sens.* **2025**, *17*, 189.
572. Molaeinasab, A.; Tarkesh, M.; Bashari, H.; Toomanian, N.; Aghasi, B.; Jalalian, A. Spatial modeling of soil chemical properties in an arid region of Central Iran using machine learning and remote sensing data. *Model. Earth Syst. Environ.* **2025**, *11*, 152.
573. Srivastava, P.K.; Srivastava, S.; Singh, P.; Gupta, A.; Dugesar, V. Soil chemical properties estimation using hyperspectral remote sensing: A review. In *Earth Observation for Monitoring and Modeling Land Use*; Elsevier: Amsterdam, The Netherlands, 2025; pp. 25–43.
574. Rogovska, N.; Blackmer, A.M. Remote sensing of soybean canopy as a tool to map high pH, calcareous soils at field scale. *Precis. Agric.* **2009**, *10*, 175–187.
575. Khanal, S.; Fulton, J.; Klopfenstein, A.; Douridas, N.; Shearer, S. Integration of high resolution remotely sensed data and machine learning techniques for spatial prediction of soil properties and corn yield. *Comput. Electron. Agric.* **2018**, *153*, 213–225.
576. Šestak, I.; Mihaljevski Boltek, L.; Mesić, M.; Zgorelec, Ž.; Perčin, A. Hyperspectral sensing of soil ph, total carbon and total nitrogen content based on linear and non-linear calibration methods. *J. Cent. Eur. Agric.* **2019**, *20*, 504–523.
577. Jain, S.; Sethia, D.; Tiwari, K.C. Developing novel spectral indices for precise estimation of soil pH and organic carbon with hyperspectral data and machine learning. *Environ. Monit. Assess.* **2024**, *196*, 1255.
578. Scudiero, E.; Corwin, D.L.; Anderson, R.G.; Yemoto, K.; Clary, W.; Wang, Z.; Skaggs, T.H. Remote sensing is a viable tool for mapping soil salinity in agricultural lands. *Calif. Agric.* **2017**, *71*, 231–238.
579. Bai, L.; Wang, C.; Zang, S.; Wu, C.; Luo, J.; Wu, Y. Mapping soil alkalinity and salinity in northern songnen plain, China with the hj-1 hyperspectral imager data and partial least squares regression. *Sensors* **2018**, *18*, 3855.
580. Metternicht, G.I.; Zinck, J.A. Remote sensing of soil salinity: Potentials and constraints. *Remote Sens. Environ.* **2003**, *85*, 1–20.
581. Lazzeri, G.; Milewski, R.; Förster, S.; Moretti, S.; Chabrillat, S. Early Detection of Soil Salinization by Means of Spaceborne Hyperspectral Imagery *Remote Sens.* **2025**, *17*, 2486.
582. Gorji, T.; Sertel, E.; Tanik, A. Monitoring soil salinity via remote sensing technology under data scarce conditions: A case study from Turkey. *Ecol. Indic.* **2017**, *74*, 384–391.
583. GORJİ, T.; YILDIRIM, A.; SERTEL, E.; TANIK, A. Remote sensing approaches and mapping methods for monitoring soil salinity under different climate regimes. *Int. J. Environ. Geoinform.* **2019**, *6*, 33–49.
584. Aldabaa, A.A.A.; Weindorf, D.C.; Chakraborty, S.; Sharma, A.; Li, B. Combination of proximal and remote sensing methods for rapid soil salinity quantification. *Geoderma* **2015**, *239*, 34–46.

585. Jingwei, W.; Vincent, B.; Jinzhong, Y.; Bouarfa, S.; Vidal, A. Remote sensing monitoring of changes in soil salinity: A case study in inner Mongolia, China. *Sensors* **2008**, *8*, 7035–7049.
586. AbdelRahman, M.A.E. An Overview of Land Degradation, Desertification and Sustainable Land Management Using GIS and Remote Sensing Applications; Springer International Publishing: Cham, Switzerland, 2023; Volume 34, ISBN 0123456789.
587. Ruf, T.; Gilcher, M.; Udelhoven, T.; Emmerling, C. Implications of bioenergy cropping for soil: Remote sensing identification of silage maize cultivation and risk assessment concerning soil erosion and compaction. *Land* **2021**, *10*, 128.
588. Liu, S.; Dong, A.; Niu, B.; Xu, F.; Xu, J.; Yin, L.; Wang, S. Maize/cover crop intercropping mitigates soil erosion and enhances yield of ridge cultivation in Chinese Mollisol region. *Catena* **2025**, *255*, 109012.
589. Fahd, S.; Waqas, M.; Zafar, Z.; Soufan, W.; Almutairi, K.F.; Tariq, A. Integration of RUSLE model with remotely sensed data over Google Earth Engine to evaluate soil erosion in Central Indus Basin. *Earth Surf. Process. Landf.* **2025**, *50*, e70019.
590. Zhang, X.; Qin, C.; Ma, S.; Liu, J.; Wang, Y.; Liu, H.; An, Z.; Ma, Y. Study on the Extraction of Topsoil-Loss Areas of Cultivated Land Based on Multi-Source Remote Sensing Data. *Remote Sens.* **2025**, *17*, 547.
591. Gammoudi, A.; Guesmi, H.; Tebini, A.; Attia, R.; Chahed, T.S.; Trabelsi, H. Soil degradation risk prediction in an arid region (Northern Tataouine, Tunisia): Using an empirical model coupling with remote sensing and GIS. *Environ. Res. Commun.* **2025**, *7*, 015019.
592. Molua, O.C.; Ukpene, A.O.; Ighrakpata, F.C.; Emagbetere, J.U.; Nwachuku, D.N. Review on Nondestructive Methods of Detecting Compacted Soils and Effects of Compacted Soil on Crop Production. *Open J. Agric. Sci.* **2023**, *4*, 1–16.
593. Bento, N.L.; Ferraz, G.A.e.S.; Santana, L.S.; Faria, R.D.O.; Rossi, G.; Bambi, G. Plant Height and Soil Compaction in Coffee Crops Based on LiDAR and RGB Sensors Carried by Remotely Piloted Aircraft. *Remote Sens.* **2025**, *17*, 1445.
594. Mikhailova, E.A.; Post, C.J.; Zurqani, H.A.; Hutton, P.C.; Nelson, D.G. Enriching Earth Science Education with Direct and Proximal Remote Sensing of Soil Using a Mobile Geospatial Application. *Earth* **2025**, *6*, 8.
595. Lambot, S.; Wu, K.; Bates, J.; Fluhrer, A.; Montzka, C.; Henrion, M.; Peichl, M.; Dill, S.; Bruecker, P.; Engel, M.; et al. Multi-Sensor Drone Fleet for Soil and Crop Analyses: Integrating Gpr, Sar, Lidar, Multispectral and Infrared Imaging. *SSRN* **2025**.
596. Kulkarni, S.G.; Bajwa, S.G.; Huitink, G. Investigation of the effects of soil compaction in cotton. *Trans. ASABE* **2010**, *53*, 667–674.
597. Bento, N.L.; Silva Ferraz, G.A.e.; Santana, L.S.; de Oliveira Faria, R.; da Silva Amorim, J.; de Lourdes Oliveira e Silva, M.; Silva, M.M.A.; Alonso, D.J.C. Soil compaction mapping by plant height and spectral responses of coffee in multispectral images obtained by remotely piloted aircraft system. *Precis. Agric.* **2024**, *25*, 729–750.
598. Milewski, R.; Schmid, T.; Chabrillat, S.; Jiménez, M.; Escribano, P.; Pelayo, M.; Ben-Dor, E. Analyses of the Impact of Soil Conditions and Soil Degradation on Vegetation Vitality and Crop Productivity Based on Airborne Hyperspectral VNIR–SWIR–TIR Data in a Semi-Arid Rainfed Agricultural Area (Camarena, Central Spain). *Remote Sens.* **2022**, *14*, 5131.
599. Serrano, J.; Marques, J.; Shahidian, S.; Carreira, E.; Marques da Silva, J.; Paixão, L.; Paniagua, L.L.; Moral, F.; Ferraz de Oliveira, I.; Sales-Baptista, E. Sensing and Mapping the Effects of Cow Trampling on the Soil Compaction of the Montado Mediterranean Ecosystem. *Sensors* **2023**, *23*, 888.
600. Kuemmerle, T.; Fernandez, P.D.; Baumann, M.; Burton, J. Uncovering patterns of cattle intensification across South America's dry diagonal. *Environ. Res. Lett.* **2025**, *20*, 074004.
601. Gómez Giménez, M.; de Jong, R.; Della Peruta, R.; Keller, A.; Schaepman, M.E. Determination of grassland use intensity based on multi-temporal remote sensing data and ecological indicators. *Remote Sens. Environ.* **2017**, *198*, 126–139.
602. De Vroey, M.; Radoux, J.; Defourny, P. Grassland Mowing Detection Using Sentinel-1 Time Series: Potential and Limitations. *Remote Sens.* **2021**, *13*, 348.
603. Potočnik Buhvald, A.; Račič, M.; Immitzer, M.; Oštir, K.; Veljanovski, T. Grassland Use Intensity Classification Using Intra-Annual Sentinel-1 and -2 Time Series and Environmental Variables. Remote Sens. 2022, 14, 3387.
604. Rivas, H.; Touchais, H.; Thierion, V.; Millet, J.; Curtet, L.; Fauvel, M. Nationwide operational mapping of grassland first mowing dates combining machine learning and Sentinel-2 time series. *Remote Sens. Environ.* **2024**, *315*, 114476.
605. Bekkema, M.E.; Eleveld, M. Mapping Grassland Management Intensity Using Sentinel-2 Satellite Data. *GI_Forum* **2018**, *1*, 194–213.
606. Wu, R.; Hong, Z.; Du, W.; Shan, Y.; Ying, H.; Wu, R.; Gantumur, B. A Generalized Spatiotemporally Weighted Boosted Regression to Predict the Occurrence of Grassland Fires in the Mongolian Plateau. *Remote Sens.* **2025**, *17*, 1485.
607. Molema, T.R.; Tesfamichael, S.G.; Fundisi, E. Optical and radar remote sensing for burn scar mapping in the grassland biome. *Remote Sens. Appl. Soc. Environ.* **2025**, *38*, 101548.
608. Mofokeng, O.D.; Adelabu, S.A.; Durowoju, O.S.; Adagbasa, E.A. Grass curing-driven fire danger index in a protected mountainous grassland using fused MODIS and Sentinel-2. *Int. J. Remote Sens.* **2024**, *45*, 5359–5384.

609. Hu, X.; Jiang, F.; Qin, X.; Huang, S.; Yang, X.; Meng, F. An Optimized Smoke Segmentation Method for Forest and Grassland Fire Based on the UNet Framework. *Fire* **2024**, *7*, 68.
610. Marčiš, M.; Fraštia, M.; Lieskovský, T.; Ambroz, M.; Mikula, K. Photogrammetric Measurement of Grassland Fire Spread: Techniques and Challenges with Low-Cost Unmanned Aerial Vehicles. *Drones* **2024**, *8*, 282.
611. Watzig, C.; Schaumberger, A.; Klingler, A.; Dujakovic, A.; Atzberger, C.; Vuolo, F. Grassland cut detection based on Sentinel-2 time series to respond to the environmental and technical challenges of the Austrian fodder production for livestock feeding. *Remote Sens. Environ.* **2023**, *292*, 113577.
612. Reuß, F.; Navacchi, C.; Greimeister-Pfeil, I.; Vreugdenhil, M.; Schaumberger, A.; Klingler, A.; Mayer, K.; Wagner, W. Evaluation of limiting factors for SAR backscatter based cut detection of alpine grasslands. *Sci. Remote Sens.* **2024**, *9*, 100117.
613. Dujakovic, A.; Watzig, C.; Schaumberger, A.; Klingler, A.; Atzberger, C.; Vuolo, F. Enhancing grassland cut detection using Sentinel-2 time series through integration of Sentinel-1 SAR and weather data. *Remote Sens. Appl. Soc. Environ.* **2025**, *37*, 101453.